COMPUTATIONAL ANALYSIS FOR MIXING OF FLUIDS FLOWING THROUGH MICROCHANNELS

A Thesis Submitted
In Partial Fulfillment of the Requirements
for the Degree of

DOCTOR OF PHILOSOPHY

by

RANJAN PRAKASH
(2K18/PH.D./ME/16)

Under the Supervision of

Dr. MOHAMMAD ZUNAID
(Assistant Professor, DTU)

Dr. SAMSHER
(Professor, DTU)

Department of Mechanical Engineering

DELHI TECHNOLOGICAL UNIVERSITY
(Formerly Delhi College of Engineering)
Shahbad Daulatpur, Main Bawana Road, Delhi-110042, India

October, 2023

CERTIFICATE

Certified that **Ranjan Prakash (Roll No. 2K18/Ph.D./ME/16)** has carried out their research work presented in this thesis entitled **"Computational Analysis for Mixing of Fluids Flowing through Microchannels"** for the award of the degree of **Doctor of Philosophy** from Delhi Technological University, Delhi, under our supervision. The thesis embodies results of original work, and studies are carried out by the student himself and the contents of the thesis do not form the basis for the award of any other degree to the candidate or to anybody else from this or any other University/Institution.

Dr. MOHAMMAD ZUNAID
SUPERVISOR,
(Assistant Professor)
Department of Mechanical Engineering,
Delhi Technological University,
Delhi-110042,
INDIA

Dr. SAMSHER
CO-SUPERVISOR,
(Professor)
Department of Mechanical Engineering,
Delhi Technological University,
Delhi-110042,
INDIA

Date: 09/10/2023

CANDIDATE'S DECLARATION

I, Ranjan Prakash, Roll No. 2K18/Ph.D./ME/16 student of Ph.D., hereby declare that the research work proposed in this thesis entitled **" Computational Analysis for Mixing of Fluids Flowing through Microchannels"** which is submitted by me to the Department of Mechanical Engineering, Delhi Technological University, Delhi in partial fulfillment of the requirement for the award of the degree of Ph.D. is original and not copied from any source without proper citation. This work has not previously formed the basis for the award of any Degree, Diploma Associateship, Fellowship or other similar title or recognition.

Ranjan Prakash

Place: Delhi **(RANJAN PRAKASH)**

Date: 09/10/2023

ABSTRACT

An explication of mixing performance of microchannels having bend turns is introduced by CFD work. Species carriage model are interpreted through a group of equations of conservation that is Navier-Stokes equation, Continuity equation, and equation of Convection-Diffusion. Reynolds number has opted in extent from 30 to 500. At first, mixing index of T-form unbending as well as T-form having bend turns are likened. For a supreme Reynolds number, a micromixer T-form having bend turns provides a supreme mixing index ($M_i = 46\%$). The outcomes display that as long as Reynolds number enhances, mixing index esteem, and pressure downfall esteem also enhances. Ahead, the impression of bend's structure is analyzed for superior mixing efficiency. To this target, three bend structures of varied radii of 1mm, 2mm, and 3mm as well as identical mixing channel lengths were simulated. The outcomes exhibit that as long as channel radius enhances, mixing quality enhances.

After that, the numerical dissection on mixing quality of T-form straight microchannel, offset insertions T-form microchannel, and offset insertions T-form having bend turns mixing channel by simulation work. CFD software package solves conservation of mass equation, conservation of momentum equation, and conservation of energy equation within the boundary condition. In the concern of offset insertions T-form microchannel, as aspect ratio (height to width proportion) of mixing channel enhanced then mixing index also enhanced as well as offset insertions T-form having bend turns is a conjunction of enhanced aspect ratio and chaotic advection, thus it gives promoted mixing quality than offset insertions T-form microchannel and T-form straight microchannel. Pressure downfall in offset insertions T-form microchannel is more than T-form straight microchannel even then barely inferior to offset insertions T-form having bend turns. Chaotic advection rooted micromixer generates secondary flow which impulsive an advanced pressure downfall in micromixer.

The intention of this perusal is to collate mixing index of a plane spiral microchannel as well as a spiral with spiral obstacle microchannel by simulation work and study of parameters like an impression of increasing inlet velocity (Reynolds number), an impression of channel's curvature (initial channel radius), an impression of microchannel's cross section (different aspect ratios), and impact of distance amid two consecutive turns of spiral with spiral obstacle microchannel. The set of conservation equations is unriddled by CFD software. Simulation procedures were executed at various Reynolds numbers (1, 30, 50, 80, 112, 125) for plane spiral micromixer and spiral with spiral obstacle micromixer. The variation of mixing index and concentration distribution with equal length were numerated for both the microchannels. The mixing index and pressure drop esteem mainly rely on Reynolds number. By increasing Reynolds number, get a supreme esteem of pressure fall and mixing index. Even at a lower value of Reynolds number, a spiral with a spiral obstacle microchannel gives higher mixing quality than a plane spiral microchannel. The pressure downfall in the spiral with spiral obstacle micromixer is more supreme than the plane spiral micromixer. In the indorsation exercise, the process of a Lab on a Chip device is not impressed by pressure fall. The design performs a prominent contribution, here upon this spiral with spiral obstacle micromixer has an appropriate potential to utilize in a Lab-on-a-Chip device.

The influence of cylindrical, rectangular, and triangular obstacles in the case of spiral microchannel has also been studied. It is found that a spiral with spiral obstacle micromixer provides highest mixing index value. Spiral with rectangular obstacles provides the next higher mixing index value after the spiral with spiral obstacle micromixer. Further, a spiral with rectangular obstacles micromixer gives highest pressure drop at Reynolds number 112 and 125, while at Reynolds number 1, 30, 50, and 80, a spiral with cylindrical obstacles gives highest pressure drop.

A comparative interpretation of mixing index of micromixers of duo cross-sections square and circular in spiral shape is proponed by simulation analysis. To execute the manifestation, geometric factors such as axial length of micromixers and hydraulic diameter are opted identical for duo cases. CFD

codes clear up equation of Continuity, equation of Navier-Stokes, as well as equation of Convection-Diffusion.

Interpretation of liquid flow, as well as a combination, has been done via a range of Reynolds numbers 1 to 125. The outcomes decode that circular section spiral micromixer grants a superior mixing performance likened to square section spiral micromixer. Moreover, in case of a circular section spiral mixer, mixing index value has gained 92% at Re =125. For the duo section microchannel, the value of mixing index increment is abrupt on Reynolds numbers. For a pair of cases, pressure fall has been numerated for micromixers of identical lengths. The value of pressure drop in square section spiral microchannel is more than circular section spiral microchannel. The simulation results displayed that circular section spiral microchannel is a dominant design for microfluidic systems such as Lab-on-a-chip (LOC).

A computational interpretation of the mixing quality of twisted spiral micromixer and collated the outcomes with plane spiral micromixer. The fluid motion and mixing performance were explored numerically by mass transporting 3-D Convection-diffusion and Navier-stokes equations. The species transport model is utilized in present work. The Reynolds number is picked in the limiting from 1 to 125. The variations of mass fraction dispensations as well as mixing quality throughout the spiral length and with Reynolds number were evaluated for a twisted spiral microchannel and a plane spiral microchannel. At a higher Reynolds number, a twisted spiral microchannel gives higher mixing quality ($M_i = 98\%$). It can be concluded that the proposed twisted design in three-dimensional is an emphatic method to enhance fluids mixing in microfluidic microdevices. Further, for both cases, pressure drop has been examined. The plane spiral micromixer shows a smaller pressure drop than a twisted spiral micromixer.

ACKNOWLEDGEMENTS

First and foremost, I want to reveal my thankfulness to my supervisors Dr. Mohammad Zunaid and Dr. Samsher for their valuable guidance, support, and encouragement throughout my Ph.D. program. This thesis could not have accomplished its current form without their supervision, direction, and interest in the research work. Their diligent efforts, methodical approach, and individual help made it possible for me to complete this work on time.

I reveal my gratitude to Prof. S.K. Garg, Chairman of DRC, and SRC members, Prof. Avdhesh Kumar Sharma, Prof. M.M. Hasan, Prof. Raj Kumar Singh, and Prof. Amrish Kumar Pawar for giving precious remarks and suggestions. I am grateful to all faculty and staff members of the Mechanical, Production & Industrial, and Automobile Engineering Department for their sustained considerable foster. I eulogize reviewers of research papers and industry people for sparing their precious time and constructive remarks.

I desire to thank my parents, brothers, sisters, family members, and friends whose blessings made this work reality. I'd like to present my sincere thankfulness to my deceased dear mother, Sangeeta Devi for her major contribution to my life and their numerous sacrifices for me. I sincerely thank my wife Mona Kumari for their perseverance, endorsement, and loving participation in accomplishing this research work. I would also like to recognize the support and direction of my father Ajit Prasad. Last, but not least I am grateful to the almighty God for granting me the physical and mental strength to work sincerely, diligently, and honestly and for helping and guiding me during my life and throughout my study.

Ranjan Prakash

RANJAN PRAKASH

..

Title	Page No.
Certificate	ii
Candidate's Declaration	iii
Abstract	iv
Acknowledgments	vii
List of Contents	viii
List of Tables	xii
List of Figures	xiii
List of Symbols, Abbreviations and Nomenclature	xvii
CHAPTER 1: INTRODUCTION	**1-10**
1.1 Introduction to Microfluidics	1
1.2 About the Micromixers	2
1.3 Classification	3
1.3.1 Active Micromixers	3
1.3.2 Passive Micromixers	5
1.4 Dean Flow in Curved or Spiral Channel	6
1.4.1 Visualization of Dean Vortices	7
1.5 Applications	8
1.5.1 Biomedical Diagnostics	8
1.5.2 Analysis of biological macromolecules	8
1.5.3 Drug Delivery and Blood Extraction	9
1.5.4 Electronic Cooling and Thermal Management	9
1.5.5 Mixing and Reactive System Analysis	10

CHAPTER 2: LITERATURE REVIEW 11-40

2.1 Introduction 11

2.2 Review 11

2.2.1 T-junction and Y-junction Micromixer 11

2.2.2 Serpentine Micromixer 27

2.2.3 Spiral and Helical Micromixer 37

CHAPTER 3: OBJECTIVE OF THE STUDY 41-45

3.1 Introduction 41

3.2 Research Gaps 41

3.3 Research Objectives 42

3.4 Expected Research Outcome 43

3.5 Limitations associated with the simulation study 43

3.6 Assumptions of present study 44

3.7 Potential sources of errors in the results 44

3.8 Challenges in Simulation Study 45

CHAPTER 4: METHODOLOGY AND MODELING 46-74

4.1 Model and domain description 46

4.2 Governing Equations 56

4.2.1 The continuity equation 56

4.2.2 Navier-stokes Equations 57

4.2.3 The species transport equation 58

4.3 Newtonian Fluids 59

4.4 Method of Solution 59

4.4.1 Some basic details regarding CFD 60

4.4.1.1 Usages of CFD 61

4.4.1.2 Procedure of CFD 62

4.4.1.3 Advantages 62

4.4.1.4 Disadvantages 63

4.4.1.5 CFD Code 63

4.4.1.6 CFD Procedure 63

4.4.1.7 Steps 64

4.4.2 Coupling and spatial discretization schemes 64

4.4.3 Boundary Conditions 65

4.5 Mixing Index Calculation 66

4.6 Mesh Generation and sensitivity explication 66

4.7 Endorsement of computational work 72

CHAPTER 5: RESULTS AND DISCUSSIONS 75-110

5.1 Mixing and flow analysis in T junction unbending and T junction having bend mixing channel 75

5.1.1 Impact of Design 75

5.1.2 Impact of inlet velocity 76

5.1.3 Impact of bend's structure 78

5.2 Mixing and flow analysis in T form straight microchannel, offset insertions T form straight microchannel, and offset insertions T microchannel having bend shape mixing channel 79

5.2.1 Impact of Geometry 79

5.2.2 Effect of increasing inlets velocity 80

5.3 Mixing and flow analysis in plane spiral micromixer and spiral micromixer with spiral obstacle 83

5.3.1 Effect of Geometry 83

5.3.2 Effect of increasing inlets velocity in terms of Reynolds number 87

5.3.3 Impact of Channel's Structure 88

5.3.4 Impact of microchannel's cross-section 89

5.3.5 Impact of the distance amid two consecutive turns of spiral with spiral obstacle micromixer 90

5.4 Mixing and flow analysis in a spiral microchannel with cylindrical obstacles, rectangular obstacles, and triangular obstacles 91

5.4.1 Impact of Geometry 92

5.5 Mixing and flow analysis in square section spiral microchannel and circular section spiral microchannel 96

5.5.1 Influence of Configuration 96

5.5.2 Effect of increasing inlets velocity in terms of Reynolds number 100

5.6 Mixing and flow analysis in plane spiral microchannel and twisted spiral microchannel 102

5.6.1 Effect of Geometry 102

5.6.2 Effect of increasing inlets velocity 107

CHAPTER 6: CONCLUSIONS 111

Scope for Future Work 115

References 116- 129

List of Publications Founded On Research Work 130

Biographical Profile of Researcher 131

LIST OF TABLES

Table No.	Title	Page No.
4.1	Geometry description of T-form unbending and T-form with bend turns	47
4.2	Geometry descriptions of T-form unbending, offset insertions T-form mixer and offset insertions T-form mixer having bend turns.	49
4.3	Geometry description of square section spiral microchannel and circular section spiral microchannel	54
4.4	Geometry Descriptions of Plane Spiral and Twisted spiral micromixer	55
4.5	Numerical schemes used for CFD Solutions	65
5.1	Mixing index at several Reynolds numbers	95
5.2	Pressure drop at several Reynolds numbers	95

LIST OF FIGURES

Fig. No.	Title	Page No.
1.1	Kinds of Active Micromixer	5
1.2	Types of Passive Micromixer	6
1.3	Delineation of flow outline and secondary flow creation as Dean vortices eventuate	7
4.1	Geometry of T-form microchannel: (a) straight (b) bend turns	47
4.2	Geometry of micromixer T-design: (a) T form unbending (b) offset insertions T form mixer (C) offset insertions T form mixer having bend turns.	48
4.3	A Plane Spiral Micromixer	50
4.4	A Plane Spiral Micromixer with spiral obstacle	50
4.5	A Plane Spiral Micromixer with cylindrical obstacle	51
4.6	Layout of a triangular configuration of cylindrical obstacle array (all dimensions are in μm)	51
4.7	A Plane Spiral Micromixer with rectangular Obstacle	52
4.8	A Plane Spiral Micromixer with triangular obstacle	53
4.9	A Plane Spiral Micromixer having circular cross-section	53
4.10	A Twisted Spiral Micromixer	55
4.11	Numerated mixing index versus the number of the grid elements	67
4.12	Tetrahedral mesh of spiral with spiral obstacle micromixer	68
4.13	Tetrahedral mesh of spiral with cylindrical obstacles micromixer	69
4.14	Tetrahedral mesh of spiral with rectangular obstacles micromixer	69
4.15	Tetrahedral mesh of spiral with triangular obstacles micromixer	70
4.16	Tetrahedral mesh of circular cross-section mixer	70
4.17	Tetrahedral mesh of twisted spiral mixer	71
4.18	Mixing quality versus the number of grids	71
4.19	Mixing index esteem similitude of current T mixer and existing work with T mixer.	72

4.20 Mixing quality similitude of extant plane spiral micromixer and residing work with plane spiral micromixer 73
4.21 Numerated mixing index versus mixing channel length for experimental validation. 74
5.1 Fraction of mass contours of micromixer T-form at an outlet for (a) T junction unbending (b) bend turns at Re =500. 76
5.2 Numerated mixing quality for a T- junction unbending and T- micromixer having bend turns at various Reynolds numbers. 77
5.3 Pressure falls in a T-form uncurving and T-form having bend turns at various Re. 78
5.4 Mixing index across the mixing-channel length for the mixtures. 78
5.5 The mixing quality of three bend micromixers having varied radii versus mixing-channel length. 79
5.6 Mass fraction contours of T mixer at an outlet for (a) straight (b) offset insertions (c) offset insertions T mixer having bend form at Re =500. 80
5.7 Mixing quality for a T form straight microchannel, offset insertions T form straight microchannel as well as offset insertions T mixer having bend turns at varied Reynolds numbers 81
5.8 Pressure drop esteems in a T form straight mixer, offset insertions T form straight mixer as well as offset insertions T mixer having bend turns at different Re. 82
5.9 Mixing index esteem across down channel length for T form straight microchannel, offset insertions T form straight microchannel and offset insertions T mixer having bend turns mixing channel. 82
5.10 Mass fraction contours of micromixer at an outlet for (a) plane spiral (b) plane spiral with a spiral obstacle at Re = 80. 84
5.11 Contour of mass fraction along the spiral length at the central plane for (a) plane spiral (b) plane spiral with a spiral obstacle at Re = 80. 85
5.12 Streamlines rely on species concentration for (a) plane spiral (b) plane spiral with a spiral obstacle at Re = 80. 86

5.13 Numerated mixing index to the plane spiral microchannel and spiral with spiral obstacle microchannel at several Reynolds numbers 87

5.14 Pressure fall in the plane spiral microchannel and spiral with spiral obstacle microchannel at several Re 88

5.15 Calculated mixing index of three spiral with spiral obstacle micromixers with different initial channel radius 89

5.16 Calculated mixing index at an outlet of four spiral with spiral obstacle micromixers with different rectangular cross-sections. 90

5.17 Calculated mixing index versus down-channel length at an outlet for the four spiral with spiral obstacle micromixers with a different centre-to-centre distance. 91

5.18 Contours of mass fraction of micromixer at an outlet for (a) cylindrical obstacles (b) rectangular obstacles (c) triangular obstacles at Re = 80. 92

5.19 Contour of mass fraction along the spiral length at the central plane for (a) cylindrical obstacles (b) rectangular obstacles (c) triangular obstacles at Re = 80. 93

5.20 Streamlines rely on species concentration for (a) cylindrical obstacles (b) rectangular obstacles (c) triangular obstacles at Re = 80. 94

5.21 Fraction of mass contours of micromixer (a) square cross-section (b) circular cross-section at Re = 125. 96

5.22 Concentration contour throughout the spiral length for (a) square cross-section micromixer (b) circular cross-section micromixer at Re = 125. 97

5.23 Streamlines rely on a fraction of mass for a micromixer of (a) square cross-section (b) circular cross-section at Re = 125. 98

5.24 Contour of a fraction of mass at four varied positions beginning from junction point for micromixer of (a) square cross-section (b) circular cross-section at Re = 125. 99

5.25 Plot of velocity vectors for micromixer of (a) square cross-section (b) circular cross-section at Re = 125. 100

5.26 Mixing index esteems to the square and circular cross-section micromixer at several Reynolds numbers. 100

5.27 Variation of the pressure downfall versus Reynolds number for duo cross-section. 101

5.28 Variation of mixing index across mixing channel length at Re =125. 101

5.29 Contours of a fraction of mass of micromixer at an outlet for (a) plane spiral (b) twisted spiral at Re = 112 102

5.30 Contour of a fraction of mass across the spiral length for (a) plane spiral (b) twisted spiral at Re = 112. 103

5.31 Streamlines rely on a fraction of mass for (a) plane spiral (b) twisted spiral at Re = 112. 105

5.32 Species concentration contour at five varied positions for (a) plane spiral (b) twisted spiral at Re =112. 106

5.33 Velocity vectors plot at an outlet of (a) plane spiral micromixer (b) twisted spiral micromixer at Re = 112. 107

5.34 Numerated mixing index to the plane spiral microchannel and twisted spiral microchannel at several Reynolds numbers. 108

5.35 Pressure downfall in the plane spiral microchannel and twisted spiral microchannel at several Re 109

5.36 Mixing index along the mixing channel length to the plane spiral microchannel and twisted spiral microchannel. 109

5.37 Mixing index variation at four variegated locations throughout the length of the mixing channel for twisted spiral micromixer. 110

NOMENCLATURE

D_h	Hydraulic diameter
D_i	Diffusion coefficient
M_i	Mixing index
C	Concentration
Re	Reynolds number
u	Velocity along x-direction
v	Velocity along y-direction
w	Velocity along z-direction
R	The curvature radius of the microchannel
p	Pressure
N	Number of points taken on a particular plane
C_i	Mass fraction at i sampling point
C_{mean}	Average value of the mass fraction
De	Dean number
w	Width of channel
h	Height of channel
s	Center-to-center distance of spiral
r_i	Inner-most initial channel radius
n	Number of spiral loops
d	The wire diameter of spiral obstacle
D	Mean diameter
t	Time

∇	Del operator
$\vec{V}$	Velocity vector
b_i	Body force
C_A	Concentration of species A
D_{AB}	Molecular diffusivity coefficient
V_m	Mean velocity of the flow

Subscripts

f	Fluid
i	Index
max	Maximum
r	Radius

Greek Symbols

σ_{max}	Maximum value of standard deviation
σ	Standard deviation of the mixture at any cross-section
μ	Dynamic Viscosity
ρ	Density of fluid (kg/m^3)
υ	Kinematic viscosity
τ	Shear stress
$\tau_{i\,j}$	Stress tensor
$\delta_{i\,j}$	Kronecker delta
λ	Volumetric dilation coefficient
$\dot{\gamma}$	Shear rate

Abbreviations

SIMPLE	Semi-Implicit Method for Pressure-Linked Equations
CFD	Computational Fluid Dynamics
MUSCL	Monotonic Upstream-centered Scheme for Conservation Laws
LBM	Lattice Boltzmann Method
LOC	Lab-on-a-Chip
FVM	Finite Volume Method
μ TAS	Micro-Total Analysis Systems
SAR	Split and Recombination
EHD	Electro-hydrodynamic
DC	Direct current

AC	Alternating Current
SAW	Surface Acoustic Waves
PDMS	Polydimethylsiloxane
rpm	rotation per minute
POC	point-of-care
LSM	Laser Scanning Microscope
µ LIF	Micro Laser Induced Fluorescence
µ PIV	Micro Particle Image Velocimetry
MSMA	Micromixer with a simplified model of Plan A
MSMB	Micromixer with a simplified model of Plan B
MSMC	Micromixer with a simplified model of Plan C
$TMRF_{0.75}$	Topological micromixer with reversed flow
MC-BMP	Metal Capped Bimorph
MHD	Magneto-hydrodynamic
VOF	Volume of fraction
PMMA	Polymethyl methacrylate
TDHM	Three-dimensional helical micromixer

CHAPTER-1

INTRODUCTION

1.1 Introduction to Microfluidics

The perusal of liquid streams on a micro level which means dimensions of microchannels existent in the mode of microns is called Microfluidics. The conviction of miniaturization of several biological, biomedical, and chemical explication bears huge benefits. Firstly, there is a valuable quantity of deficiency in the requisition of reagents per analysis. That outcome in great skimping of expensive reagents per analysis, also such a small volume of reagents aids in rapid explication and diagnosis. Secondly, the shrinkage of the real size of biochemical/biomedical laboratories to the size of a chip, which builds the laboratory portable and compact. Lab on a chip (LOC) system is an illustration of a microsystem which resides in one or more than one lab affairs on a single chip. These chips will give us improved susceptibility and selectivity. Because of these benefits, Lab on a Chip (LOC) devices has transacted various finding aptitudes in the past few dickers, especially for uses in biomedical as well as biochemical regions.

Even though in microelectronics the conduct of electrons stays nearly equal alike at nano and micro levels, all the same, the diegesis for fluids at the micro level is varied regarding the conduct at macro levels. The fluid flow physics alters drastically by length diapasons. Reynolds number is a significant dimensionless number that is utilized to delineate the liquid flux. The flux on micro-levels is governed by viscous forces of liquid adverse to macro-levels where inertia forces transact a dominant preamble in fluid dynamics. Whether we have to envision natation at a micro level, our stirring will clog incontinently because of the conflicting viscous forces now those in macro levels we comply with the movement to sustain to longer duration

and deviation because of the existence of inertia.

1.2 About the Micromixers

Micromixers are an important portion of microfluidics devices like Lab-on-a-Chip (LOC) as well as micro-Total Analysis Systems (μTAS). In versatile microfluidic usages, mixing quality of microchannels may impress the gross performance of whole microfluidics devices. For instance, rapid mixing of organic solutions, reagents, and cells is necessary for numerous biomedical, biochemical frameworks, and nanomaterial agglutination. Potential mixing not only enhances the inventory sensitivity but as well fetches climb down the explication time by a remarkable motive. The physical circumstance of combination alters at micro levels when collated with the amalgam at macro levels. At macro levels, the amalgam mainly keeps on convection mass carriage which rises escorted by the turbulent character of liquid flux because of an increase in momentum transposition, in spite of, the flux at microscale is intensely laminar and streamlined with no disturbance irregular movement of fluid. Therefore, the amalgam circumstance is regulated by molecular scattering species carriage because of the prevalence of viscous forces which solicits the amalgam liquids to remain in touch for a long duration of time and as well desire prolonged mixing channels. So far as maintaining the lengthy mixing channels send down the fundamental opinion and conviction abaft miniaturization of explication systems, it is important to evolve mixers that are adequate for providing dominant combination within a stocky duration and lengths.

1.3 Classification

Rooted on the manoeuvre engaged for amalgaming the fluids, mixers can be mainly segregated into two kinds, viz, Active and passive mixers.

1.3.1 Active Micromixers

Active mixers use up an exterior origin of power such as magnetic field, electrical field, acoustic, pressure, temperature gradient, piezoelectric drive, etc as a stimulation to the amalgam procedure in the micromixers [Nouri, D. et al. 2017]. These mixers are intricated and solicit extra ingredients which constitute it stiff to unify into Lab-on-Chips (LOC) and micro-Total Analysis Systems (μTAS). All the same, they provide superior command atop the flow and the degree of combination.

Micromixers transacted through magnetic regions having magneto-liquids which are subordinated to Lorentz forces with the aid of electric regions as well as magnets. Magnetic field can cater both as a pump and mixer to transact flux via micromixer [Qian, S. & Bau, H. H. 2005]. Electrodes are located throughout the length of conduit as well as the direction and magnitude of magnetic field can be variegated to command dynamics of flow in an electrolyte solution. Few designs as well inclusive swivelling magnets within the microchannels to rise stirring function which will increase the mixing quality [Veldurthi, N. et al. 2015]. Micromixers driven by an Electrical field utilize the agitation of fluids with electrically charged in an electric region (DC or AC) to unsettle the interface of amalgam fluids which increases the scattering species carriage. Present circumstance is entitled as Electro-Hydrodynamic (EHD) instability [Eribol, P. & Uguz, A. K. 2015]. Micromixers driven acoustically are rooted

on bubble creation inside mixing channel to increase the convective amalgam. Few mixers adopt benefit of walls surface roughness of poly-dimethyl-siloxane (PDMS) to create one or more than one bubble. One more type of micromixer transacted by sound is which usage of Surface Acoustic Waves (SAW). This acoustic wave departed to solid surface of a micromixer. Sound running raises the stirring impact which increases mixing index. Micromixers driven by pressure fields are many usual micromixers due to their convenient structure and creation. The fundamental design embraces a T-junction microchannel having double micropumps to interpose fluid in rotation into a mixing channel creating a pulsatile flow. Assigning present manner of system vastly increases interfacial area outcoming in enhanced mixing quality [Cortes-Quiroz, C. A. et al. 2014]. Also, little work has been presented on having bubbles in a micromixer driven by a pressure field. The bubbles when created at an exclusive frequency will unsettle interface of amalgam liquids rendering superior mixing quality [Khoshmanesh, K. et al. 2015].

In a temperature-stimulated active micromixer, liquids at varied temperatures are melange in a micromixer as well as a temperature gradient was generated utilizing deuce Peltier modules in conjunction with a micromixer [Ishii, K. et al. 2020]. An electrokinetic micromixer uses electrokinetic flow to carry liquid. Electro-kinetic amalgam is influenced via unrepeatable voltage resources together with microchannels dimensioned to have the hoped-for voltage division [Jacobson, S. C. et al. 1999]. A new dielectrophoretic mixer is using parallel microelectrodes to avail polymer particles as well as create a vortex that can beetle liquid to gain combination [Deval, J. et al. 2002]. In electro-osmotic mixing, explication of a stream as well as mixing index in two-dimensional (2D) micromixer with nonuniform zeta potential on microchannel walls is well-grounded [Hadigol, M. et al. 2011]. A micromixer driven by piezo-electrical force urges the enunciation of an interpolated piezoelectric actuator together with the wiring of a piezoelectric actuator for the outsider energy procure [Shimizu, H. et al. 2022].

Figure 1.1 interpret and briefs the categorization of active micromixers [Chen, X., & Shen, J. 2016].

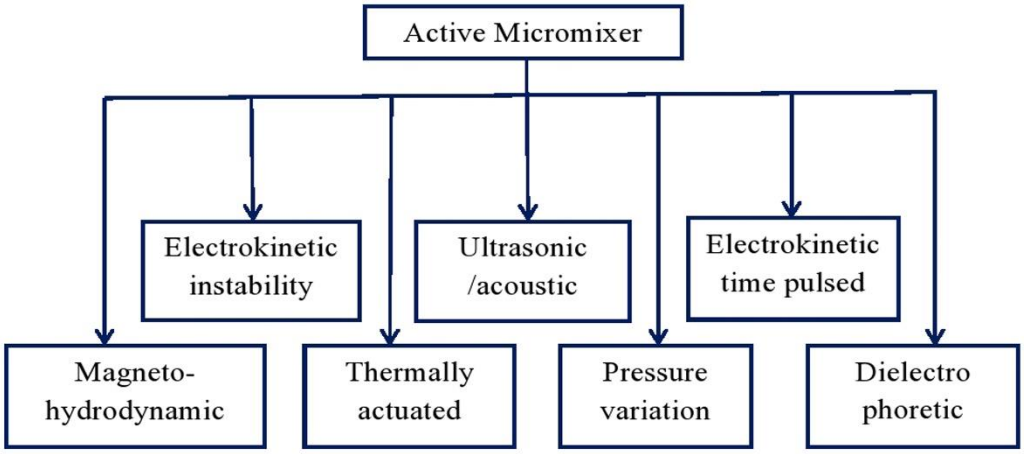

Figure 1.1 Kinds of Active Micromixer [17]

Besides, a few mixers as well exploit centrifugal forces furnished because of revolve to get better amalgam. For instance, the lab on CD micro-Total Analysis System has different ingredients kept on the disc which is swiveled around an axis to detachedly superimpose the liquids. The Coriolis impact infests into the picture because of revolving and here by mixing is coercively contingent on this part of the force. Revolution per minute (rpm) of a disc can be variegated to command the degree of combination expected as stated by requisition [Haeberle, S. et al. 2005].

1.3.2 Passive Micromixers

As stated aloft, active mixers use exterior power resources to increase the species diffusion procedure. All the same, a passive mixer also called a static mixer is discontiguous in intubation that it utilizes transformation in size, appearance, and mixing channel geometry to generate

chaotic advection, create vortices, etc. The key conception of a passive mixer is to fold as well as stretch flowing liquid so many times which increases interfacial area of amalgam liquids enhancing diffusion species transport within a small time and lengthiness. The main benefit of a passive mixer is that it is easy to fabricate and unified into a framework and hereby, the expense of manufacturing as well as running is much lower creating a seductive micromixer for investigation as well as various kinds of mixers are processed by different technologist and scholars. Figure 1.2 depictures the kinds of passive mixers [Chen, X., & Shen, J. 2016]. Since the present workout of this handout is rely on passive mixers, specified framework knowledge together with literature scrutiny are given in Chapter 2.

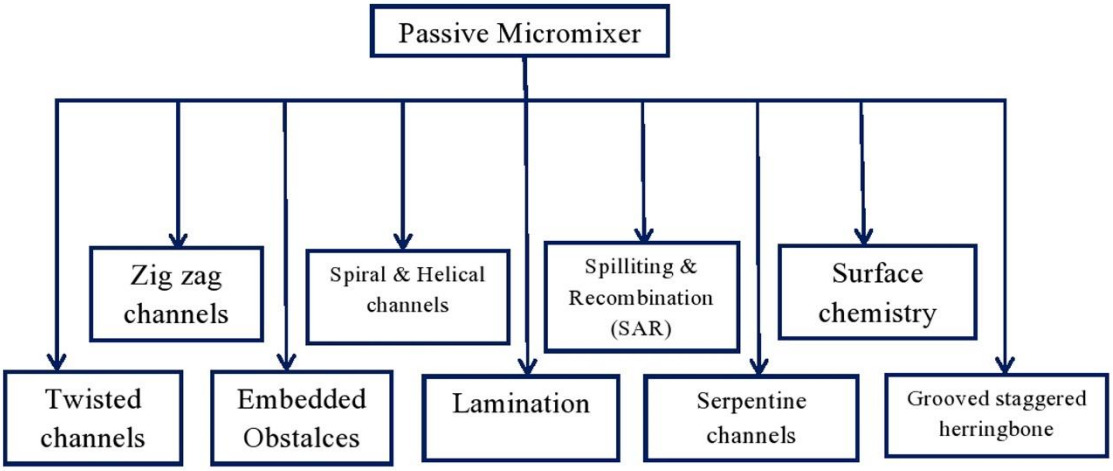

Figure 1.2 Types of Passive Micromixer [17]

1.4 Dean Flow in Spiral or Curved Channel

The fluid flow region interior a spiral microchannel was primarily inspected by Dean. The use of spiral channels creates secondary flow take the form of pair vortices in upper and lower halves of micromixer in view of centrifugal force. The presence of pair vortices (Dean Vortices) provides an enhancement in mixing. The creation of Dean Vortices as well as dignity of the secondary flow (Dean Flow) is depicted by Dean number as [Vatankhah et al. 2018]:

$$De = Re\sqrt{\frac{D_h}{2R}} \quad (1.1)$$

Where-abouts, R denotes channel curvature radius, D_h denotes Channel hydraulic diameter and Re denotes Reynolds number.

Supposing the esteem of Dean number is less than 1, the combination of pair liquids is mainly gained by diffusion. Though Dean number is more than 10, the first double vortex generates and enhances micro mixing process.

1.4.1 Visualization of Dean vortices

Figure 1.3 interprets the creation of Dean vortices via the visitation of pair counter-rotating vortices created because of a mismatch of the turn-propelled centrifugal force as well as stream velocity in the axial direction. The development of secondary flow in appearance of Dean vortices is envisaged via confocal microscopy.

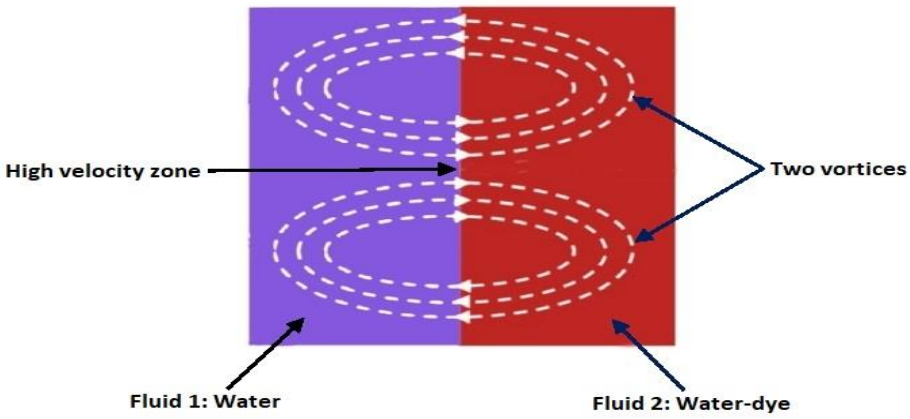

Figure 1.3 Delineation of flow outline and secondary flow creation as Dean vortices eventuate [11].

The Dean vortices are designated by visitation of pair counter-rotating vortices created on both halves of a plane as well as are usually seen at Dean number greater than ten.

1.5 Applications

Microfluidics are widely utilized in the biomedical and biochemical sciences for laboratory research. Various usages of Microfluidics are debated underneath:

1.5.1 Biomedical Dignosis

One of the important Microfluidics usages is in the medicinal industry. Presently, several microfluidic systems are being utilized for gestation check-ups, HIV pathology, monitoring of glucose biosensors, and drug abuse. Present microfluidics province is designated Point-of-Care (POC), which demands many findings to provenance various other devices that bear inexpensive, are simple to utilize, and are portative, forming it practicable for a more significant segment of the community alike existing in rural regions.

1.5.2 Explication of biological macromolecules

To comprehend the character as well as the conduct of biological macromolecules such as RNA, proteins, DNA, etc, reasonable sequencing and stranding are demanded. One of the illustrations is DNA Hybridization via Microfluidics. It insets demolition duplex-stranded DNA framework into a unique-stranded DNA sequence for forward explication of an infection or disease.

1.5.3 Drug dispensation and Blood Extrication

Traditional techniques of administering drugs and drawing blood inset the use of sharp, painful syringes. Another disadvantage of using needles to deliver drugs is that it takes a prolonged time to convey the drug to the affected organ or area. It can be utilized to delegate drugs directly to the vicinity of the affected area, mpressively reducing the time by narrowing the "drug path". There are also various micro devices existing to monitor blood sugar. It is of great serve to people with diabetes who need to maintain their sugar levels.

1.5.4 Thermal Management and Electronic Cooling

By the rebating in mensuration of electronic parts such as Integrated circuits, microprocessors, etc. there infests a fundamental necessity for the dominant disappearance of heat from these ingredients to work under the secure range. Even though the mensuration of electronic ingredients is obtaining smaller, all the same, the energy input expected to make go persists the same, and hereby, eliminating an extra thermal power from circumscribed micro steads is defiance. Various droplets rooted cooling of microfluidic frameworks as well as abstruse heat pipes has infested forth to be strenuous rectification to these issues. Present region is a comprehensive field of ongoing findings as well as stable efforts have been rendered to fabricate optimum thermal designs to permit dominant passive cooling for energy ingredients as well as modules.

1.5.5 Mixing as well as Reactive System Explication

Various biomedical as well as biochemical usages such as polymerization, organic synthesis, and micro-chemical reactors postulation fast combination of liquids to get homogenized samples and rapid reactions amid the liquids. The present handout embraces an exploration of passive micromixers as well as a detailed Section 1.2 and Section 1.3 enclose the area of these micromixers disserting different kinds, working, and implementations.

The main aim of microfluidic research is designing standalone microfluidic systems which could be able to operate without needing a specialist; these microfluidic systems are called micro-Total Analysis systems (μ TAS) and Lab-on- Chips (LOC).

Recently, a new system concept has been proposed for micro-fluidic system, i.e., introducing some deformable solid structures in the micro-channels, so that the so-called embedded micro-fluidic system is formed. In the future, the potential application of this new system concept Soft Microfluidic System (SMS) for drug delivery and testing, micro-sphere generation, tissue regeneration, 3D printing technique, and deep X-ray lithography technique.

CHAPTER-2

LITERATURE REVIEW

2.1 Introduction

An ongoing chapter explicates the comprehensive intelligence linked to mixing phenomena in a micromixer with Newtonian and Non- Newtonian fluids. In this chapter, several research papers are reviewed which have intimation linked to micromixer flow.

2.2 Review

2.2.1 T-junction and Y-junction Micromixer

Jacobson, S. C. et al. [1999] proposed microfluidic instruments for electrokinetically transacted serial and parallel combination. Parallel combination instrument is contemplated having a sequence of independent T-crossroads, together with serial combination instrument is rely on an array of cross scissions as well as sample shunting. These instruments were calibrated by combination a sample with a buffer in the mitigation experimentation.

Hengzi, W. et al. [2001] calibrated mixing quality of a Y-junction microchannel having cylindrical obstacles arranged in eight different configurations. The mixing fluids used in this microchannel were ethanol and water. The simulation outcomes show that as long as the number of obstacles rises, mixing quality also rises. The outcomes also exhibit that the mixing quality is increased as the pressure downfall rises.

Wong, S. H. et al. [2003] explored the mixing efficiency of a microchannel in a cross shape that has grooves in the mixing channel. In this case, out of three inlets one inlet for enzymes and two inlets for antibiotics for rapid mixing. The efficiency of microchannel without grooves and with grooves is collated. The simulation explication of combination in a cross-shaped micromixer with grooves consolidated in mixing channel exhibits improves mixing performance more than a microchannel without grooves. Also, rising the number of grooves and consolidating the grooves at junction again enhances mixing efficiency.

Wong, S. H. et al. [2004] erected and tested a T-junction micromixer to calibrate their workability as a fast mixing microchannel. In present paper, experimental work as well as CFD simulation have been performed. The working fluids utilized in this micromixer were blue dye and colourless liquid. Various pressures are enforced at the inlets of T-junction microchannel as well as their analogous mixing quality is inspected with the help of an optical microscope. This perusal exhibits that fast amalgam can be gained in a T-junction microchannel in Reynolds number limit from 400 to 500.

Engler, M. et al. [2004] analyzed computationally and experimentally rising vorticity in static T-junction microchannel having rectangular cross-sections obtained at inferior Reynolds numbers as well as their impact can be utilized to enhance mixing performance. Furthermore, they differentiate between three flow regimes viz Stratified stream regime, Engulfment stream regime, and Vortex stream regime. They also erected a sequence of microchannels having rectangular cross sections and made an appropriate experimental setup to liken the simulation outcomes to the actual mixing manners.

Haeberle, S. et al. [2005] introduced a new centrifugal micromixer rely on Coriolis-induced mixing. The Coriolis microchannel excels with rapid mixing at high-volume throughputs. Also, the possibility to control the flow ratios and flow rates by varying the frequency and sense of rotation has been explained.

Nguyen, T. N. T. et al. [2008] designed a Y-type square wave microchannel inside square obstacles. By inserting square obstacles, chaotic advection was created which will enhance mixing ability. In this mixing process, the working fluids NaOH and phenolphthalein were taken. The mixing features of microchannel were calibrated by altering the rate of flow and width of micromixer. The outcomes exhibited that mixing was accomplished in a small number of seconds after passaging through the fourth stage of mixing.

Tsai, T. H. et al. [2009] investigated amalgam process amid ferro-nanofluid (Fe_3O_4 nanoparticles as well as water solution) and pure water in the Y-shape semi-active microchannel. An everlasting magnet having a power of 2200G was installed at the position behind Y-shape micromixer to enhance mixing quality of water and ferro-nanofluid. Equal rates of flow for both the water and ferro-nanofluid were analyzed in duplet channel widths. Three separate rates of flow were tested to find the impact of flow rates on mixing of solutions in microchannel. Actually, nanoparticles in solutions are impressed by a magnetic field, calculated results exhibit that fast mixing between water and ferro-nanofluid can be obtained instantly downstream of a magnet for entire rates of flow and each microchannel width studied in the present paper.

Sökmen, C. N. [2010] calibrated numerically the impact of alteration of supercritical water characteristics having pressure as well as temperature on mixing of flows having varying temperatures in the T-junction micromixer. In this paper, mixing fluids hot stream and cold stream were taken. The impact of characteristic alterations on the results of combination is

much vital for inferior Reynolds numbers and hot stream entrance temperatures aloft pseudo-critical temperature as well as so obtain non-uniform temperature dispensation at an outlet.

Xu, Z. et al. [2011] presented staggered oriented ridges micromixers and their geometric impacts on fluid mixing process. They studied the changing of the inflow direction i.e. vertical inlet configuration and parallel inlet configuration, ridge height ratio, ridge asymmetry index, pressure downfalls, and methods of fluid flow. The outcomes exhibit that vertical inlet configuration is more efficient than parallel inlet configuration.

Hadigol, M. et al. [2011] read out the influences of shear relying on viscosity of Non-Newtonian liquids in 2-D microchannel having non-uniform zeta potential dispensations across the microchannel walls. The simulation outcomes indorsed that shear relying viscosity has a valuable impact on extent of mixing quality. It was obtained that for an employed electric field as well as zeta potential, mixing quality reduces when Reynolds number exceeds, also dilatant fluids are much susceptive to Reynolds number transformations in proportion with pseudoplastic fluids. The pseudoplastic fluids can achieve supreme mixing quality in broad limits of Reynolds number.

Seo, H. S. & Kim, Y. J. [2012] calibrated mixing process in the hybrid micromixer mingled with both passive and active action. The simulation of passive micromixer with triangular, rectangular, and cylindrical obstacles is exploited, which are imposed on top and bottom walls. The mixing phenomena of active action with an applied electric field are also studied and then likened mixing quality of both types of micromixers.

Mouheb, N. A. et al. [2012] screened the species transport within cross-shaped and T-junction microchannels utilizing Confocal LSM and CFD. They compared the species concentration profile of both cross and T geometries. For comparison purposes, Reynolds number and flow rate at an inlet of both geometries were taken the same. They concluded that due to two outlets

in cross geometry, extent of fluid freedom increases in microchannels and also permits easy rotation of flow in proportion with T junction geometry. So cross-shaped microchannel verges to rise mixing quality earlier by formation of 3-D flows.

Hsieh, S. S. et al. [2013] calibrated the impact of angles in a Y-shape micromixer utilizing μLIF and μPIV optical techniques. To examine the mixing quality, they quantified the concentration profile and velocity fields in the Y-shape microchannel. An optimum mixing angle was gained rely on mixing index and mixing length. Also impact of joule heating on mixture was monitored.

Afzal, A., & Kim, K. Y. [2013] numerically analyzed the combination of two fluids in a staggered herringbone micromixer. For optimization, width and depth of grooves were taken as design alterables. Three execution parameters, i.e. overall friction factor, mixing sensitivity, as well as mixing quality at an outlet of microchannel were assigned as objective functions.

Solehati, N. et al. [2014] designed a T-joint microchannel having a wavy form lead to secondary flow for improved mixing index. They developed a mathematical model for combination in T shape micromixer with a wavy form. Single-phase mixing is considered in this model. This mathematical model settles mass conservation, energy conservation, and momentum conservation. They also introduced a performance index which means a proportion of mixing index to pressure drop. The outcomes exhibit that mixing index and performance index improves appreciably for micromixer T shape mixer with wavy form, particularly at the supreme Reynolds number.

Rahimi, M. et al. [2014] interpreted the impact of channel angles, a ratio of flow rate, as well as flow rate on mixing quality in passive asymmetrical micromixers. Flow properties for each configuration were tested by CFD simulation and experimental work. The results expose that mixing quality rely on microchannel configuration, entrance rate of flow

ratios, and total rate of flow. The mixing quality was not good in T junction micromixer at a lower flow rate. It improved by increasing the rate of flow. At supreme Reynolds numbers, by rising the angles and rate of flow ratio the mixing index increased. Also, the mixing effectiveness was measured for all micromixers.

Cortes-Quiroz, C. A. et al. [2014] examined a microfluidic method constituted by two valveless micropumps linked to a T-junction microchannel. A parametric perusal is performed on this microfluidic device with the help of CFD. The phase distinction and frequency of periodic flow velocities as well as angle made by inlets were utilized as design parameters and pressure drop, mixing index, and maximum shear strain rate in microchannel was used as performance parameters.

Quiroz, C. A. C. et al. [2014] performed a simulation of three dimensional T- micromixer and a typical T-micromixer with same dimensions of mixing channel length and cross-section and also same flow rates. This perusal exhibits that the three-dimensional T-micromixer gives an appreciable increase in mixing and provides less pressure drop and same degree of shear stress collated with a typical T-micromixer.

Calado, B. & Santos, A. D. et al. [2015] designed three T shape microchannels with asymmetric entrances and various heights to estimate their mixing quality with various Reynolds numbers. The outcomes allow discerning five mixing regimes. Mixing quality for every regime is examined with duplet variables along a T-junction. First one is fluid concentration and the second one is complementary index. The outcomes exhibit that the rise of asymmetry level of entrances enhances the mixing quality.

Afzal, A. & Kim, K. Y. [2015] proposed T with a convergent-divergent mixing channel and also introduced pulsatile flows in the micromixer having time-dependent velocities at entrance 1 and entrance 2. These velocities are a superposition of steady flow (first term) and sinusoidal

flow (second term). The impacts of the sinusoidal waves on the mixing quality in a convergent-divergent micromixer were investigated. A convergent-divergent micromixer presented the most effective flow comparison to a straight channel, square-wave channel, zig-zag channel, and sinusoidal channel.

Eribol, P. & Uguz, A. K. [2015] applied an electrical field to unsettle the interface between duplet Newtonian and immiscible fluids flowing in the rectangular micromixer. The fluids taken in the experiments are a combination of castor oil, olive oil, ethylene glycol, and different viscosity silicone oils. The electrohydrodynamic instability was examined for different parameters like flow rates, viscosities, width of micromixers, and applied electric field direction.

Khoshmanesh, K. et al. [2015] introduced a hydrodynamically actuated bubble-based microfluidic device. Combination of vicinal liquids is accomplished with vacillate the bubble at lusted displacement as well as frequencies. The flux control is obtained by forcing the bubble to fully or partially shut the main channel.

Puccetti, G. et al. [2015] offered an experimental analysis of flow patterns in gas-liquid (air-water) two-phase mixing in a T-junction microchannel. In this microchannel having a rectangular cross-section, a water-air combination is prepared by inoculation of air in the direction perpendicular to straight water flow. To create a flow pattern map, 256 experimental trials having various values of superficial velocity have been done.

Quiroz, C. A. C. et al. [2016] proposed three dimensional T junction micromixer having both entrances at different horizontal levels and a parametric readout with the help of CFD was done on the substratum of the prime three-dimensional T-junction micromixer to cognize the design assortment that improves mixing much fastly in Reynolds number limit of 50 to 700. The width

and height of mixing channel were utilized as configuration factors, which are changed to create different configurations with distinguishing aspect ratios and relative levels between the entrance channels.

Xia, G. D. et al. [2016] monitored experimentally and numerically features of species transport and fluid flow in a microchannel with baffles and gaps. The pressure downfall and mixing index were calculated in Reynolds number limit from 0.1 to 60 considering impact of baffles and gaps, sudden contraction or expansion, split and recombination, and multiple vortices. It is exhibited that the field synergy regulation gives a substitute path to calculate the mixing quality. The extensive performance of microchannel is calibrated by the performance index and field synergy principle.

Ritter, P. et al. [2016] offered a passive microchannel having repetitive nozzle-diffuser shape obstructions. LBM simulation of two fluids was implemented for Reynolds number limit of 1 to 100 and at Schmidt numbers 1 and 50. Numerical simulation hubs on a calculation of mixing index of novel design as well as an explication of species transport as a concern of Peclet number. The outcomes are compared with a plain rectangular microchannel.

Li, T. & Chen, X. [2017] designed three simplified microchannels of plan A (MSMA), plan B (MSMB), and plan C (MSMC) as stated by the topological microchannel $TMRF_{0.75}$ which is presented in 2016. The mixing in all three microchannels is simulated in Reynolds number range of 0.01 to 100. All three microchannels MSMA, MSMB, and MSMC have achieved higher mixing index. The mixing quality of MSMA and MSMC is superior to MSMB since both have more contact area.

Chen, X. & Zhao, Z. [2017] proposed the optimization of square and cylindrical obstacles in three-dimensional T junction microchannel. Numerical simulation exhibits that flow direction

changes frequently due to obstacles, which creates chaotic advection and raises mixing efficiency. The results show that multi-unit obstacles microchannel is more efficient than simple T junction microchannel.

Santana, H. S. et al. [2017] designed two micromixers first one T junction micromixer with static elements and the second T junction micromixer without static elements. The flow explication was delineated in Reynolds number range 0.1 to 100. The micromixer with static elements exhibited better performance than a simple T junction microchannel. The supreme mixing index was gained at Reynolds number 100. The utilization of these static elements in the microchannel improved biodiesel synthesis.

Silva, J. P. et al. [2017] designed T junction microchannels with alterable entrances widths and applied pulsed signal at the entrances to see the effect on mixing quality. The outcomes demonstrate that the use of pulsed signal at entrances is extremely favourable, with highest mixing quality rises 100% in case of symmetrical microchannels and 90.6% for most asymmetrical microchannels. Moreover, as the frequency increases, mixing quality decreases.

Nouri, D. et al. [2017] deciphered a fast combination of water as well as ferrofluid in the Y junction micromixer utilizing a permanent magnet by COMSOL software and experimental work. COMSOL software solves Maxwell equations to get magnetic potential. After that magnetic force was evaluated. The simulation outcomes are likened to experimental outcomes to verify the simulation outcomes. The impact of numerous parameters like concentration of nanoparticles, rate of flow, as well as magnetic field's strength on mixing quality is studied.

Lobasov, A. S. & Minakov, A. V. [2018] studied impact of various fluids properties on mixing quality in a T junction microchannel. It was shown that the densities and viscosities, opening

temperatures, and rheology of combination fluids have valuable impacts on mixing quality of the mixture. In this analysis, it was gained the mass fraction of components, pressure drop, and velocity field distribution in the microchannel.

Dauyeshova, B. & Monaco, E. [2018] used LBM scheme to read out mixing quality of the T-shaped micromixer having obstructions in the mixing channel. In this study, water as well as ethanol were taken as operating fluids. They studied mixing quality of T-shaped microchannel with circular obstacles, T-shaped microchannel with rectangular obstacles, and Grooved T-mixer.

Nezhad, J. R. & Mirbozorgi, S. A. [2018] analyzed the effect of triangular baffles, circular baffles, and elliptical baffles on mixing quality in terms of mixing efficiency and performance index by applying immersed boundary-lattice Boltzmann method. The outcomes show that the use of various shape baffles enhances the mixing quality. Also as the baffles distance decreases, the mixing quality increases.

Casanova, J. O. & Lai, C. H. [2018] used mixed motion of pitching and heaving of a square cylinder situated in mid of a rectangular micromixer to magnify the mixing of fluids. The features of five input parameters and output outcomes are investigated. The input parameters have two amplitudes and two frequencies. The output outcomes are mixing quality, mixing energy cost, and input power coefficient.

Xu, W. et al. [2018] presented the influence of varied entrance conditions on mixing quality of microchannel having triangular and rectangular baffles. Twenty-eight microchannels with various parameters were studied by simulations. The relevancy of simulation results and experimental results reaffirm the convincement

of research technique and the accuracy of simulation. The results exhibit that by increasing the number of entrances and varying the angle of entrances, we can improve mixing quality of micromixer.

Izadpanah, E. et al. [2018] deliberated a combination of two liquids in the three-dimensional T junction and double T junction microchannel using a finite volume method with a Reynolds number range of 75-400. The outcomes display that by reducing the angle of branches in a double T junction microchannel, mixing index increases. It is also noticed that mixing quality of fluids raises along the mixing channel length.

Dundi, T. M. et al. [2019] presented the swirl component of velocity at entrances of T junction microchannel to improve amalgam. Numerical outcomes were exhibited that inverse orientation of swirl at entrances desirable sooner initiation of engulfment regime which improved mixing in Reynolds number range 66 to 180. At Reynolds number greater than 266, same orientation of swirl at entrances improved swapping of samples at the junction point which appreciably increased mixing. Inverse orientation of swirl improved by 300% to 500% mixing index in the Reynolds number range 160 to 180 and the same orientation of the swirl improved by 30% to 70% mixing index in Reynolds number range 266 to 372 as collated to the T junction without swirl.

Haghighinia, A. & Movahedirad, S. [2019] compared the simulation results of two-dimensional and three-dimensional microchannels. The blockage ratio of obstacles to resist the direction of flow was near zero or one, and the outcomes of two-dimensional simulations outlook to three-dimensional simulation results. The value of mixing index of two dimensional simulations and three dimensional simulations achieved prominent incompatibility at a

blockage ratio of 0.75. At a blockage proportion of 0.5, the existence of the vortices motivated by secondary flow achieved a higher mixing index and the subsequent divergence of two-dimensional results in comparison to three-dimensional results.

Liu, X. & Lu, Y. [2019] used a fast and tunable combination technique to manage the gathering of Fe_3O_4 nanoparticles. Present technique insets shear mixing in the T-shaped microchannel. Changing the rate of mixing and scrip of magnetic suspension permitted for malleable settlement of nanocluster size while keeping homogeneously sized magnetic nanoclusters.

Rahmannezhad, J. & Mirbozorgi, S. A. [2019] optimized grooved microchannels with square, diamond-shaped, and circular obstructions by CFD analysis and response surface methodology. The impact of obstacles dimension and offset in various ranges are calibrated on mixing energy cost, pressure drop, and percentage of mixing. The results demonstrate that mixing percentage raises with an increase in obstruction dimension in all range esteems of offset to all three obstacle shapes. Same pattern is seen with a rise in the offset. Further outcomes show that pressure downfall and mixing energy cost rise with the rise of obstruction dimension at all offset values and for all shape obstructions. On the contrary, the mixing energy cost and pressure drop decrease as the offset increases. Ultimately, pressure downfall, mixing percentage, and mixing energy cost (mec) are recognized as objective functions to optimize grooved microchannel performance having obstructions.

Xu, C. et al. [2019] introduced a dispersed double T junction micromixer for amalgam of liquids. At an entrance velocity of 0.6 m/sec and microfiltration mesh size of 10 micrometers, high mixing quality was obtained. The outcomes propound that surface etymology of Tio2 films generated by micromixing can be readily commanded in proportion with that of specimen created by conventional stirring amalgam procedure.

Cetkin, E. & Miguel, A. F. [2019] proposed three designs of microchannels namely branching ducts with obstacles, branching ducts having sphere mixing chamber, and branched system of ducts, and analyzed three degrees of freedom first one ratios of diameters, second one ratios of lengths, third one ratio of length and diameter. The mixing quality of all designs is evaluated by simulation results. The outcomes uncap that the divaricate microchannel must have a long mother conduit having a greater diameter than daughter conduits. The outcomes exhibit that branching ducts with obstacles and having sphere mixing chambers improve mixing quality. As well microchannel with sphere mixing channel at junction has better mixing quality than microchannel with inserted obstacles into the mother duct channel.

Santana, H. S. et al. [2019] introduced a microchannel having triangular baffles as well as circular obstacles. The optimization of geometric alterables was done taking into account mixing efficiency and pressure drop. Various binary mixtures like ethanol/water and vegetable oil/ethanol were used. Reynolds number limit was taken from 0.01 to 200. A mixing index of 99% was obtained for ethanol/oil mixture for various microchannel widths and heights at inferior Reynolds number 0.1 as well as also in high Reynolds number range 50 to 100.

Zhang, S. et al. [2019] proposed the mixing quality of microchannel having stagger Koch fractal baffles. It was positioned at bottom and top of T-microchannel. Mixing quality of secondary Koch fractal microchannel and primary Koch fractal microchannel is likened to four different Reynolds numbers. As long as the baffles angle varies, it subscribes to increase chaotic convection of microchannel. The mixing quality of microchannel is greater than 95% at Reynolds number values 0.05 and 100.

Rao, L. T. et al. [2019] examined the mixing quality of T form microchannel with various obstacles. In this work, the impact of a single obstacle having various shapes and positions was investigated. Various shapes like circular, diamond, ellipse, triangle inside, and triangle outside were utilized as obstacles. Simulation was performed using COMSOL software. Rely on mass fraction, pressure downfall, mixing quality, and mixing length, it was obtained that diamond shape obstacle provides best mixing quality collated to other obstacles.

Dundi, M. et al. [2019] introduced a new design T-T microchannel at several Reynolds numbers. The outcomes exhibit a prominent rise in mixing quality of T-T microchannel for Reynolds numbers inferior to 200 and also for Reynolds number greater than 400. This appreciable increase with a T-T micromixer is achieved at an outlay of a minor increase in pressure downfall likened to a simple T micromixer. The interlude between double T micromixer was optimized and obtained that gap of 5 to 20 micrometer in a double T micromixer is superior. They also studied the effect of different velocities at inlets.

Kurnia, J. C. & Sasmito, A. P. [2019] inserted twisted tape inside the T shape micromixer and collated mixing index result with simple T shape micromixer. This is the case of single-phase mixing, laminar flow, and Newtonian fluid. Various parameters were studied like inlet velocity, the width of the twisted tape, twisted tape nature either solid or porous, and porous tape permeability. By adding twisted tape inside T junction micromixer the mixing index increases twice that of simple T junction micromixer. Porous tape at permeability $10^{-10}\ m^2$ provides best mixing quality at obscure to moderate Reynolds numbers and solid twisted tape rises mixing quality at supreme Reynolds numbers.

Ishii, K. et al. [2020] proposed a new non-contact microchannel that utilizes two Peltier modules as well as creates a temperature distinction within a micromixer to create a helical

flow. In present work, mechanism of spiral flow was analyzed by numerical computation. This spiral flow was created by natural convection. The natural convection impression on microchannel volume was huge at millimeter level as well as it was obtained that temperature distinction can be utilized more fruitfully for amalgam.

Tokas, S. & Zunaid, M. [2020] examined the flow and mixing behaviour in T microchannel with water and blood as a working fluid having a width-to-height ratio of microchannel two in the Reynolds number range 2 to 320 for water as well as corresponding mass flow rates for blood. It obtained different mixing and flow behaviour for blood and water. The results show that initially mixing quality for water reduces, as long as Reynolds number exceeds particular values of Re then further mixing quality rises with the rise in Reynolds number. On the contrary in case of blood analysis, mixing quality decreases as the mass flow rate increases.

Madana, V. S. T. & Ali, B. A. [2020] analyzed single-phase flow in T junction microchannel by numerical simulation. For single-phase flow analysis, a 3D transient numerical simulation was carried out. The engulfment flow has occurred at critical Reynolds number 300. To obtain engulfment flow at a lower Reynolds number, inlets of T junction micromixer are altered as convergent (C) and divergent (D) sections, as well as its impact on engulfment flow is examined. The pressure fall is obtained to be minimal at a C/D proportion of 9:1.

Termizi, S. N. A. A. et al. [2020] used to explore the fluid mixing in T micromixer by CFD simulation. The water-ethanol and water-glycerol were taken as working fluids. T junction microchannel was created by AutoCAD software. The impact of entrance velocity as well as width size on mixing quality was examined. Mixing index of two mixtures having different diffusion coefficients exhibited same pattern for various inlet velocities and width sizes of mixing channel.

Yuan, S. et al. [2021] explored flow behaviour and combination process of ethanol and water mixture in the cross-shaped microchannel inside laminar regime. Firstly impact of rising an operative parameter on local mixing quality along micromixer is examined. Secondly, the influence of varied factors like mixing angle, aspect ratio, as well as blockage on the mixing index are studied and velocity profile as well as mass fraction distribution was exhibited. Furthermore, the effect of microchannel surface roughness was also analyzed.

Prakash, R. et al. [2021] explored mixing index of the microchannel having a bend shape mixing channel by CFD simulation and compared the results with simple T junction microchannel. The results exhibit that T shape with bend curvature gives better performance than simple T shape microchannel. Also, as long as Reynolds number exceeds, mixing index and pressure downfall value exceeds. Furthermore, impact of bend shape at different radii 1mm, 2mm, and 3mm was studied. It was found that as long as the radius of curvature rises, mixing index rises.

Prakash, R. et al. [2021] proposed the three types of microchannel geometries T junction unbending, offset headers T junction, as well as offset headers T junction with bend form mixing channel. It was gained that offset gateways T junction with bend form mixing channel provides improved mixing index than T junction unbending as well as offset inlets T junction unbending.

Shimizu, H., & Uetsuji, Y. [2022] offered a novel actuator in which a metal cap is connected having a bimorph piezoelectric element. Two drive modes were taken namely a single actuator for top surface of circular tank and double actuator for both lower as well as upper surfaces. In fluid shifting execution test, it was obtained that the rate of flow was enhanced by 19 times in single MC-BMP (Metal Capped Bimorph) as well as around 82 times in double MC-BMP

likened to conventional BMP (Bimorph). In mixing quality calibration, it was obtained that mixing quality was enhanced 2.3 times in single MC-BMP as well as around 2.9 times in double MC-BMP likened to conventional BMP.

2.2.2 Serpentine Micromixer

Deval, J. et al. [2002] proposed a dielectrophoretic microchannel that motivates chaotic trajectories of interposed particles through a combination in time and space of electrical actuation and local microchannel design alteration. In this simple design, mixing time is choreographically reduced.

Qian, S., & Bau, H. H. [2005] designed and tested a magneto-hydrodynamic (MHD) stirrer. The stirrer contains conduits connected with specifically controlled electrodes situated longwise its opposite walls. Conduit is impregnated having electrolyte solution as well as situated in the uniform magnetic region. This system can execute as both a pump and a stirrer. So far as this system has no movable segments, the concept is appropriate for microfluidic applications.

Mouza, A. A. et al. [2008] presented a chaotic microchannel having a combination of curved channels for generation of the secondary flow, split and recombination, as well as flow separation because of backward and forward facing steps. It was found that this new design provides superior mixing performance at low Dean numbers.

Hossain, S. et al. [2009] proposed a simulation analysis for combination and flow behaviour in micromixers having various serpentines such as curved, square-wave, as well as zig-zag. For simulation, geometric parameters like microchannel cross-section, microchannel height, microchannel axial length, and number of pitches are taken equal for all three microchannels.

The outcomes exhibit that square wave micromixer gives best mixing quality and zig-zag and curved micromixer show approx. same mixing quality for maximal Reynolds number.

Ansari, M. A. & Kim, K. Y. [2009] numerically studied amalgam of fluids in microchannels having mixing chambers in circular form. These mixing chambers in the circular form are textured to generate self-circulating flow that works on inferior Reynolds numbers. Simulations have been carried out in a structure that consists of four mixing chambers in circular form connected with constriction channels. In this perusal, mixing of fluids is analyzed for Reynolds number limit from 1 to 250. As well the impact of the proportion of width of the constriction channel to the diameter of circular chamber and angle amid connection channel and the external walls of chamber on mixing have been analyzed. The mixing quality at the end of system design rises sharply with Re.

Ansari, M. A. & Kim, K. Y. [2009] investigated the combination of two fluids in a 3-D serpentine micromixer with L-shaped repeated structure. The Reynolds numbers for simulation were taken 1, 10, 35, and 70. The effects of ratio of microchannel height to microchannel width as well as proportion of outright microchannel length in L-shaped to microchannel width have been evaluated at four Reynolds numbers.

Alam, A. & Kim, K. Y. [2012] proposed the planar microchannel having a circular mixing chamber as well as two connection channels crossing each other. Mixing quality of this presented microchannel is simulated and liked the results with three other microchannels. Computational analysis of mixing and flow is carried out by utilizing 3-D Navier-Stokes equations for Reynolds number range 0.1 to 100. The proportion of the width of connection channel to the circular chamber diameter was taken as 1/8. The mixing is estimated by numerating the mixing performance. The proposed microchannel exhibits best mixing

performance for Reynolds number less than 50 and exhibits worst mixing quality for Reynolds number greater than 50.

Alam, A. & Kim, K. Y. [2012] numerically examined mixing of fluids in curved micromixer having rectangular grooves utilizing 3-D Navier-Stokes equations. Firstly, the mixing and flow behaviour is explored in Reynolds number limit from 0.5 to 90. Secondly, the influence of depth and width of rectangular grooves on mixing quality is examined. It was found that mixing index of a grooved microchannel produces better mixing quality than a smooth micromixer for Reynolds number of more than ten.

Wang, L. et al. [2013] presented a constructal tree-shaped micromixer for fast mixing of liquids. The mixing behaviour of present configuration was examined by simulation and then fostered experimentally. In this study, by increasing Reynolds number three flow regimes such as vortex regime, stratified regime, and engulfment regime were distincted. The results exhibited that high mixing quality was obtained at a low Reynolds number in case of constructal tree-shaped configuration.

Ansari, M. A. et al. [2013] studied the modified geometry of square wave bend micromixer to improve mixing quality. The microchannel zone is splited into double layers of same height. The bilayer bends microchannel exhibits improved mixing quality compared to a normal bend microchannel. Also, bilayer bend microchannel shows creation of various vortices at varied locations.

Alam, A. et al. [2014] investigated mixing phenomena in the passive microchannel having number of various cylindrical obstacles inside a curved micromixer. Mixing was analyzed by Navier-Stokes equation and Convection-diffusion equation between ethanol and water for Reynolds number range 0.1 to 60. The proposed microchannel exhibits superior mixing quality

than a simple curved microchannel and T-junction microchannel with circular obstacles.

Veldurthi, N. et al. [2015] presented a simulation of mixing process in a cylindrical chamber having the micro-rotor utilizing CFD. The chamber was joined with two inlets and one outlet. Mixing index at various rpm of the micro-rotor was calculated. Also, simulations were performed for various locations of micro-rotor. Mixing index value of 90% was obtained at 1500 rpm when the position of the micro-rotor was on the summit of the chamber.

Chen, X. et al. [2016] analyzed species mixing quality of three structures namely zig-zag, multi-wave, and square-wave. In this research, blue ink and yellow ink were taken as working fluids and Reynolds number limits vary from 0.1 to 100. The mixing quality decreases in Reynolds number limit 0.1 to 1 and increases in Reynolds number limit 1 to 100. All three structures exhibit identical mixing quality at Re = 0.1 as well as 100. The outcomes exhibit that square wave microchannel is more efficient than multi-wave and zig-zag micromixers.

Chen, X. & Shen, J. [2016] investigated the pressure drop and mixing quality of two 3-D microchannels first is a stacking E-form microchannel (SESM) and the second is a folding E-form microchannel (FESM). Both geometries contain chaotic advection and split and recombination mechanism. The outcomes exhibit that as long as Reynolds number enhances, the pressure downfall and mixing quality enhances. FESM shows enhance mixing performance than SESM for Reynolds numbers greater than and equal to 30. Furthermore, mixing efficiency has achieved 95% at Reynolds number equal to 50.

Pradeep, A. et al. [2016] developed a highly efficient passive microchannel with alternatively varying cross-sectional diameter. The mixing quality in microchannels for different configurations was examined and an extreme efficient microchannel was again optimized for best mixing quality. Experimental investigation of simulation outcomes was performed by

injecting coloured solutions via the PDMS microchannels.

Raza, W. et al. [2017] proposed the three-dimensional split and recombine serpentine form to obtain advanced mixing quality at an inferior Reynolds number, even in a short length. The flow and mixing quality was analyzed by an equation of Navier-Stokes and for species transport, equation of convection-diffusion was used in the Reynolds number limit 0.1 to 200. A parametric perusal was carried out utilizing five geometric parameters of microchannel.

Ruijin, W. et al. [2017] designed a novel Baker-based micromixer on the ground of a chaotic mixing concept. In such a micromixer, simulations were performed and compared the results with two split and merging micromixers namely Smale and Helical mixer. The numerical outcomes show that the Baker micromixer is more efficient than Smale and Helical microchannel at low Reynolds numbers.

Gidde, R. R. et al. [2017] offered the planar passive mixer having a square as well as circular mixing chamber located equidistant along the length. For flow and mixing performance analysis, equation of Navier-Stokes as well as equation of convection-diffusion was unriddled through CFD codes. In this study, four performance parameters such as performance index, pumping power, pressure downfall, and mixing index were evaluated for different designs of configurations. The outcomes show that performance index of microchannel with a square chamber is much than microchannel with circular chambers.

Husain, A. et al. [2017] offered a new three-dimensional split and recombination microchannel having offset entrances. Extent of mixing is numerated by mixing index. The effects of various design parameters like depth and width of channel, length, height, and pitch of mixing chamber on mixing efficiency were analyzed. The offered microchannel showed transcendent mixing

quality in a broad limit of Reynolds number.

Wu, J. W. et al. [2018] reported a micromixer which is combination of pulsatile flow and divergent chamber. The testing outcomes exhibit that design works well at high viscosities and high flow rates. At 40 ml/min, the mixing index can achieve 97%. Also, efficient mixing can be obtained at a viscosity ratio of 10.

Khaydarov, V. et al. [2018] monitored flow regimes in micromixers with a chicane mixing geometry. Two effects namely swirling and recirculation were identified by CFD modeling for the convective mixing process. It is observed that a high extent of combination in vortex flow is likened to stratified flow.

Mondal, B. et al. [2018] reported the comparison of mixing quality between serpentine micromixer and raccoon micromixer. In this study, three discontiguous flow dispensations are accredited hanging on factors impacting the mixing index. The outcomes exhibit that raccoon micromixer is more efficient than serpentine micromixer. As well, the pressure downfall in raccoon mixer is higher than serpentine mixer.

He, M. et al. [2019] introduced an overbridged E-shape split and recombination micromixers, to renovate mixing quality in a wide limit of Reynolds numbers. They calibrated numerically mixing quality of six overbridged E-form microchannels through three-dimensional Navier-Stokes equations. The results exhibit that double bridged E-shape micromixer-3 has classic mixing quality of more than 95% in the Reynolds number limit 0.5 to 100.

Xu, J. & Chen, X. [2019] designed Y-shape and T-shape micromixer rely on Murray's Law. They monitored impact of configuration factors and pressure downfall on mixing quality. For Y-shape microchannel, impact of various branch angles like 30°, 60°, and 90° on mixing quality

was examined as well as results exhibit that the 30° Y-shape microchannel has the best mixing quality.

Zare, P. & Talebi, S. [2019] numerically analyzed the mixing process in the microchannel having repeating L-shaped units in 3-D space. Firstly in three-dimensional space, Geometry second and Geometry third are designed by extending Geometry first. Secondly, L-shaped microchannel, 60° V-shaped microchannel, and 90° V-shaped microchannel are examined. It is seen that Geometry first as well as Geometry second execute superior in comparison to Geometry third. Also, an L-shaped microchannel is excess versed than a 60° V-shaped microchannel and a 90° V-shaped microchannel.

Shi, X. et al. [2019] presented six types of mixer models having four varied obstacle shapes round, square, right triangular, and left triangular. It is found that the square obstacles shape is best out of the four obstacles, because of chaotic advection effect generated by the square obstacle mixer is higher than the other three.

Qian, J. Y. et al. [2019] analyzed the pressure downfall and mixing performance of two-phase liquid-liquid mixture in serpentine microchannels. In this work, mixing quality at the pair droplet-creating stage and droplet travelling stage are examined by the VOF method. The outcomes reveal that the shorter dispersed phase fraction and shorter bend curvature exhibit superior mixing quality.

Alijani, H. et al. [2019] investigated experimentally the impacts of curve angle on mixing in three curved serpentine microchannels. Microchannel having fragments with 280° curve angle gives supreme mixing index esteems up to Dean number equal to 60. It is obtained that at Dean number greater than 70, no difference was seen in the performance of microchannels.

Zhang, S. & Chen, X. [2019] studied the process of making micromixer by bonding the PMMA sheets. The mating strength of microchannel is increased by secondary bonding with advanced influence. The impacts on multi-layer and single-layer micromixers are likened to low-influence and high-influence bonding.

Nazari, M. et al. [2019] proposed a new design induced-charge electrokinetic microchannel having a conductive mixing chamber. Square, circular, rhomboid, and triangular armpits are taken to monitor the impacts of mixing chamber configurations. Also likened to one portative surface mixing chamber and two portative surface mixing chamber. The results show that microchannel with a rhomboid mixing chamber having one portative edge and a portative surface provides optimum mixing quality than other cases.

Mondal, B. et al. [2020] proposed and elaborated a rapid procedure for fabrication of micromixer with poly-di-methyl-siloxane. Two wavy mixers raccoon mixer and serpentine mixer are constructed. The overall generation process of micromixer was operated in two steps mainly mold preparation and fabrication.

Shinde, A. B. et al. [2021] reported impact of topological transformations on mixing quality of ethanol and water in split and recombine micromixer having various configurations. Finite Element Method was utilized for simulation inspection. The impact of constriction height, different pillar shapes, and inlet angles on mixing quality was examined. It is observed that U-form pillar split and recombine microchannel exhibited better mixing quality as likened to other configurations.

Mashaei, P.R. et al. [2020] proposed a Non-planar curved microchannel to enhance mixing performance. The geometry consists of four segments arranged in a non-planar way. The impacts of Reynolds number as well as aspect ratio on mixing quality, velocity region, pressure downfall, streamlines, entropy generation, and energy efficiency factor are examined, and compare the results with a simple curved micromixer.

Lobasov, A. S. et al. [2020] investigated mixing quality of fluids in microchannel having a cylindrical section of swirl flow. It is obtained that as long as number of segments rises, mixing quality and pressure drop also increases in Reynolds number 1 to 300.

Shah, I. et al. [2020] proposed three new designs for calculating mixing quality needed for biodiesel preparation. The present task is rooted on the transesterification of ethanol and sunflower oil to extensive on the use of these micromixers for biodiesel synthesis in Reynolds number limit of 0.5 to 100. These designs are combination of split and recombination and cantor fraction structure. It is found that out of these three designs Y-junction with circular-square mixing unit of split and recombine is better than Y-junction with circular mixing extent of split and recombine and Y-junction with square mixing extent of split and recombine.

Jain, S. & Unni, H. N. [2020] reported the experimental and simulation validation of new configurations of micromixers that are destined for biological mixing utilizations. The impact of inserted obstacles was studied to comprehend the impact of channel impetigo on mixing. Mixing quality of different channel configurations was likened and improvement in mixing efficiency was discussed by changing the Reynolds number and Dean number values.

Qamareen, A. et al. [2021] calibrated the impression of aspect ratio on mixing quality in a curved serpentine micromixer having Reynolds number limits from 1 to 210. The aspect ratio of micromixer delineates a prominent preamble in creation of secondary flow. It obtained a higher mixing quality for aspect ratio of 1.5 in Reynolds number limit 50 to 100. For Reynolds numbers greater than 150, all the aspect ratio geometries exhibited good mixing quality because of creation of strong multiple pairs of Dean vortices.

Kouadri, A. et al. [2021] compared four different configurations of passive mixers namely two-layer crossing channels mixer, semicircular serpentine mixer, curved mixer with grooves, and C-shaped mixer. The simulation has performed at inferior Reynolds numbers through ANSYS Fluent to settle the three-dimensional continuity equation, momentum equation, and species transport equation. It is obtained that two-layer crossing channels micromixer has a better mixing index than other micromixers.

Zou, L. et al. [2021] designed a two-dimensional (2D) passive mixer rely on unbalanced convergence-divergence splits and reverse collision recombination. It is found that multiple vortex as well as reverse collisions recombination created a direction of diverted fluid flow as well as enhanced mixing quality in a proposed microchannel.

Mondal, B. et al. [2021] offered a process for creating a serpentine square wave microchannel with PDMS. The fabrication process of microchannel includes the duplet steps first mold preparation and second microchannel fabrication. The mold of microchannel was prepared by wire electric discharge machining as well as after utilizing these molds, a square wave channel of serpentine form was prepared by the soft lithography technique.

2.2.3 Spiral and Helical Micromixer

Scherr, T. et al. [2012] presented a planar microchannel design rely on logarithmic spirals. Mixing quality was analyzed via numerical simulation and microscopy. The proposed design was likened to other planar configurations like Meandering S- mixers and Archimedes spiral. The proposed design provides better mixing performance than other reported planar mixers.

Yang, J. et al. [2013] presented a three-dimensional microchannel that persists two layers of spiral channels overlapped together vertically. To renovate mixing quality, the parameters have been optimized by utilizing CFD code. By optimizing the flow rate the mixing index value of 90% has been obtained.

Ghadami, S. et al. [2017] introduced a new inertial separation technology utilizing spiral micromixer with stair-like cross-section. It is found that in comparison to normal spiral microchannel in which Dean vortices are situated latitudinal, Dean vortices are uniquely situated longitudinally in stair-like cross-section.

Duryodhan, V. S. et al. [2017] studied numerically and experimentally mixing behaviour of spiral microchannel in Reynolds number limit 1 to 468 and Dean number limit from 0.1 to 75. The impact of cross-sectional aspect ratio upon mixing behaviour was studied. It is found that spiral micromixer have supreme aspect ratio outcomes in superior mixing as likened to shorter aspect ratio micromixer.

Balasubramaniam, L. et al. [2017] examined the augmentation of mixing performance in spiral micromixer of several cross-section geometries (trapezoidal, semi-circular, square, and rectangular) and varying hydraulic diameters. The formation of Dean vortices was

experimentally contemplated throughout the micromixer length by confocal microscopy as well as after that likened to simulation results. It is obtained that semi-circular and trapezoidal cross-section microchannel get the highest mixing quality because of their improved swirling strength.

Vatankhah, P. & Shamloo, A. [2018] proposed a spiral micromixer to stimulate chaotic advection as well as improve mixing phenomena. It is found that spiral micromixer is much verseed than straight T junction micromixer. The pressure downfall in spiral microchannel is slightly superior to T junction microchannel. Mixing quality of spiral micromixer enhances by rising the entrance velocity. The initial radius of spiral micromixer also performs a significant preamble in the increasing mixing procedure. The various cross-sectional effects concluded that square cross-section provides a higher mixing index.

Wang, T. et al. [2020] investigated the mass transfer characters in a spiral micro-supported liquid membrane (micro-SLM) device by three-dimensional numerical simulation. In this work, five different mass transfer mechanisms were evaluated and discussed. To segregate amid these mechanisms of mass transfer as well as to create a mechanism zoning map, two dimensionless numbers were explained.

Tokas, S. et al. [2020] proposed a three-dimensional helical passive microchannel and compared the results with a simple T microchannel. Visitation of the mixing quality and flow patterns has been performed utilizing momentum equation, continuity equation, as well as species transport equation having Newtonian and non-Newtonian fluid in the limit of 0.2 to 320 Re as well as the rate of mass flow 0.00005 to 0.091 kg/h, respectively. It was found that TDHM provides superior mixing quality than simple T microchannel at every esteems of Reynolds number and mass flow rates taken in this perusal.

Javed, S. F. & Zunaid, M. [2020] compared the mixing performance and flow behaviour of simple T-form and Helical T-form microchannels with and without nanofluids. The helical T-shape microchannel with nanofluid creates the vortices and induces swirling at a lower Reynolds number as likened to a simple T- shape micromixer. The proposed helical microchannel is more effective in mixing compared to a simple T-shape mixer.

Ngo, I. L. et al. [2020] reported a parametric analysis of mixing quality in the spiral mixer utilizing Finite Element Method. For improving the mixing performance, various parameters like Peclet number, Reynolds number, flow rate ratio, and diffusion coefficient ratio were analyzed. It is obtained that mixing quality of dean flows in spiral micromixer increases with increasing the Reynolds number at a low Peclet number.

Altay, R. et al. [2021] assessed mixing quality of five loop spiral micromixer with elliptical structures having various commencing aspect ratios having altering radius of curvature. The performance of these microchannels was calculated in terms of mixing index. Elliptical spiral micromixer provides mixing index of upto 98% at Reynolds number equal to 20.

Tokas, S. et al. [2021] numerically calibrated performance of a 3-D spiral microchannel, able to fast mixing in small axial length through induction of chaotic advection. The flow behaviour and mixing outcomes were likened to simple T mixer at same axial length. Blood is taken as a working fluid. It is found that simple T micromixer provides poor mixing quality with a rise in blood flow rate while a 3-D spiral micromixer gives better mixing having 97% performance at lowest esteem of blood flow rate.

Prakash, R. et al. [2022] proposed an offset inlets spiral micromixer and likened the results of mixing quality with a simple spiral mixer. An offset entrances spiral mixer gives a superior mixing quality likened to the simple spiral micromixer. For both microchannels, as long as Reynolds number rises pressure drops and mixing quality also rises. The esteem of pressure drop in an offset entrances spiral mixer is more than a simple spiral mixer.

CHAPTER-3

OBJECTIVE OF THE STUDY

3.1 Introduction

The present chapter deals with the research gaps for the current analysis. Based on the research gap research objectives have been formulated.

3.2 Research Gaps

So many researchers have worked on Micromixer with different geometry like T junction microchannel, O micromixer, H micromixer, Spiral micromixer, Curved microchannel, Square wave microchannel, Zig-Zag microchannel, Tear-drop micromixer, chain 1 micromixer, Y-junction micromixer, Multi-wave micromixer, Tree shape micromixer and so on. The intention of these explorations is to find two aims which are supreme mixing index and inferior pressure downfall at varied Reynolds Numbers. Some researchers have also done numerical analysis for several parameters such as fluids properties, inlet velocities, microchannel's cross-sectional sizes, the diffusion coefficient of fluid, as well as mixing angles for investigating their effects on mixing performance. Some researchers have plotted Reynolds number versus inlet velocity, Peclet number versus mean inlet velocity, mixing length versus inlet velocity in mixing channel, and fraction of mass for each species at the entrance and midsection as well as outlet of mixing channel.

Some researchers have proposed obstacle-based passive micromixers. Obstacle structures are

cylindrical obstacles, square and rectangular obstacles, and triangular obstacles as well as Microchannels with patterned Grooves. The simulation result shows that mixing quality rises as the number of obstacles rises.

i) From the literature survey it is found that less research work has been performed in concern of T micromixers with bend mixing channels and offset insertions T-mixer with bend mixing channels.

ii) From the literature review I have found that less work has been done in case of spiral microchannel.

iii) Also it is noticed that no significant work has been made regarding the use of obstacles like spiral shape obstacles, cylindrical obstacles, rectangular obstacles, and triangular obstacles in a spiral microchannel.

iv) Furthermore, from the available literature it is found that less research has been conducted for comparison of different cross-sectional geometry

v) The effect of twisted spiral geometry has also not been explored much.

3.3 Research Objectives

Keeping in view of the intervals in literature, the under-mentioned objectives have been formulated for performing the current research work out.

1) An interpretation of mixing index in T-form unbending and T-form micromixer having bend mixing channel at varied radii.

2) Numerical analysis of mixing quality in T form straight microchannel, offset insertions T form straight microchannel, and offset insertions T junction having bend form mixing channel.

3) Computational analysis of mixing in a spiral microchannel with spiral obstacle and study of parameters like impact of increasing the inlet velocity, impact of microchannel's curvature, impact of channel's cross-section, and impact of distance amid two consecutive turns of spiral microchannel.

4) To obtain the impact of cylindrical obstacles, rectangular obstacles, and triangular obstacles in case of spiral microchannel.

5) Comparison between square section spiral microchannel as well as circular section spiral microchannel.

6) The effect of twisted spiral geometry on mixing phenomena.

3.4 EXPECTED RESEARCH OUTCOME

1) We know that the spiral microchannel is much verseed in comparison to a straight microchannel mixing-wise. Moreover, from the literature review, we have learned that mixing index rises as the number of obstacles rises in case of a straight microchannel. Therefore, a combination of both i.e. spiral microchannel with a number of obstacles could be even more effective.

2) Effective sample preparation for assays and drug delivery.

3.5 Limitations associated with the simulation study

1) A convenient simulation model may be very costly. Simulation often needs a significant amount of computer time and is therefore costlier.

2) It is a trial and error method that may produce different solutions in repeated runs.

3) The difficulty in finding the optimal values increases due to an increase in the number of parameters.

3.6 Assumptions of present study

1) Flow is in a steady state.

2) Fluid viscosity and density will not be changed.

3) Neglect surface tension and gravity.

4) Incompressible Newtonian liquid.

5) No slip boundary condition.

3.7 Potential sources of errors in the results

1) Physical Approximation Error- Physical modelling errors are those due to uncertainty in the formulation of the model and deliberate simplifications of the model.

2) Computer Round-Off Error- Computer round-off errors develop with the representation of floating point numbers on the computer and the accuracy at which numbers are stored.

3) Iterative Convergence Error:- The iterative convergence error exists because the iterative methods used in the simulation must have a stopping point eventually. The error scales to the variation in the solution at the completion of the simulations.

4) Discretization Errors- Discretization errors are those errors that occur from the representation of the governing flow equations and other physical models as algebraic expressions in a discrete domain of space (finite-difference, finite-volume, finite-element) and time. The discrete spatial domain is known as a grid or mesh.

3.8 Challenges in Simulation Study

1) Accuracy of geometry

2) Surface and volume gridding

3) Accuracy of numerical solution

4) Multiple solutions

5) Slowing growth of computing power

6) Accuracy of physical modelling

CHAPTER-4

METHODOLOGY AND MODELING

Numerical methodology to calibrate passive micromixing comprises evolution of flow domain, grid creation, making use of Computational Fluid Dynamics solver to iteratively unriddle the discretized governing equations, as well as ultimately, post-processing of CFD to conceptualize the flow as well as mass transport amid the fluids. Chapter 4 dissertates essential governing partial differential equations that are the Navier-Stokes, continuity, as well as species transport equations to sanction molecular diffusion throughout mixing. The present perusal embrace exploring the character of Newtonian fluid water (liquid-liquid mixing). The conclusive boundary stipulations as well as schemes utilized in CFD solver are also altercated in elaboration in segment 4.4. Segment 4.6 intricates on grid creation incidence and grid-independent test, i.e., collating the outcomes colligation the size of mesh utilized in flow domain. At last, in segment 4.7, the validation of the computational work destined in this handout is proponed.

4.1 Model and Domain Description

T-form unbending as well as T-form with bend turns are displayed in Figure 4.1. Water enters into the micromixer from the right inlet, and water dye enters from the left inlet. The cross-sectional area of the inlet channels is 100 µm x 100 µm, cross-sectional area of mixing channel is 100 µm x 200 µm, inlets channel total length is 800 µm, and length of mixing channel is 3000µm. To compare the T form unbending and T form with bend mixing channel, length in the y-direction is opted identical for both designs. Geometry descriptions for T-junction straight and T-junction with bend turns are given in Table 4.1.

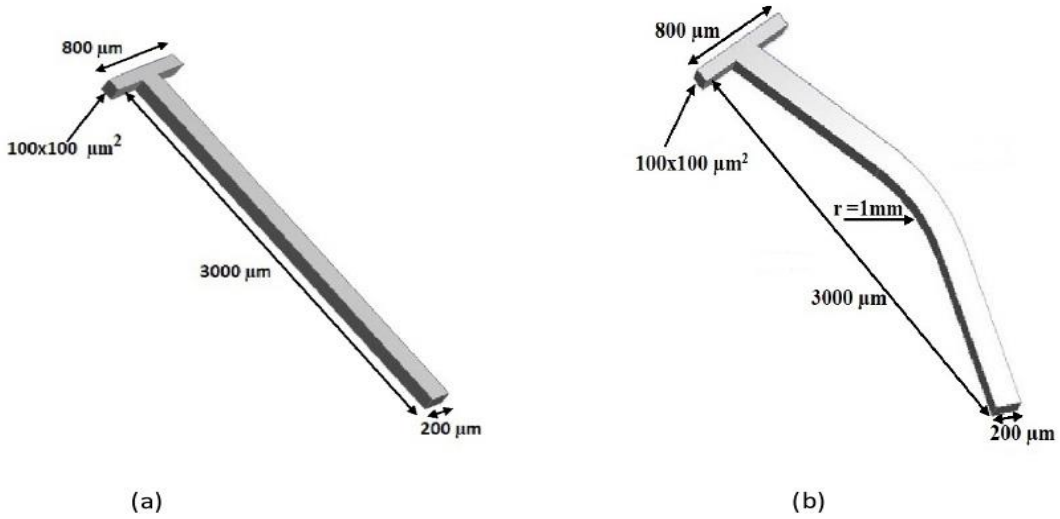

Figure 4.1: Design of T-form microchannel: (a) straight (b) bend turns.

Table 4.1: Geometry description of T-form unbending and T-form with bend turns

Type	T-mixer unbending (All mensuration in µm)	T-mixer with bend turns (All mensuration in µm)
Inlets channel length	800	800
Length of mixing channel	3000	3000
Cross-sectional area of inlets channel	100*100	100*100
Mixing channel cross-sectional area	100*200	100*200

T form unbending, offset insertions T junction, as well as offset insertions T junction with bend turns are exhibited in Figure 4.2. Water-soluble dye and water get into the inlets channel from left and right respectively. For similitude intention, hydraulic diameter of mixing channel as well as inlets channel of these three designs were selected equal. Table 4.2 exhibits the geometry details for all three design.

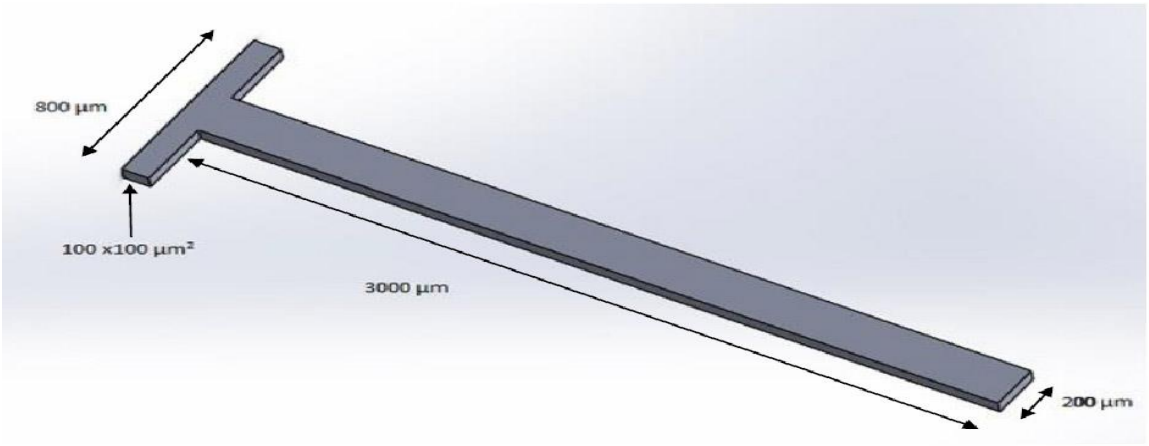

(a)

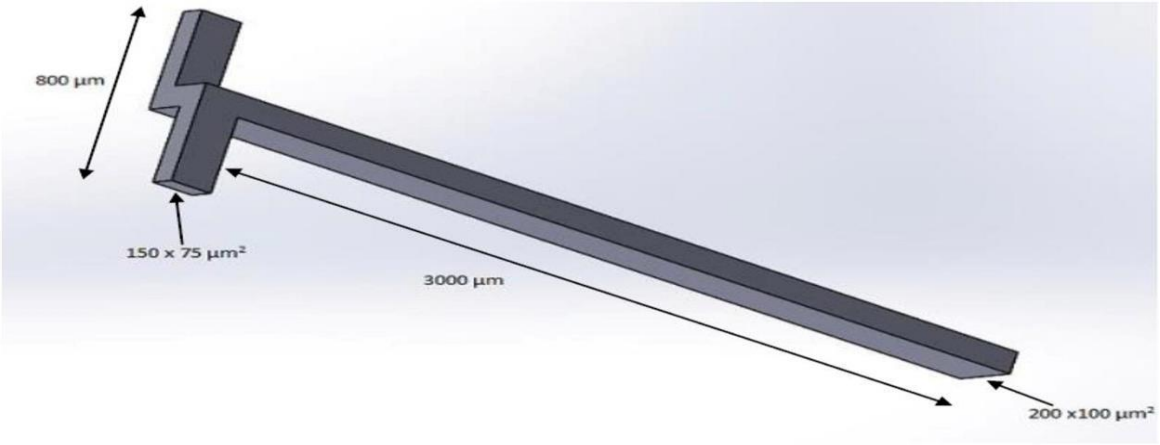

(b)

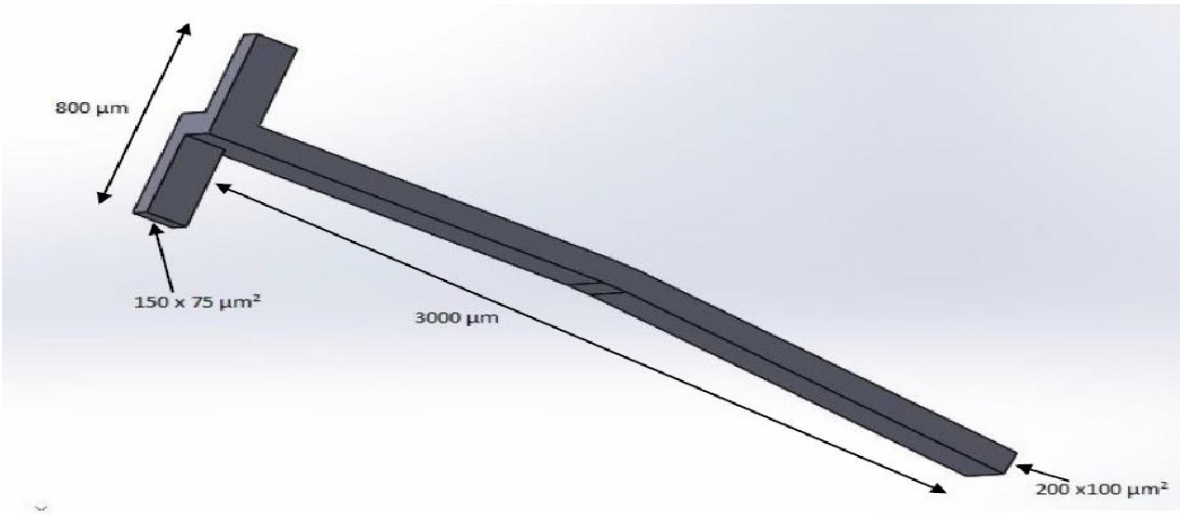

(c)

Figure 4.2: Geometry of micromixer T- design: (a) T form unbending (b) offset insertions T junction (C) offset insertions T junction having bend turns.

Table 4.2: Geometry descriptions of T-form unbending, offset insertions T junction, and offset insertions T-junction having bend turns.

Type	T-form unbending (All mensuration in µm)	offset insertions T junction (All mensuration in µm)	Offset insertions T-junction having bend turns (All mensuration in µm)
Inlets channel length	800	800	800
Length of mixing channel	3000	~3000	~3000
Cross-sectional area of inlets channel	100*100	150*75	150*75
Mixing channel cross-sectional area	100*200	200*100	200*100
Inlets channel hydraulic diameter	100	100	100
Mixing channel hydraulic diameter	400/3	400/3	400/3

The 3-D model of the micromixers is created on SOLIDWORKS. The governing equation is unriddled as well as the flow is simulated in ANSYS Fluent.

A Plane Spiral Micromixer has duplet entrances having a rectangular cross-section of side 100 µm x 200 µm ($\frac{w}{2}$ x h). The mixing channel has a square cross-section having a width (w) and height (h) of 200 µm and 200 µm respectively, the distance amid consecutive turnings (s) is 400 µm, initial channel radius (r_i) is 1mm, mixing channel total length is 15 mm, and number of turns is 2 as displayed in Figure 4.3.

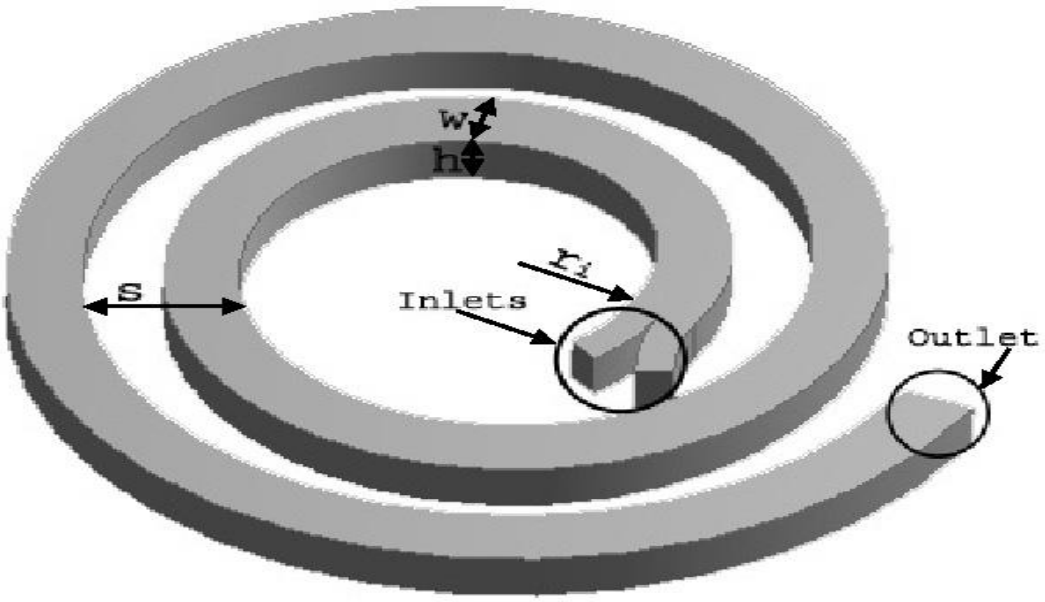

Figure 4.3: A Plane Spiral Micromixer

Figure 4.4 shows a geometric modification of Figure 4.3 after inserting a spiral obstacle having a wire diameter (d) of 0.04mm, mean diameter (D) of 0.15mm, pitch of 0.1mm, and length of a spiral obstacle is 5mm.

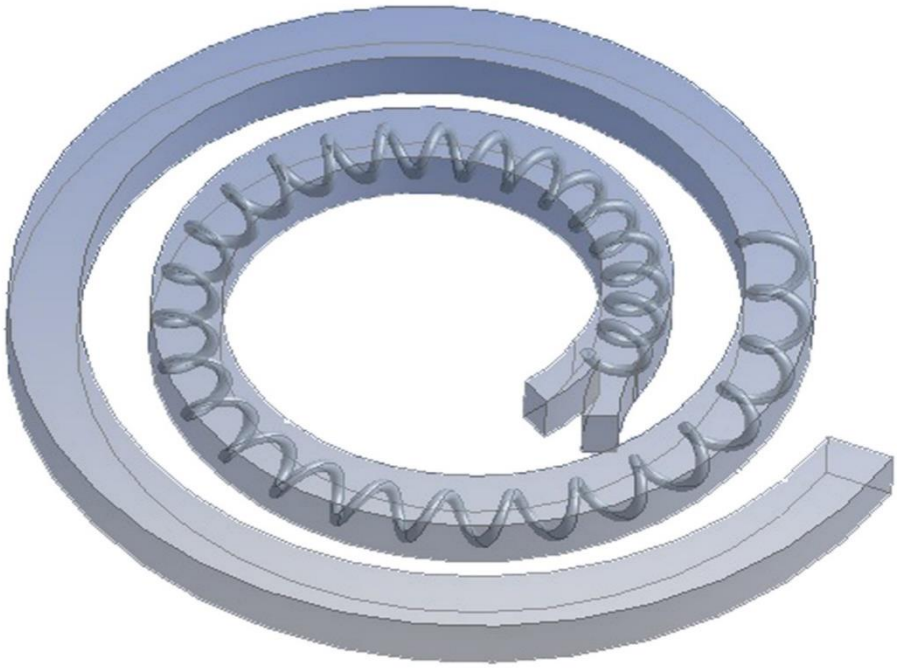

Figure 4.4: A Plane Spiral Micromixer with spiral obstacle

Figure 4.5 exhibits geometric modification of Figure 4.3 when inserting cylindrical obstacles having a diameter of 0.06mm, and height of cylindrical obstacles is 0.18mm. The details dimensions of cylindrical obstacles are shown in Figure 4.6.

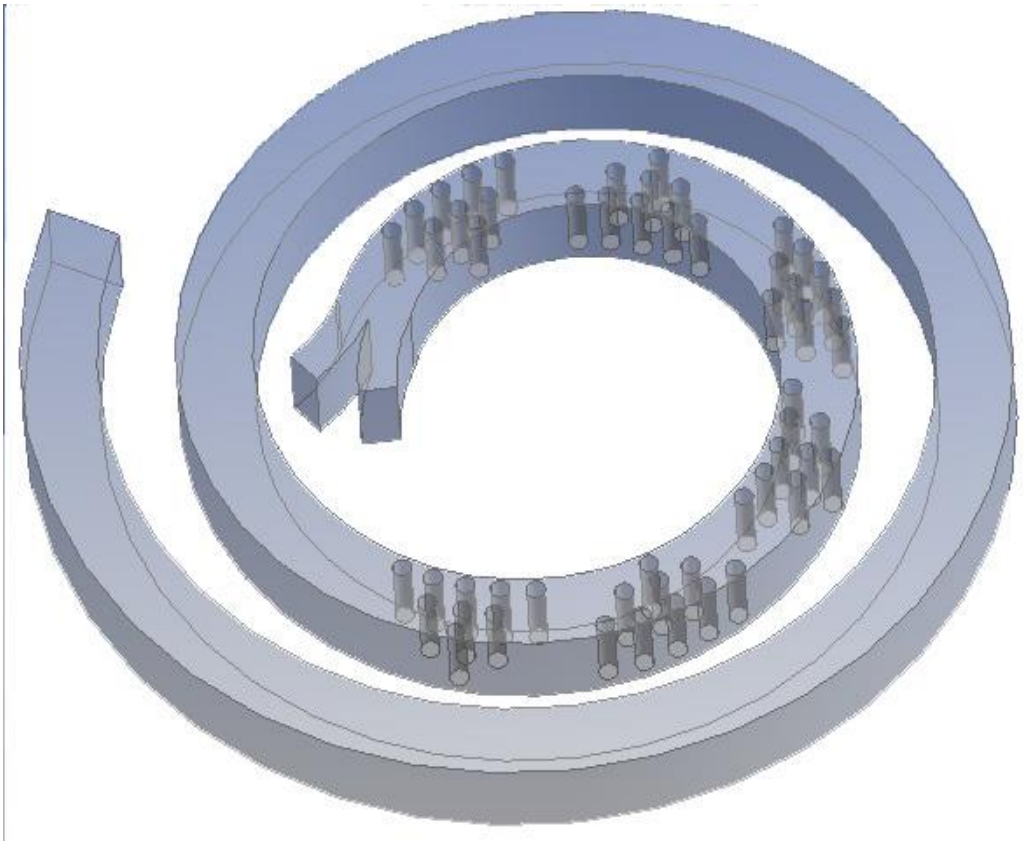

Figure 4.5: A Plane Spiral Micromixer with cylindrical obstacle

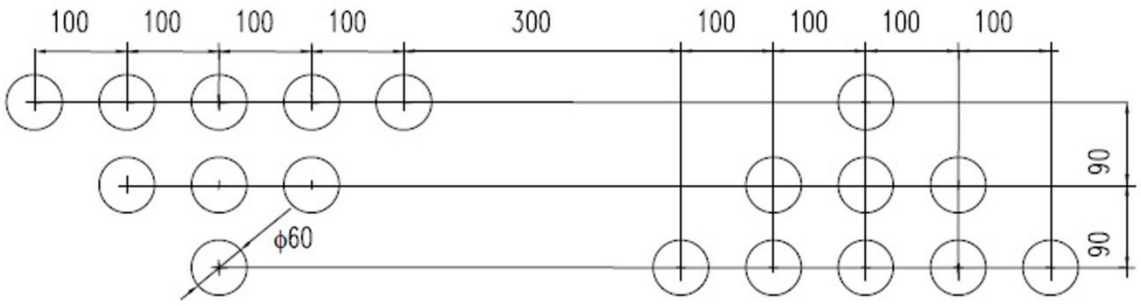

Figure 4.6: Layout of a triangular configuration of cylindrical obstacle array (all dimensions are in µm) [14]

Figure 4.7 exhibits geometric modification of Figure 4.3 when inserting rectangular obstacles with length, width, as well as height are 100 µm, 50 µm, and 180 µm respectively. The rectangular obstacles are placed offset from the centre line. The gap between two successive rectangular obstacles is 200 µm. The clearance between rectangular obstacle and main mixing channel wall is 10 µm.

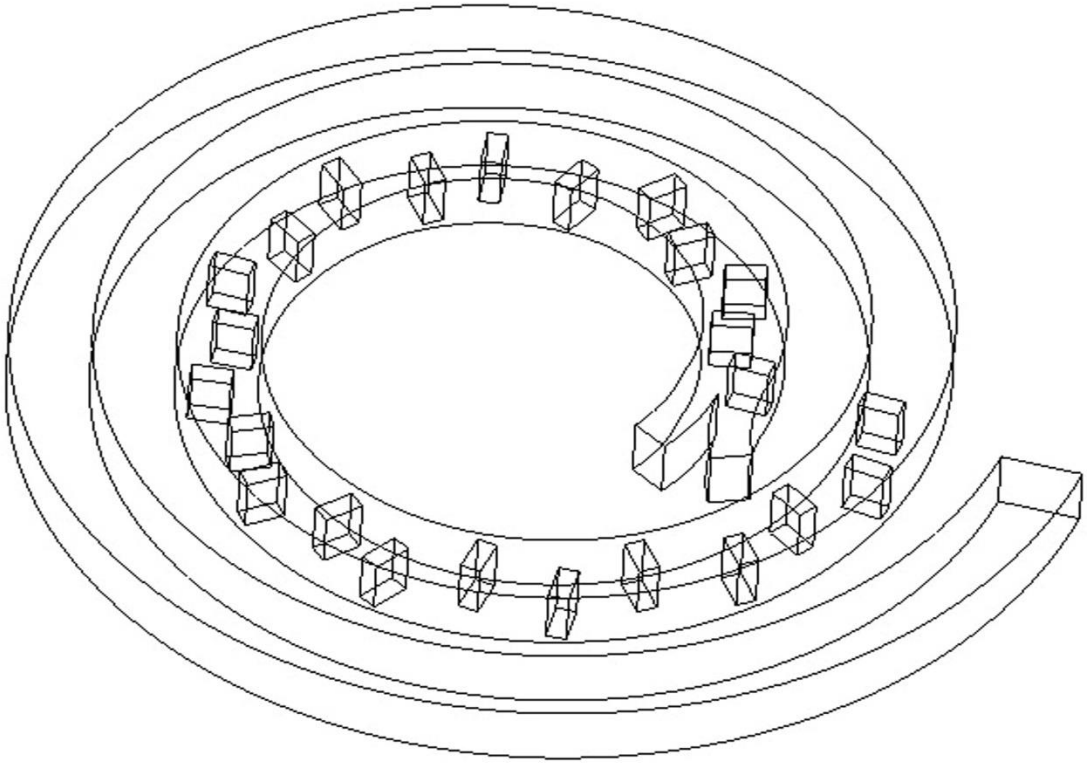

Figure 4.7 A Plane Spiral Micromixer with rectangular obstacle

Figure 4.8 exhibits the geometric modification of Figure 4.3 when inserting triangular obstacles having a base length of 200 µm, width of 200 µm, pitch length of 300 µm, and height of obstacle is 75 µm.

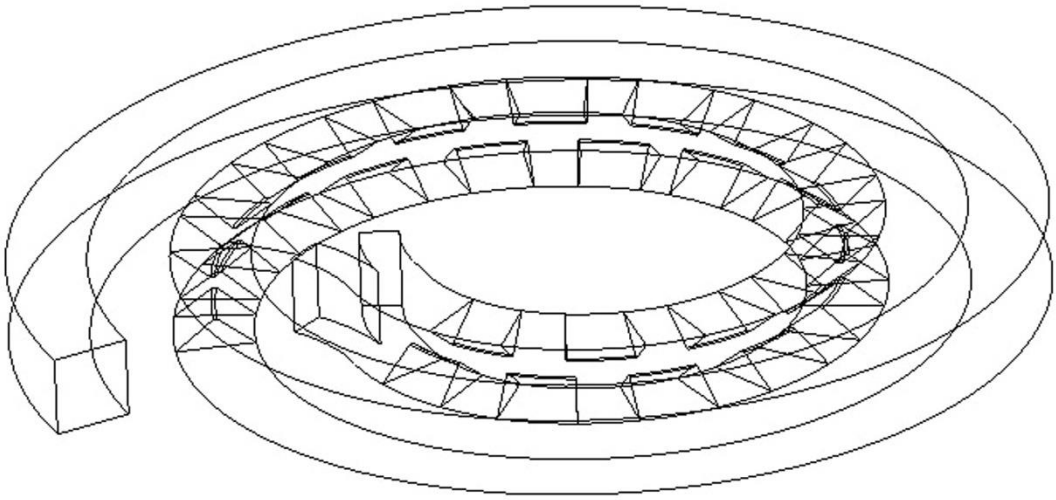

Figure 4.8: A Plane Spiral Micromixer with triangular obstacle

Figure 4.9 shows a circular cross-section micromixer. For the comparison with the square cross-section micromixer as shown in Figure 4.3, hydraulic diameter of the inlets channel and mixing channel of both geometries (circular and square cross-section) was selected as equal. Geometry descriptions for circular cross-section and square cross-section micromixers are given in Table 4.3.

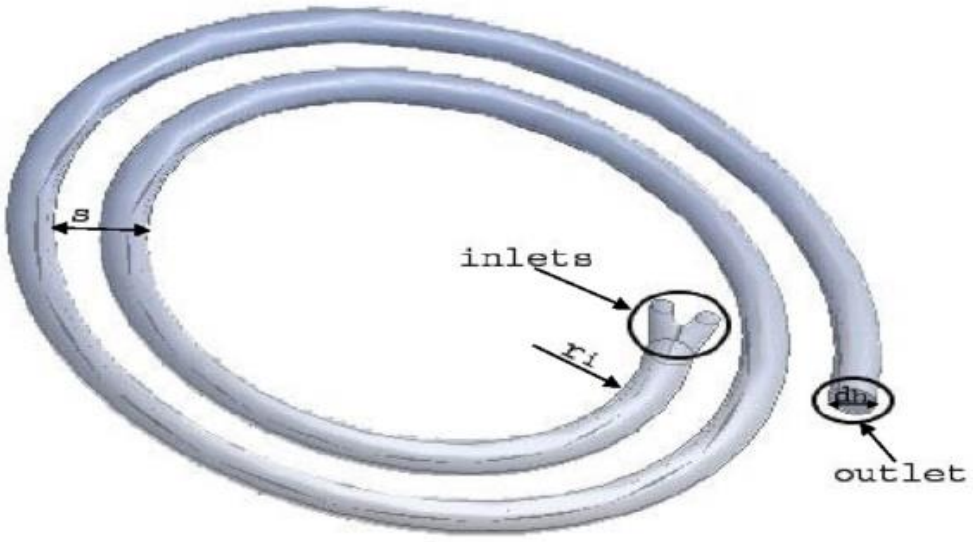

Figure 4.9: A Plane Spiral Micromixer having a circular cross-section

Table 4.3 Geometry description of square section spiral microchannel and circular section spiral microchannel

Type	Square section spiral microchannel (Figure 4.3)	Circular section spiral microchannel (Figure 4.9)
Hydraulic diameter of mixing channel	0.2 mm	0.2 mm
Hydraulic diameter of inlets channel	0.133 mm	0.133 mm
The distance between two successive turnings, s	0.4 mm	0.4 mm
initial microchannel radius, r_i	1 mm	1 mm
Number of turns, N	2	2
The total spiral length	15 mm	15 mm

Figure 4.10 exhibits the geometric modification of Figure 4.3 by twisting the geometry with an angle of 180°. For comparison between plane spiral micromixer and twisted spiral micromixer, length in profile direction is selected identical for both situations (Plane spiral and Twisted spiral micromixer). Geometry descriptions for plane spiral microchannel and twisted spiral microchannel are given in Table 4.4

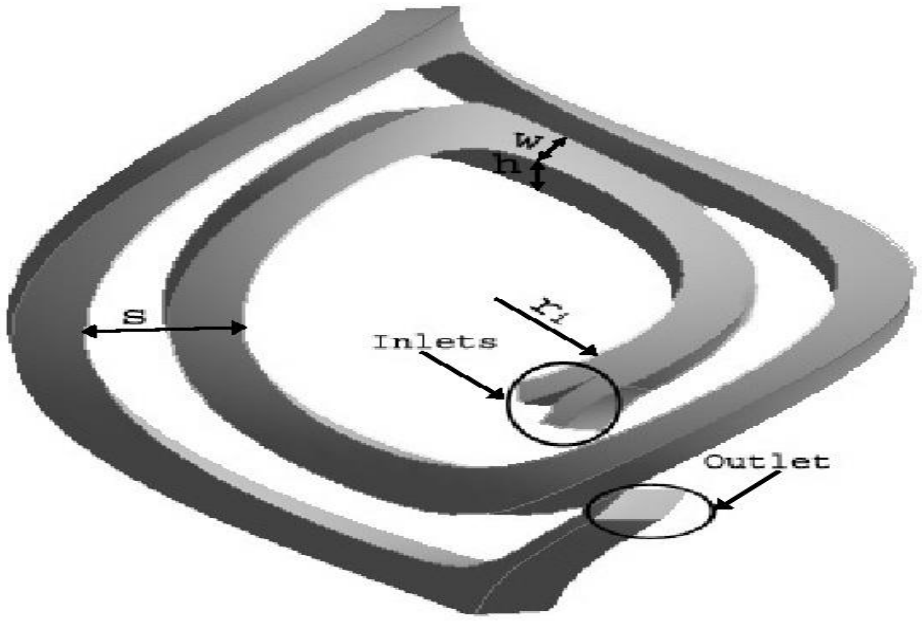

Figure 4.10: A Twisted Spiral Micromixer

Table 4.4: Geometry Descriptions of Plane spiral and Twisted spiral micromixer

Type	Plane spiral micromixer (Figure 4.3)	Twisted spiral micromixer (Figure 4.10)
The cross-sectional area of inlet channels ($\frac{w}{2}$x h)	100 µm x 200 µm	100 µm x 200 µm
The cross-sectional area of mixing channel (w x h)	200 µm x 200 µm	200 µm x 200 µm
The distance between successive turnings, s	400 µm	400 µm
initial channel radius, r_i	1mm	1mm
The mixing channel total length	15 mm	15mm
Number of turns, N	2	2
Angle of twist	-	180º

4.2 The Governing Equations

4.2.1 The Continuity Equation

Continuity equation delineates the circumstance of conservation of mass. The normal continuity equation in differential sculp cartesian coordinates is granted as [Versteeg, H., & Malalasekra, W. 2007].

$$\frac{\partial (\rho)}{\partial t} + \frac{\partial (\rho u)}{\partial x} + \frac{\partial (\rho v)}{\partial y} + \frac{\partial (\rho w)}{\partial z} = 0 \qquad (4.1)$$

Where ρ is liquid density. u, v, and w delineate velocity parts of flow region in x, y, and z directions respectively as well as t denotes time. While equation 4.1 illustrates normal form, it can be simplified due to the conditions prevailing in the experiment and several assumptions. This study deals with liquids that are incompressible fluids which means that the density is constant. Also, since flow is steady, the time derivative terms are removed from the equation. The simplified equation of mass conservation considering the conditions and assumptions stated above is given in equation 4.2.

$$\frac{\partial u}{\partial x} + \frac{\partial v}{\partial y} + \frac{\partial w}{\partial z} = 0 \qquad (4.2)$$

The equation can as well be inscribed in a surrogate style utilizing the del operator delineating the divergence of the velocity vector is granted by equation 4.3.

$$\nabla . \vec{V} = 0 \qquad (4.3)$$

Where-abouts, $\vec{V}$ denotes velocity vector as well as ∇ denotes del operator

$$\nabla = \frac{\partial}{\partial x}\hat{\imath} + \frac{\partial}{\partial y}\hat{\jmath} + \frac{\partial}{\partial z}\hat{k} \qquad (4.4)$$

$$\vec{V} = \mathrm{u}\,\hat{\imath} + \mathrm{v}\,\hat{\jmath} + \mathrm{w}\,\hat{k} \qquad (4.5)$$

The dot product of velocity and ∇ operator is recognized as a divergence of velocity region.

4.2.2 The Navier-Stokes Equations

The Navier-Stokes equations are recognized as a basic fluid dynamics equation as it is germinated from fundamental law of momentum conservation. Present equation contains the body force terms that transact on a differential fluid element when it is located in a magnetic region, electrical region, gravitational region, etc, or conjunction of these as well as surface forces inclusive both shear & normal stresses pullulating because of influence and viscid behaviour of liquid, respectively. The supreme normalized form of equation of momentum is as follows inscribed with the index notation [Versteeg, H., & Malalasekra, W. 2007].

$$\frac{\partial(\rho u_i)}{\partial t} + \frac{\partial(u_i\, u_j)}{\partial x_j} = \frac{\partial(\tau_{ij})}{\partial x_j} + b_i \qquad (4.6)$$

The right-hand side of equation delineates addition of each force working on a fluid element. While, b_i denotes body forces i.e., a force which is working on every single particle of fluid, τ_{ij} denotes stress tensor granted by:

$$\tau_{ij} = -p\delta_{ij} + \lambda\frac{\partial u_k}{\partial x_k}\,\delta_{ij} + \mu\left[\frac{\partial u_i}{\partial x_j} + \frac{\partial u_j}{\partial x_i}\right] \qquad (4.7)$$

Where δ_{ij} denotes Kronecker delta, which values is equal to one as i=j and zero as i≠j. λ denotes volumetric dilation coefficient, μ denotes coefficient of absolute viscosity as well as $\frac{\partial u_k}{\partial x_k}$

signifies the volumetric deformation, whereas $[\frac{\partial u_i}{\partial x_j} + \frac{\partial u_j}{\partial x_i}]$ denotes distortion motived because of shear stresses which work on fluid elements.

Apply in conditions of the experiment and the assumptions taken, equation 4.6 can be inscribed for x, y, as well as z-direction respectively as shown in equations 4.8, 4.9, 4.10.

$$\rho \left(u \frac{\partial u}{\partial x} + v \frac{\partial u}{\partial y} + w \frac{\partial u}{\partial z}\right) = -\frac{\partial p}{\partial x} + \frac{\partial \tau_{xx}}{\partial x} + \frac{\partial \tau_{yx}}{\partial y} + \frac{\partial \tau_{zx}}{\partial z} \quad (4.8)$$

$$\rho \left(u \frac{\partial v}{\partial x} + v \frac{\partial v}{\partial y} + w \frac{\partial v}{\partial z}\right) = -\frac{\partial p}{\partial y} + \frac{\partial \tau_{xy}}{\partial x} + \frac{\partial \tau_{yy}}{\partial y} + \frac{\partial \tau_{zy}}{\partial z} \quad (4.9)$$

$$\rho \left(u \frac{\partial w}{\partial x} + v \frac{\partial w}{\partial y} + w \frac{\partial w}{\partial z}\right) = -\frac{\partial p}{\partial z} + \frac{\partial \tau_{xz}}{\partial x} + \frac{\partial \tau_{yz}}{\partial y} + \frac{\partial \tau_{zz}}{\partial z} \quad (4.10)$$

4.2.3 The Species Transport Equation

The flow at a micro level is utterly laminar, here upon only a doable route by which combination of two fluids can occur via the molecular diffusion by one species to another once they get in the upright connexion. To envision and quantify combination circumstances, the species conservation equation needs to be unriddled in flow domain having rectified enclosure stipulations. Species transport equation in the form of advection-diffusion mode for a steady state condition is granted as follows [Tokas, S. & Zunaid, M. 2020].

$$(\vec{V} . \nabla) C_A = D_{AB} \left[\frac{\partial^2 C_A}{\partial x^2} + \frac{\partial^2 C_A}{\partial y^2} + \frac{\partial^2 C_A}{\partial Z^2}\right] \quad (4.11)$$

Where, Velocity vector,$\vec{V}$, Species A concentration, C_A and coefficient of molecular diffusivity, D_{AB}.

4.3 Newtonian Fluids

As stated by Newton's law of viscosity, at stagnant pressure and temperature, tangential stress (τ) is proportional to rate of tangential stress ($\dot{\gamma}$), as well as the constant of proportionality is called absolute viscosity (μ). It argues that tangential stress rises linearly with a rise in shear rate. Fluids that exhibit this kind of character are known as Newtonian fluids. The majority of fluids which hold inferior molecular weight like several inorganic and organic liquids, water, molten metals, and a broad variation of solutions of salt show Newtonian character when worked upon by shear stress underlying fluid flow. Viscosity of gases verges to rise, with the rise of temperature or pressure because of the augmentation in a molecular collision as long as an outcome of rise in energy is fulfilled of the gas, now those in concern of liquids viscosity reduces with rise in temperature in view of a weakening of attraction force amid molecules impending in liquid. On the absolute, the supreme viscosity of a matter, the much resistance it will show to flow and hereby will demand much energy to pump fluid and carriage it from one destination to another. In this thesis fluid motion in spiral microchannel is recognized to be Newtonian as well as incompressible. Two species of water and water mixed with dye were taken as liquid specimens to be mixed in a spiral microchannel having liquid water characters at 20°C (Water Viscosity, μ = 0.001 Ns/m^2, Water Density, ρ = 1000 kg/m^3, Mixture Diffusion Coefficient, D_i = $10^{-10}\, m^2/s$) for all the simulation. This is the liquid-liquid mixture study. This is the case of the species transport model and the flow is laminar.

4.4 Method of Solution

The flow domain of microchannels is designed utilizing readily accessible Computer-Aided Design modelling SolidWorks software. The modelled domain of flow is after that discretized into degraded elements as well as unriddled numerically utilizing Computational Fluid

Dynamics solver of ANSYS Fluent which plys the Finite Volume Method. Present segment converse about some basic details regarding Computational fluid dynamics, discretization and coupling delineations, enclosure stipulations, as well as characters of fluids utilized to unriddle discretized equations.

4.4.1 Some basic details regarding CFD

The branch of mechanics of fluids which secures a worth effective way of real flow simulation through numerical results of governing equations is called Computational Fluid Dynamics (CFD.). The Navier–Stokes formulation, one of the governing equations for Newtonian Fluid Dynamics has been used for over a hundred years. In spite of this, the advancement of decreased form of these formulations is an active region of exploration, especially the turbulent problem of Re averaged Navier-Stokes formulations. On the contrary in concern of two-phase flows, Non-newtonian fluid dynamics, and chemically reacting flows, principled evolution is at a minor promoted state. In present technique i.e. Computational method, governing differential equations has been substituted by algebraic equations which can be readily unriddled by computers. One of the prime causes for increase and embossing of Computational Fluid Dynamics is steady intensification of computer power since the 1960s. It permitted checking of circumstances that are more rigid or impossible to be evaluated experimentally and are not responsible for analytic solutions. Experimental techniques perform a main preamble in examining and validating ranges of various adjacencies to governing equations, principally rig checkup and wind tunnel hereby procuring a worthy dominant alternative. Analytic rectifications cannot be obtained for many realistic usages because of the ultimate complicacy of flow governing equations. In Computational Fluid Dynamic (CFD) problem, we utilized various codes in accredited ANSYS. In present stipulation, CFD deduce interpellation to interpellation as per source material provided. The technique constraint in uncertainty checking

scale. In utilizing thermal design problems CFD conferred simulation on the different flow techniques according to the problem. CFD cardinal on various problems on several circumstances on grid matters it decoded that fluid flow stipulation in a microchannel. It is remarked the fragment of analytic interpretation delineates the stipulation of fluid flow.

4.4.1.1 Usages of CFD

- **Aerospace**

  Several techniques of CFD are utilized in different usages (flow around an aircraft etc.) related to aerospace for the role of predicting part effectiveness.

- **Automobile**

  In the zone of automobile usage, CFD is utilized for modeling the car's aerodynamics to decrease drag in various operating stipulations and as well in other fields like engine components, auxiliary systems, etc.

- **Field of biomedical**

  Computational Fluid Dynamics is utilized to delineate and simulation of flow of blood in heart aid systems, inhalers, and flow in the heart vessels.

- **Chemical Engineering**

  Usages of Computational Fluid Dynamics in the zone of chemical engineering are massive and overplus as waste treatment recycling, food processing, fertilizers, pollution control, petrochemicals, etc.

- **Energy Engendering**

  In the zone of energy sector Computational Fluid Dynamics detects usages in an inspection of pulverized coal combustion, superheaters, low NOx burner design, and economizer, and in different zones to enhance efficiency and performance of plant.

- **Electronic Devices**

  The different thermal defiances combated by constitutes highlight the rising usages for actual and inexpensive computational draft tools to overbear intricate thermal problems delineated by their cooling. This is the thermal investigation of electronic devices by thermal management solution (TMC).

4.4.1.2 Procedure of Computational Fluid Dynamics

- Split the fluid volume (surface) up into controllable fragments (gridding)
- An equation to be made simple at demanded prerequisite.
- boundary stipulation should be imbed
- Initialization of grid esteems
- Make a simple equation via step grid at the demanded set point.

4.4.1.3 Advantages

In Computational Fluid Dynamics procedure there are under-mentioned benefits carried out. It dominates the several step procedure however it is fully effective for 3-D volume. The creation process takes a short time as time takes manually served processes.

- Computational Fluid Dynamics procedure reduces cost and time also.
- Difficult and dangerous problems can be analyzed by CFD technique.
- CFD method proposes to explore a problem in the competency of range in over its range.
- Factual immeasurable in a scale of elaboration.
- To explore outcomes draw different plots for validation of the outcome in diverse intentions utilized.
- For the nice outcome, simplification has been convenient in the manner of procedure.
- Various unfinished models to delineate multiphase, turbulence, and more difficult

problems.

4.4.1.4 Disadvantages

- Convenient to and low expenditure conduct to over marketing.
- In the beginning, expense was conferred via the setup much as par data.

4.4.1.5 CFD Code

Computational Fluid Dynamics code utilizes various classes in several usages. The utilization of these codes can enforce in the creation tool which is an accessory in Computational Fluid Dynamics explication.

- **Computational Fluid Dynamics commercial code**

  FLUIDYN, CFX, FLUENT, CFDESIGN, STAR CD, etc.

- **Computational Fluid Dynamics research code**

  CFDSHIP IOWA, COOLFLUID, etc.

- **Computational Fluid Dynamics public code**

  HYDRO, WINPIPED, etc.

- **Another Computational Fluid Dynamics codes**

  Other Codes used in creation software like GAMBIT and grid visualization like Hyper View ETC, FIELDVIEW, ENSIGHT, COMSO, ADINAAUI CFX-Post.

4.4.1.6 Computational Fluid Dynamics Procedure

- The intention of CFD is utilize to code enforcement in different usages like isolated bubbly flow via domain.
- In the usage, we see unsteady flow, massive flow, and uniform flow. In the tattles which confer conjoint assortment rate in code employ.

- Regarding code, we can embed different other usage such that biomedical, Marine, multiphase fluid, etc.
- The flow propensity in several manners judged by code enforces it. This is configuring step in embedding the code.
- It conducts to enforce code as per the step wanted in creation procedure. Throughout process configuration told the next step to conduct. If their discommodity then post the process to embed.

4.4.1.7 Steps

- Design the geometry
- Interpolate the physics
- Create mesh
- Results
- Protocol
- Comment

4.4.2 Coupling and spatial discretization schemes

"Pressure-Based" solver and "steady" model have been used in the current analysis. "Species Transport" models have been used in ANSYS FLUENT and in this case flow is laminar. For pressure-velocity coupling, "SIMPLE" algorithm has been used and for spatial discretization of pressure, momentum and continuity, "second-order upwind" has been selected. The convergence absolute criteria of residual for continuity(x-velocity, y-velocity, z-velocity) and energy were picked as $10^{-8}$and for the species (h_2o) were picked as10^{-10}. Table 4.5 extant a brief of numerical schemes assigned in computational simulations.

Table 4.5 Numerical schemes used for CFD Solutions

Gradient	Least squares cell-based
Pressure-velocity coupling	SIMPLE
Pressure	Second order
Energy	Second order upwind
Momentum	Second order upwind
Species	Third-order MUSCL

The following limitations of Fluent software are:-

- It takes a long time to compute the results.
- The results obtained by this Fluent software need validation with experimental data or previously published data.
- The design modeler of ANSYS-FLUENT is not user-friendly, so make the geometry in Solidworks or Auto CAD software and then import it into ANSYS-FLUENT software.

4.4.3 Boundary Conditions

There are two inlets for spiral micromixers. For Newtonian fluid water, water is fed in entrance 1 with a species concentration of "1" and water dye is fed in entrance 2 with a species concentration of "0". The equal velocity was taken at the inlets. Velocity of the fluids is being calculated using following equation based on Reynolds number, Re [Dundi et al. 2019].

$$Re = \frac{\rho V_m D_h}{\mu} \qquad (4.12)$$

Where, Flow average velocity, V_m , Microchannel Hydraulic diameter, D_h and Fluid Density, ρ.

No-slip prerequisite is enforced on walls of microchannel. Also, the walls are defined to have no mass flux. The 'pressure-outlet' boundary stipulation (a zero-gauge pressure at the outlet) is applied to an outlet of mixing channel.

4.5 Mixing Index Calculation

The mixing efficiency is quantified by a number termed as 'mixing index' (MI). There have been several ways put forward to define MI. The most utilized definition is a variance-based version which is demonstrated as follows [Hossain et al. 2009]:

$$M_i = 1 - \sqrt{\frac{\sigma^2}{\sigma_{max}^2}} \tag{4.13}$$

$$\sigma = \sqrt{\frac{1}{\mathrm{N}} \sum_{\mathrm{i}=0}^{\mathrm{N}} (\mathrm{C_i} - \mathrm{C_{mean}})^2} \tag{4.14}$$

where, σ^2 is variance and σ_{max}^2 represents maximum variance of species concentration. C_i is esteem of mass fraction at 'i' sampling point. C_{mean} is average esteem of fluid mass fraction at a plane pondered for the estimation i.e., the outlet cross-section. To combination embracing two same flows of fluid, the esteem of σ_{max}^2 is numerated to be 0.25. N denotes total sampling points on particular cross-section. MI can range from 0 when there is no mixing, to 100 when the mixing between the fluids is complete.

4.6 Mesh Generation and sensitivity explication

Solution gained from numerical numeration should not be subordinate to the number of grid elements. Hereupon, an optimum grid size is elected to gain enough mesh elements for which the solution is grid independent.

To the precision of outcomes of T micromixer, the impression of enhancing computational grid has been well analyzed. Figure 4.11 exhibits the alteration of mixing quality at an outlet by enhancing mesh elements in million. As viewed in Figure 4.11, mixing index esteem reduces by enhancing the grid cells. The esteem of mixing index happens approximately equal at grid elements 4.5 million and 5 million. There is only a 0.16 % distinction in mixing index esteem at grid elements 4.5 million and 5 million. The identical probations were carried out for the T mixer with bend structure at radius 1mm, 2mm, and 3mm and also for offset entrances T form microchannel as well as offset entrances T form with bend shape mixing channel.

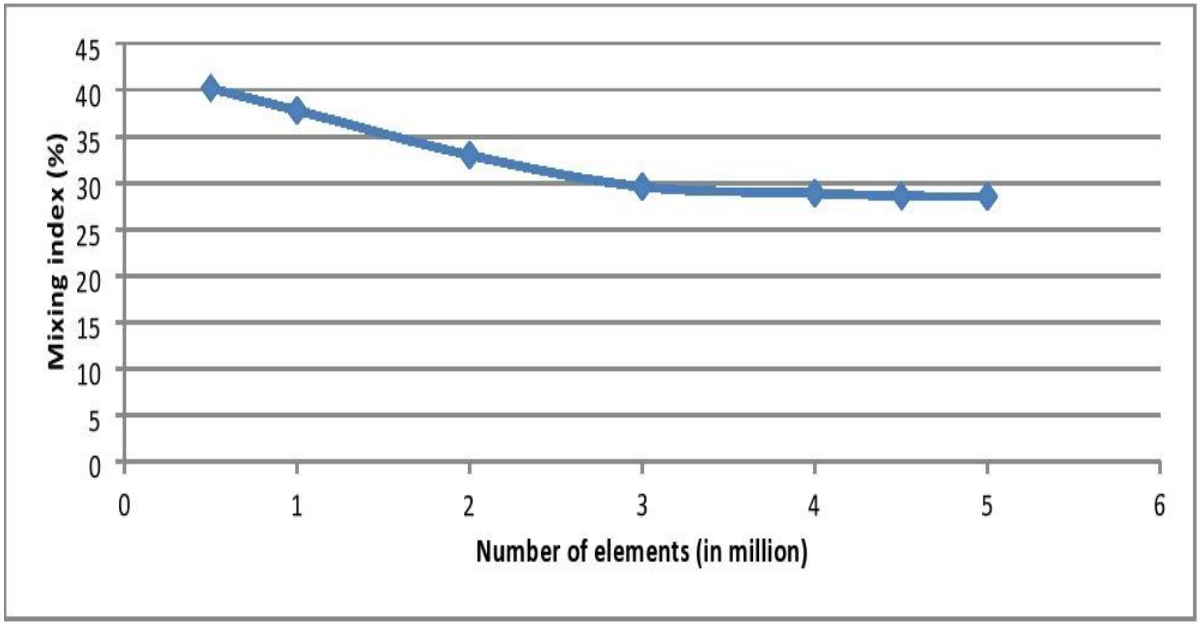

Figure 4.11: Numerated mixing index versus the number of the grid elements.

Figure 4.12, figure 4.13, figure 4.14, figure 4.15, figure 4.16, and figure 4.17 show mesh generation in a spiral with spiral obstacle micromixer, spiral with cylindrical obstacles micromixer, spiral with rectangular obstacles micromixer, spiral with triangular obstacles micromixer, circular cross-section micromixer, and twisted spiral micromixer with tetrahedral grids respectively and Figure 4.18 exhibits that the alteration of mixing quality with increasing the grids in million for plane spiral micromixer. As looked at in a Figure 4.18, as long as the number of grids increases, mixing quality decreases. Afterward, we would approach a point

where the mixing index would not alter with a further rise in the number of grids. At present stipulation, the solution gained is said to be grid independent. But a very high number of elements has the disadvantage of very advanced computational power anticipation. Hereupon, we need to opt for a certain number of elements which is optimized for accessible computational strength and satisfying outcome.

The mixing quality value gets approximately the same at 5.4 million and 6.2 million grids. There is only a significant difference in mixing quality at grids 5.4 million and 6.2 million. So grid with 5.4 million mesh elements is opted and employed for all spiral design simulations. The identical tests were performed for all the spiral designs studied in this thesis.

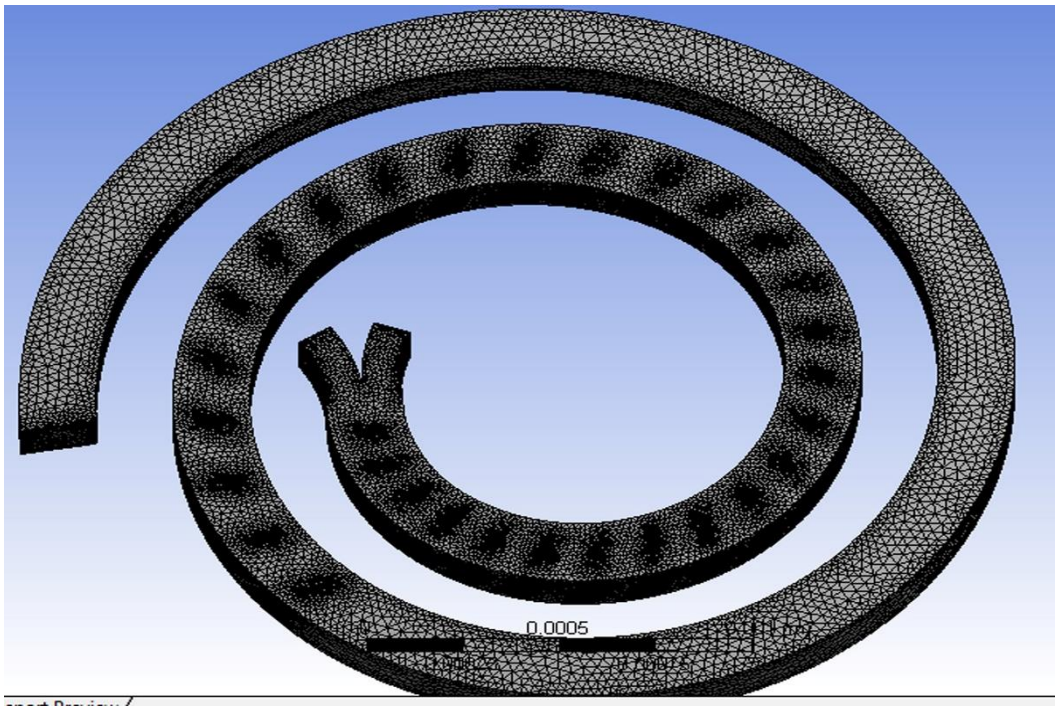

Figure 4.12: Tetrahedral mesh of spiral with spiral obstacle micromixer

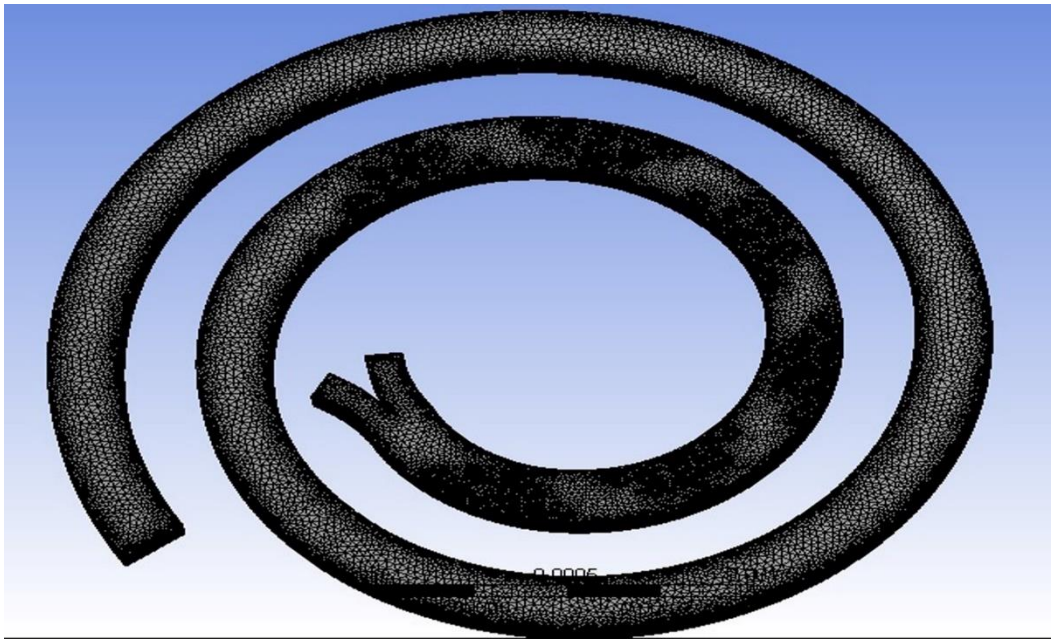

Figure 4.13 Tetrahedral mesh of spiral with cylindrical obstacles micromixer

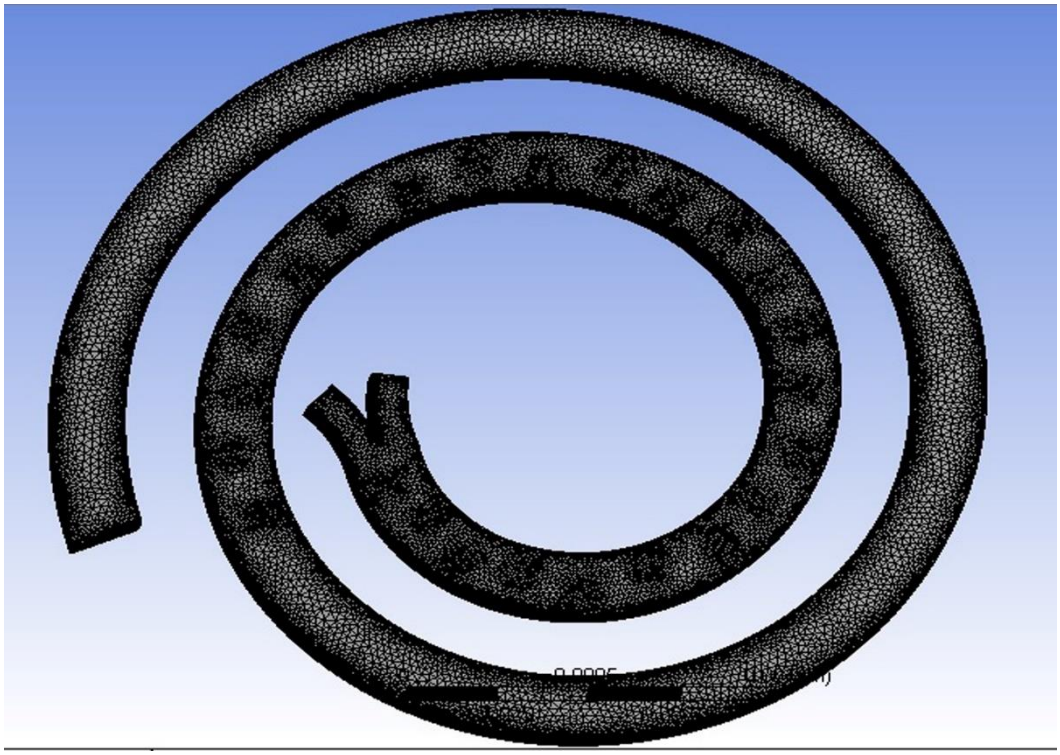

Figure 4.14 Tetrahedral mesh of spiral with rectangular obstacles micromixer

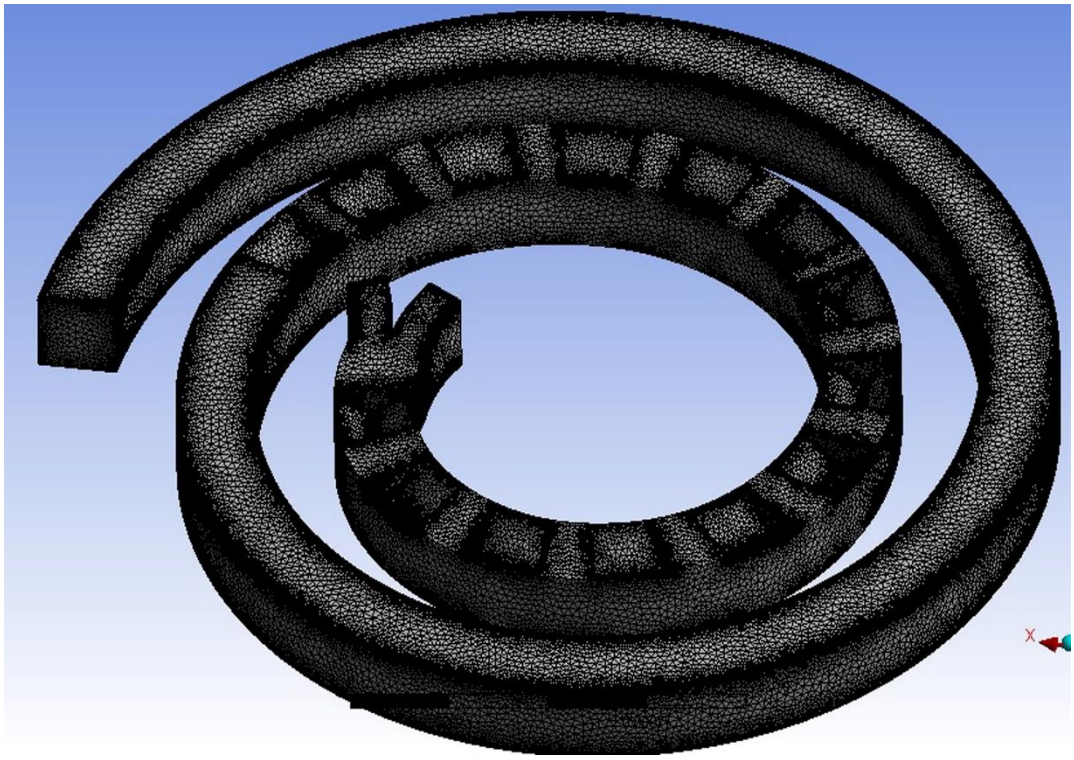

Figure 4.15: Tetrahedral mesh of spiral with triangular obstacles micromixer

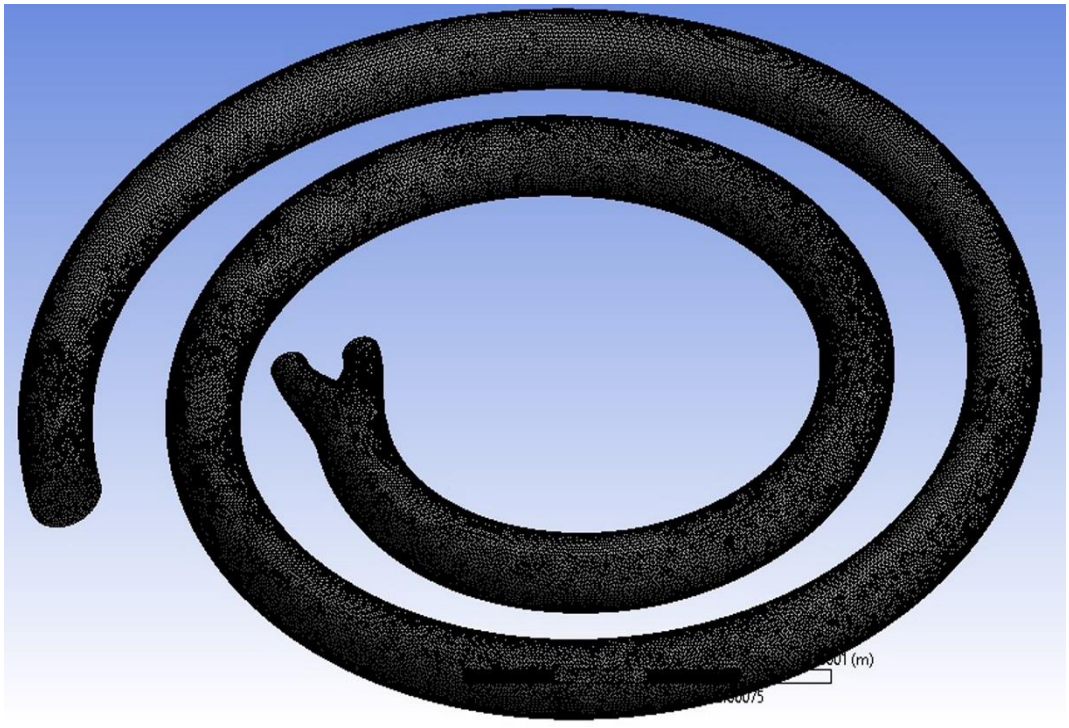

Figure 4.16: Tetrahedral mesh of circular cross-section mixer

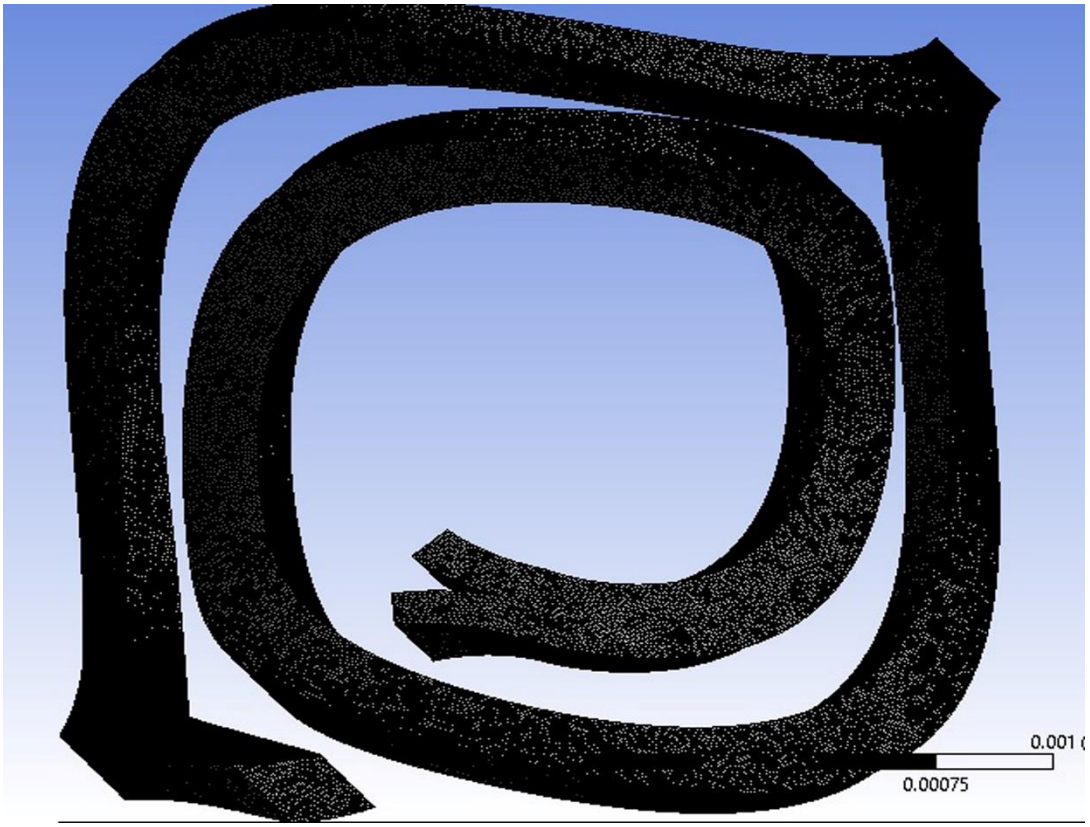

Figure 4.17: Tetrahedral mesh of twisted spiral mixer

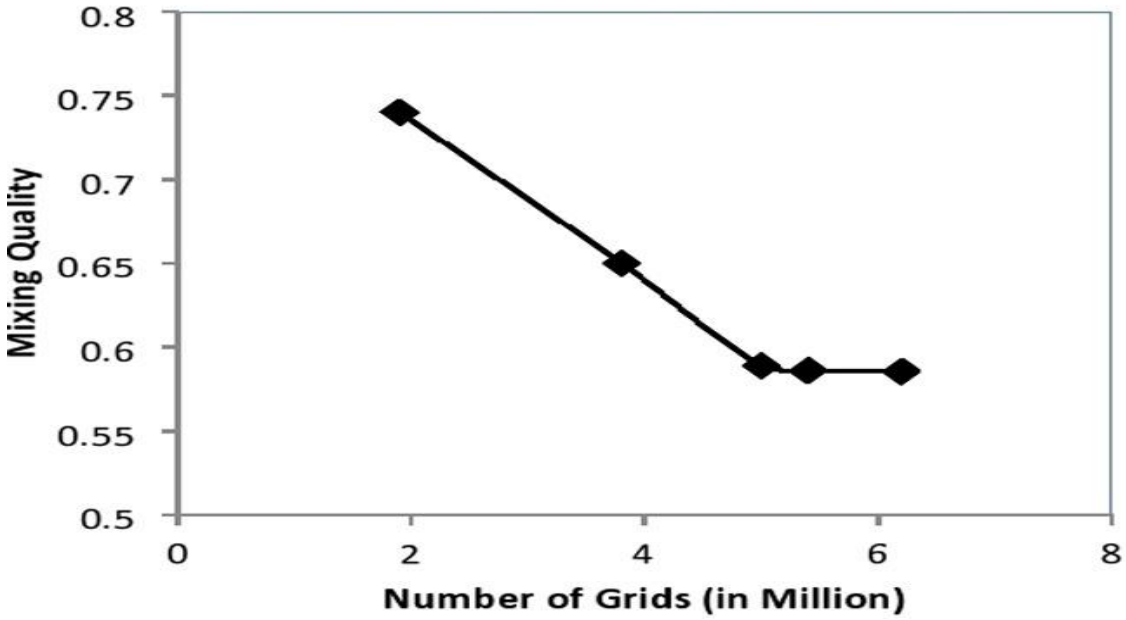

Figure 4.18: Mixing quality versus the number of the grids.

4.7 Endorsement of computational work

Numerical solutions are inclusive of several kinds of imperfections forming solutions suspect on their accuracy as well as hereby validation of computational outcomes achieved is a must with experimental data or with prevailing published research fact. Only one operating fluid that is water (Newtonian fluid) is used in this study, so validation tests are executed to examine the precision of opted approach before proceeding with actual simulations.

In this segment endorsement of a computational task is carried out. Outcomes obtained by current simulation are likened to Dundi et al. (2019). Figure 4.19 displays the similitude of outcomes of the current work and Dundi et al. (2019) outcomes. There is a good agreement between the outcomes of the current work and existing work.

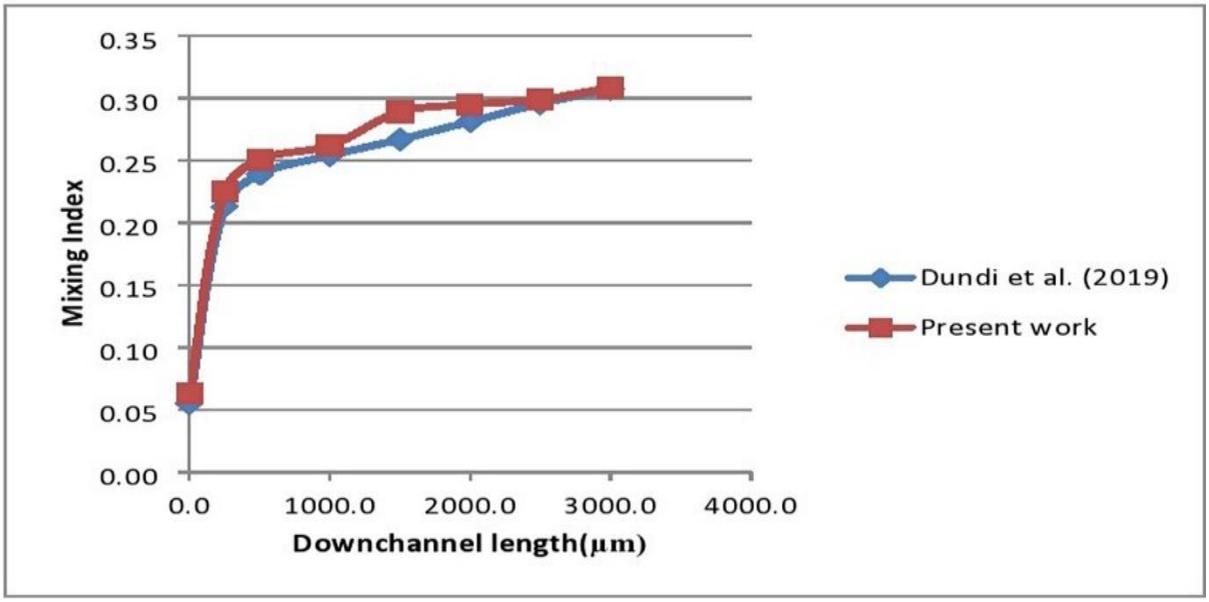

Figure 4.19: Mixing index esteem similitude of current T mixer and existing work with T mixer.

Vatankhah et al. (2018) estimated flow features as well as mixing quality of water (Newtonian fluid) in a plane spiral microchannel of length 15mm. So the outcomes of mixing quality gained from the simulations work performed utilizing identical dimensions as well as the same enclosure stipulations are likened to outcomes proposed by Vatankhah et al. (2018). Figure 4.20 exhibits the similitude of consequences of the extant work and Vatankhah et al. (2018) consequences. The consequences exhibit good agreement between the extant work-study and residing work.

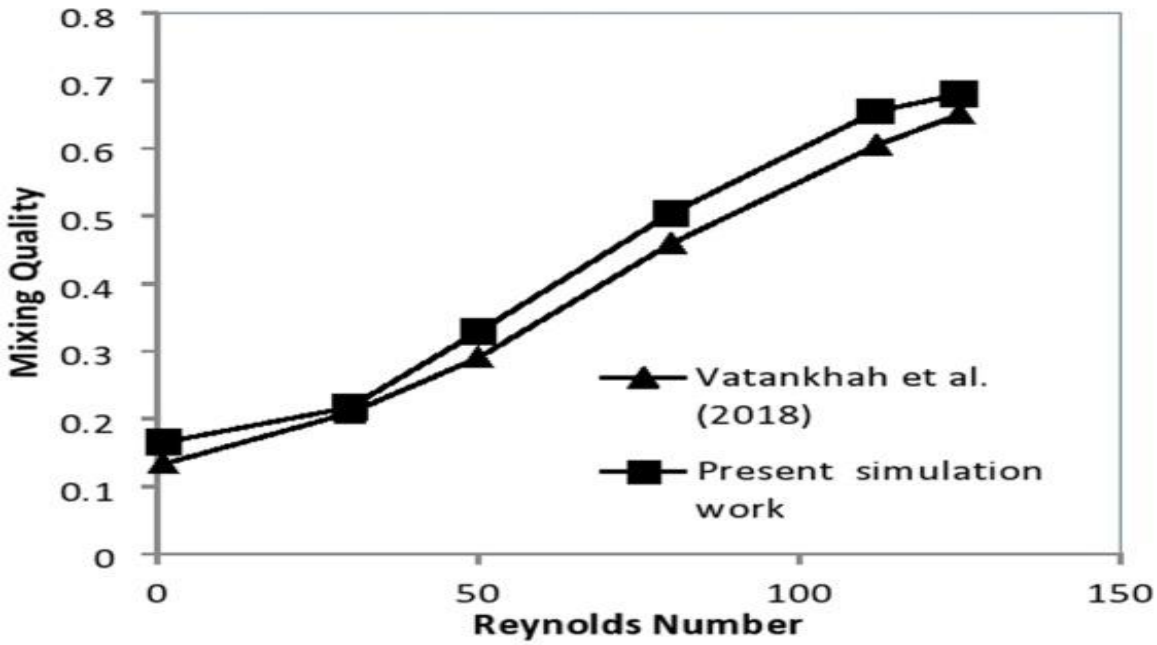

Figure 4.20: Mixing quality similitude of extant plane spiral micromixer and residing work with plane spiral micromixer

For validation of computational work with experimental data, the geometry was taken from the experimental setup of Balasubramaniam et al. (2017). The geometry contains a spiral logarithmic form having a rising curvature radius from 1.5 mm to 6 mm, providing a 75 mm total spiral length and the inlets channel length is 2 mm. The cross-section of microchannel is 600 µm x 600 µm. For grid independence analysis, three grid sizes of 30 lakhs, 66 lakhs, and

81 lakhs were studied. Figure 4.21 exhibits a graph between mixing index and down-channel length for computational simulation versus experimental results of Balasubramaniam et al. (2017). It is viewed in this graph, a good agreement amid computational work and experimental data. The minor difference amid numerated work and experimentally gained mixing index at an outlet of the spiral microchannel.

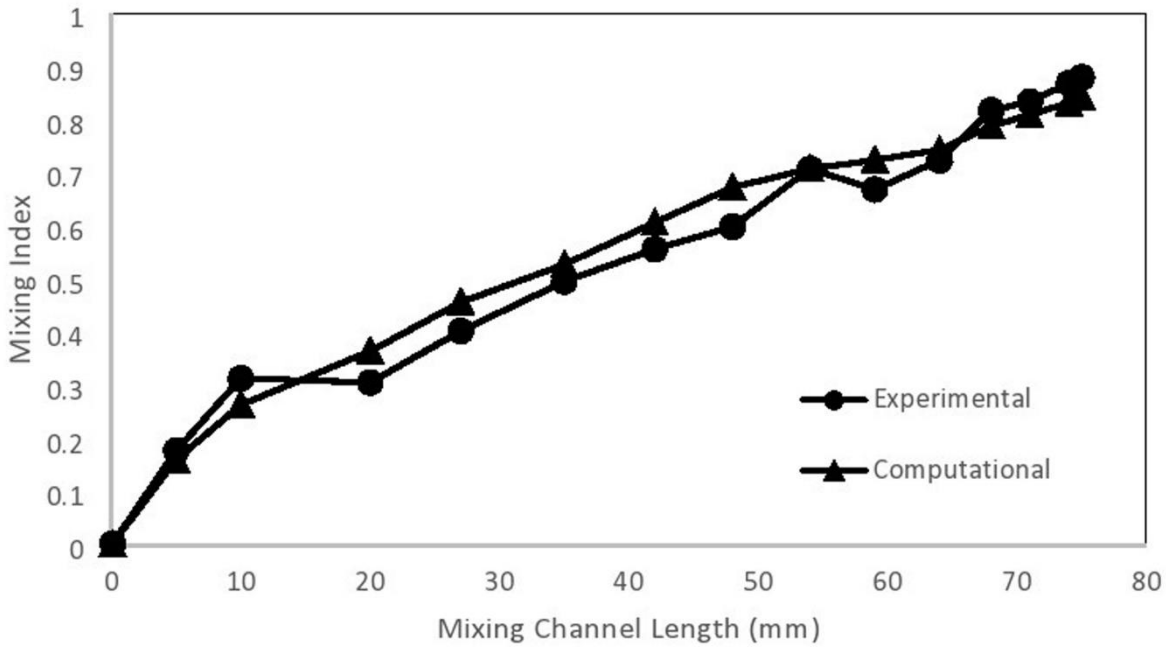

Figure 4.21: Numerated mixing index versus mixing channel length for experimental validation.

CHAPTER-5

RESULTS AND DISCUSSIONS

The present chapter procures a comprehensive deliberation of simulation outcomes gained for Newtonian fluids i.e., water in T-junction Micromixers and Spiral Micromixers. Present chapter is dispensed into six main segments. The first segment gives intimation on mixing performance and flow characterization in the T junction unbending as well as T junction having bend structure. The second section includes numerical results of T form straight microchannel, offset insertions T form straight microchannel, and offset insertions T junction having bend form mixing channel. The third segment gives intimation on mixing efficiency and flow particularization in a plane spiral micromixer and spiral micromixer with spiral obstacle and also the study of parameters like effect of increasing inlet velocity, impact of microchannel's curvature, impact of channel's cross-section, and impact of distance amid two consecutive turns of spiral microchannel with a spiral obstacle. The fourth section includes numerical results of an effect of cylindrical obstacles, rectangular obstacles, and triangular obstacles in case of a spiral microchannel. The fifth section provides a comparison between square section spiral microchannel as well as circular section spiral microchannel. The sixth section includes the effect of twisted spiral geometry on mixing phenomena.

5.1 Mixing and flow analysis in T-junction unbending and T-junction having bend mixing channel.

5.1.1 Effect of design

Fig. 5.1 deciphers the concentration contours of micromixer T form unbending and T form having bend mixing channel, in which bend curvature is explored to be superior to a T junction

unbending. Mixing index at an outlet of micromixer for the bend turns is much (M_i = 0.459) than that of T junction unbending which esteem is (M_i = 0.280). The red and blue colors denote water with dye and pure water respectively. As the color is changed into green showing a mixture.

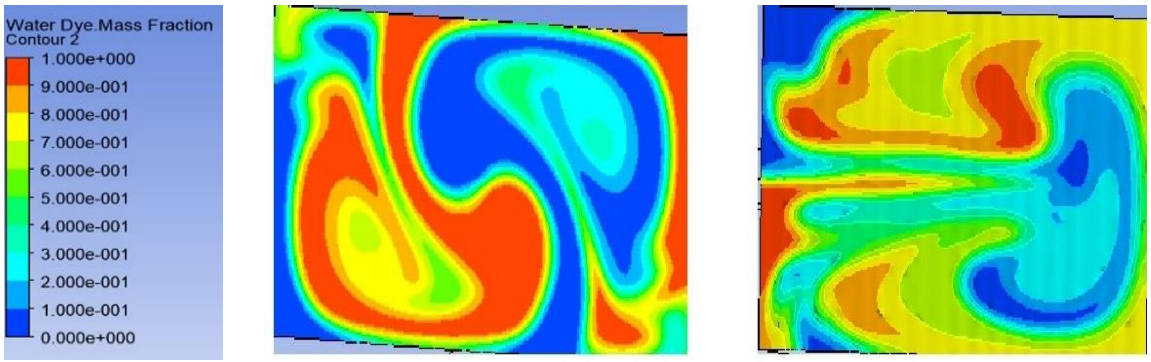

(a) (b)

Figure 5.1: Fraction of mass contours of micromixer T-form at an outlet for (a) T junction unbending (b) bend turns at Re =500.

5.1.2 Effect of Inlet Velocity

The impression of entrance velocity on mixing quality in two cases T junction unbending and T junction having bend turns were analyzed. To this goal, T form unbending and T form with bend turn having identical lengths were simulated at varied Reynolds numbers limiting from 30 to 500. Figure 5.2 exhibits mixing index numeration against Reynolds number for T form unbending and T form with bend turns. As viewed in present graph, mixing index in T form with bend turns micromixer enhances rapidly with enhancing Reynolds numbers.

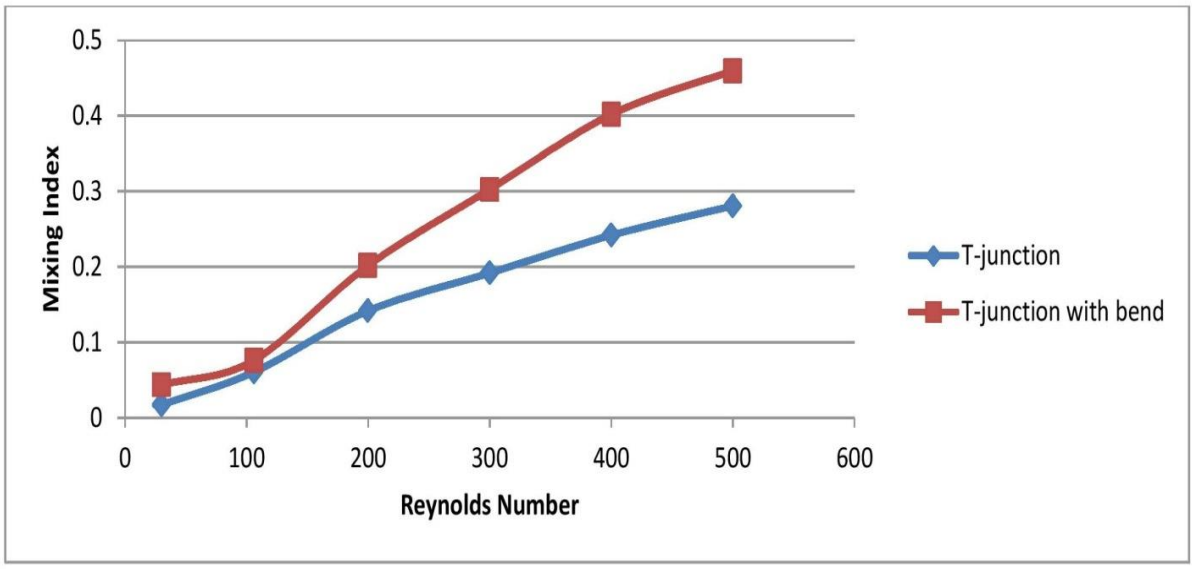

Figure 5.2: Numerated mixing index for the T- junction unbending and T- form with bend turns at various Reynolds numbers.

As altercated aloft that T-form with bend turns is much verseed than T-form uncurving. Because passive microchannels utilize only the liquid pumping power, there is no expectation to utilize any exterior powers; the consumed energy in the system can be revealed by numerated pressure fall. Fig. 5.3 exhibits pressure downfall in T-form uncurving as well as T- form with bend turns at varied Reynolds numbers. As viewed in present graph, the pressure falls in the T- form with bend turns is moderately supreme. Chaotic advection rooted microchannels induce a secondary flow that convictions a high-pressure fall in a microchannel. Ahead, mixing quality for T-form uncurving and T- form with bend turns was numerated across the mixing channel length. Fig.5.4 exhibits mixing index across mixing channel length for T-form uncurving and T-form with bend turns. From the graph, as the mixing channel length enhances, the mixing index also enhances.

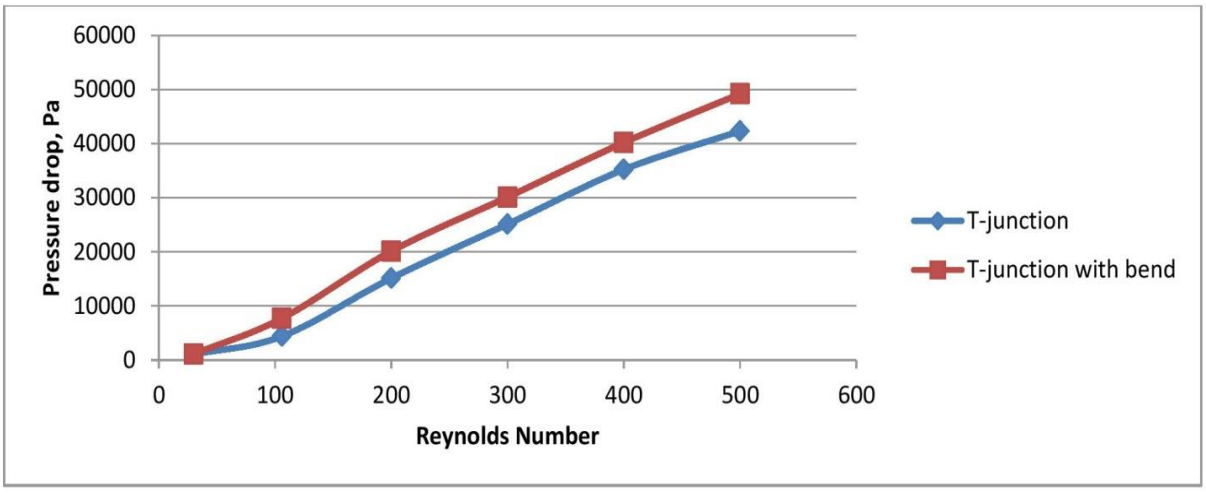

Figure 5.3: Pressure fall in T-form uncurving and T-form with bend turns at various Re.

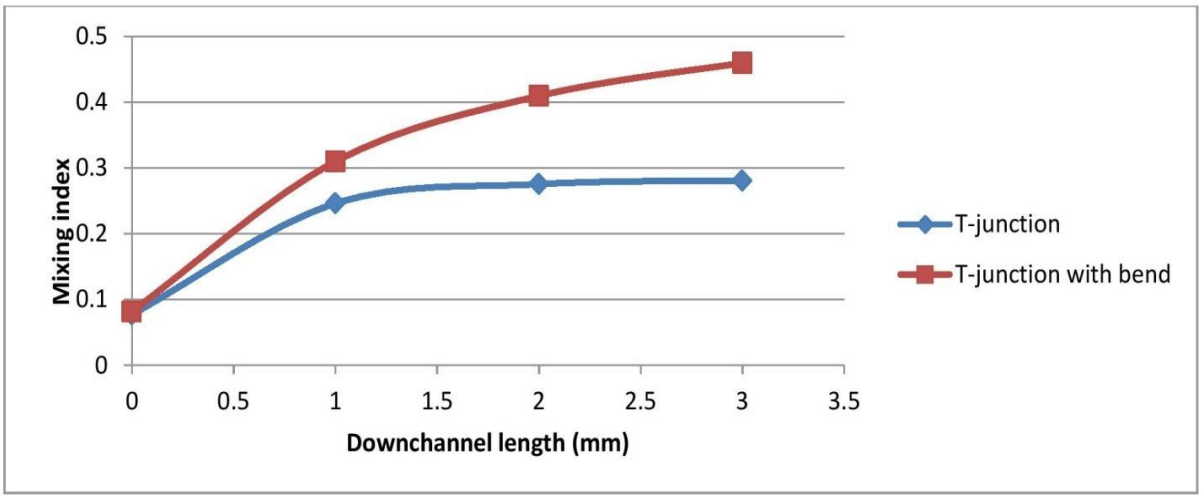

Figure 5.4: Mixing index across the mixing-channel length for the mixtures.

5.1.3 Effect of bend's structure

In this inscription, the impression of bend's turns is analyzed on mixing index of a micro-mixer. To this target, bend turns with identical lengths but having a varied bend radius of 1mm, 2mm, and 3mm were simulated. A chaotic advection mechanism is generated by either fold/bend the flow or inserting obstacles in the way of the flow. Mixing quality increases in chaotic advection based micro-channel at high Reynolds numbers. Creating chaotic advection is one of the most popular ways to increase the interfacial area between the two fluids which accelerates the

mixing process. The numerated mixing index of microchannels is exhibited in Fig.5.5. This graph displays that as the bend radius enhances, mixing index of the microchannel enhances.

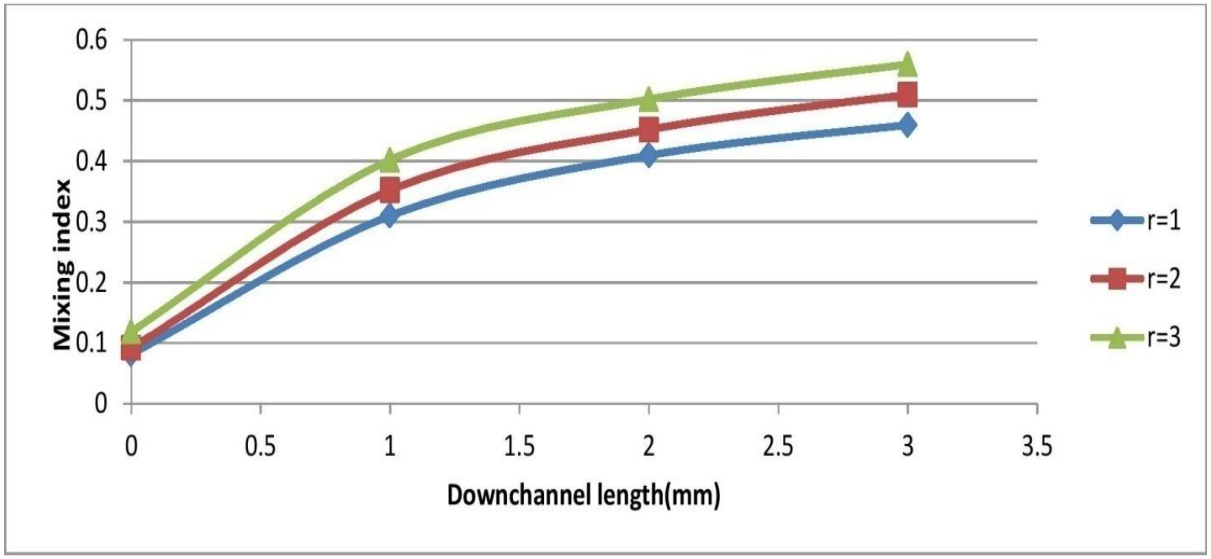

Figure 5.5: Mixing quality of three bend micromixer having varied radius versus mixing-channel length.

5.2 Mixing and flow analysis in T form straight microchannel, offset insertions T form straight microchannel, and offset insertions T junction with bend shape mixing channel.

5.2.1 Impact of geometry

Figure 5.6 exhibits mass fraction contours of T form straight microchannel, offset insertions T form straight microchannel, and offset insertions T junction having bend form, in which offset insertions T junction having bend form is infested to be superior to T form straight microchannel, as well as offset insertions T form straight microchannel. The esteem of mixing index at an outlet for offset insertions T junction having bend form is more advanced (M_i = 0.514) than that of the offset insertions T form straight microchannel (M_i = 0.468) and T form straight microchannel (M_i = 0.280).

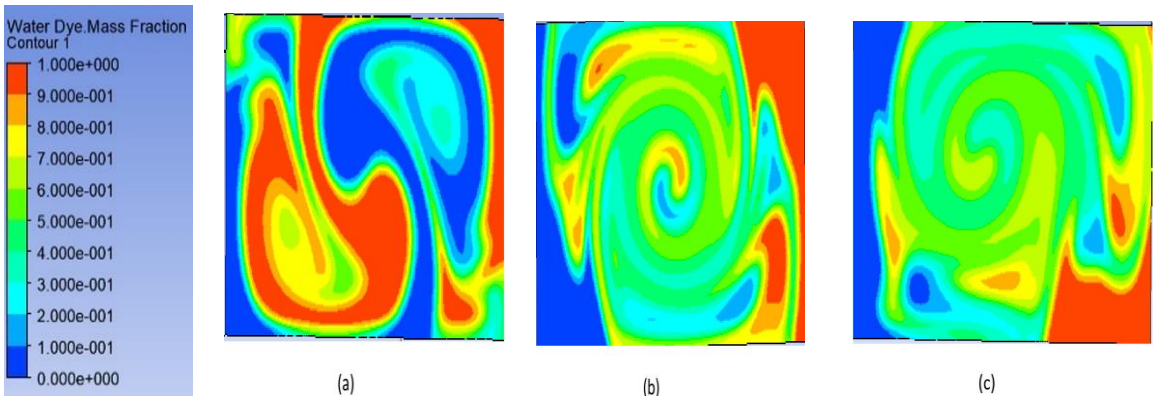

Figure 5.6: Mass fraction contours of T mixer at an outlet for (a) straight (b) offset insertions (c) offset insertions T mixer having bend form at Re =500.

5.2.2 Effect of increasing inlets velocity in terms of Reynolds number

The impression of increasing entrance velocity (Reynolds numbers) on mixing performance in a T form straight microchannel, offset insertions T form straight microchannel, as well as offset insertions T junction having bend form was displayed. To this motive, a T form straight microchannel, offset insertions T form straight microchannel, and offset insertions T junction having bend form keeping the identical down-channel length was simulated at various Reynolds numbers ranging from 30 to 500. Figure 5.7 exhibits mixing index calculation across Reynolds numbers for T form straight microchannel, offset insertions T form straight microchannel, as well as offset insertions T junction having bend form. As displayed in figure 5.7, the mixing index in an offset insertions T junction having bend form enhances sharply with enhancing the Reynolds numbers.

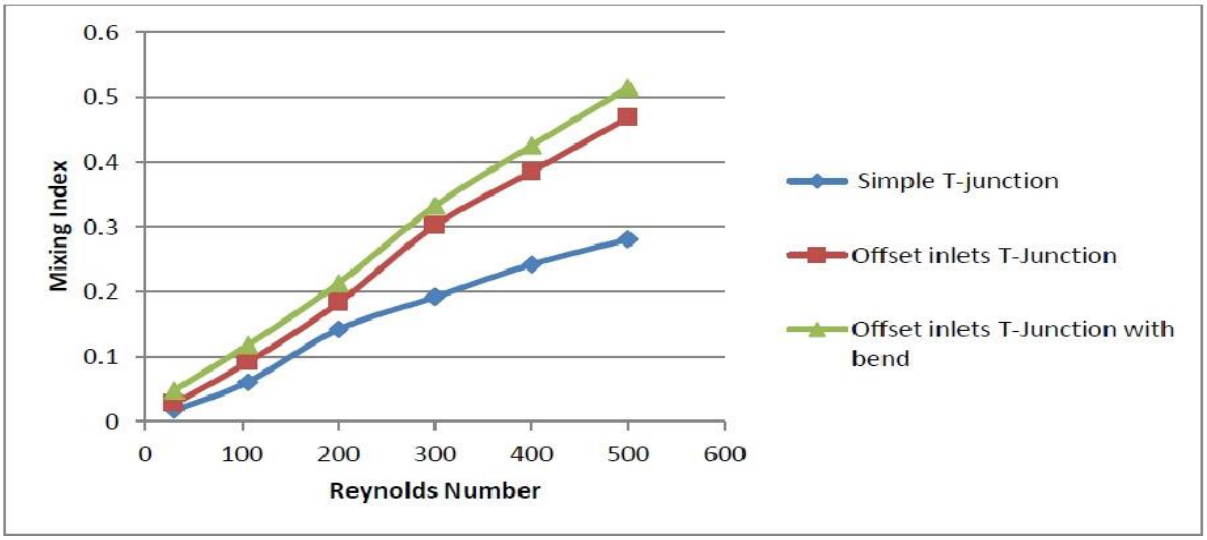

Figure 5.7: Mixing quality for T form straight microchannel, offset insertions T form straight microchannel, as well as offset insertions T form having bend turns at varied Reynolds numbers.

From the aloft outcomes, we perceive that offset insertions T junction having bend form is most efficient than the T form straight microchannel as well as offset insertions T form straight microchannel. In the concern of passive microchannels, we urge only the fluid pumping energy, without any exterior energy; the numerated pressure fall reveals the dissipated energy in the device. Figure 5.8 exhibits pressure downfall in T form straight microchannel, offset insertions T form straight microchannel, as well as offset insertions T junction having bend form at several Reynolds numbers. As exhibited in figure 5.8, pressure drop in offset insertions T mixer having bend form is moderately promoted than the offset insertions T form straight microchannel and T form straight microchannel. Since chaotic advection is generated in microchannels by a turn or inflection of mixing channel, this kind of microchannels cultivates a secondary flow conduct by centrifugal force, which causes a promoted pressure drop in a micromixer. Further, mixing quality for T form straight microchannel, offset insertions T form straight microchannel, and offset insertions T junction having bend form was estimated across the down-channel. Figure 5.9 exhibits mixing quality across mixing channel for T form straight

microchannel, offset insertions T form straight microchannel, and offset insertions T form having bend turns. As viewed in this graph, the mixing index esteem enhances by enhancing the mixing channel length.

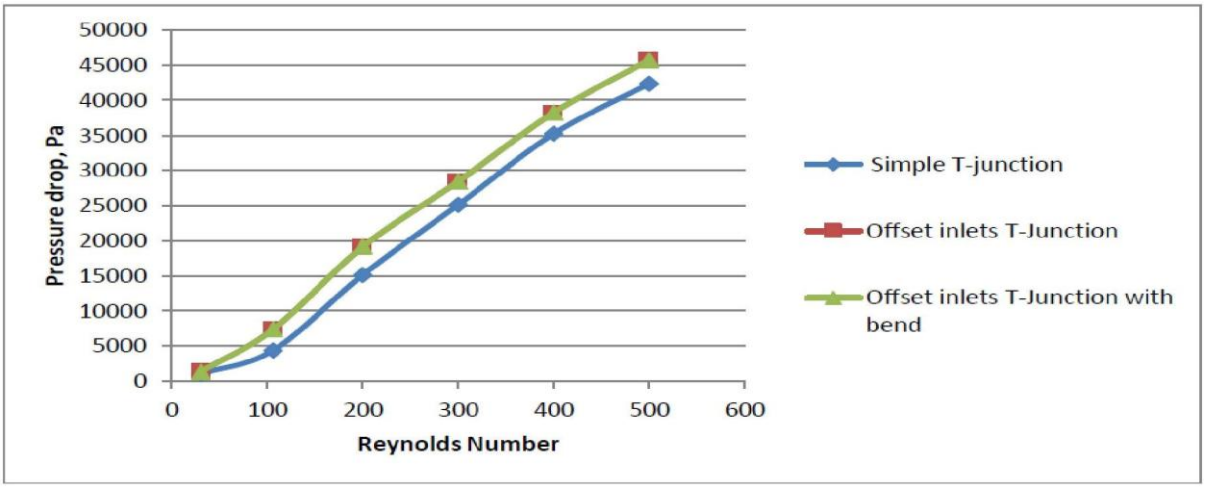

Figure 5.8: Pressure drop esteems in the T form straight microchannel, offset insertions T form straight microchannel as well as offset insertions T form having bend turns at different Re.

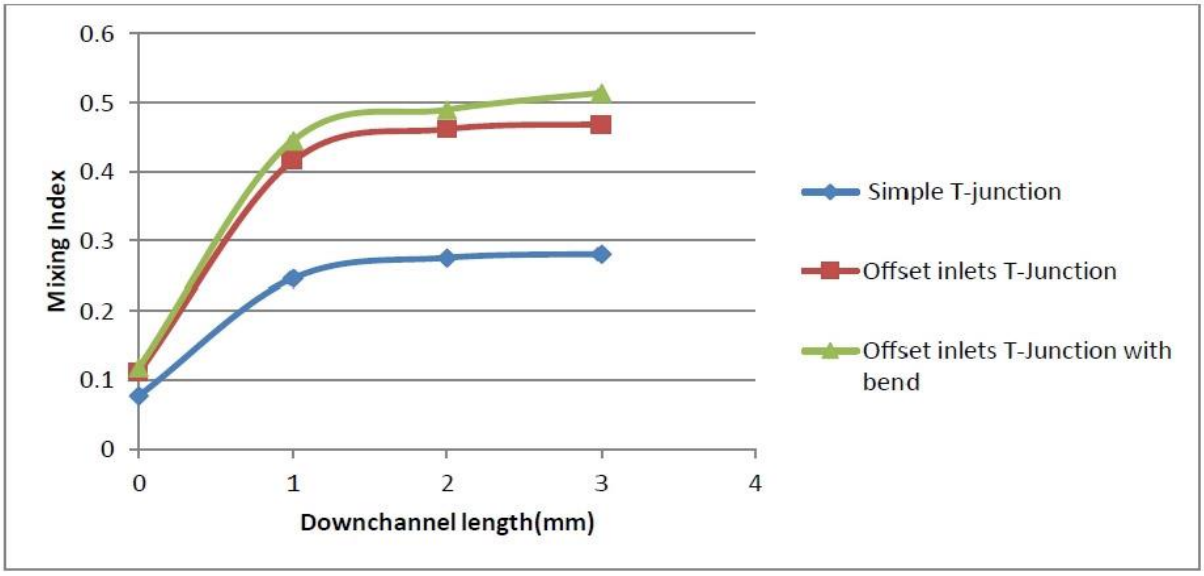

Figure 5.9: Mixing index esteem across down channel length for T form straight microchannel, offset insertions T form straight microchannel, and offset insertions T mixer having bend form mixing channel.

5.3 Mixing and flow analysis in plane spiral micromixer and spiral micromixer with spiral obstacle

As altercated in Chapter 4, length of spiral mixing channel is 15 mm having a cross-sectional area of 200 × 200 μm. The inlet channels on the other hand have a cross-sectional area of 100 × 200 μm. Distance between successive turns (s) is 400 μm, initial channel radius (r_i) is 1mm and the number of turns is 2. The spiral with spiral obstacle having wire diameter (d) 0.04mm, mean diameter (D) 0.15mm, pitch 0.1mm, and length of spiral obstacle is 5mm are analyzed. Flow and mixing behaviour of water and water dye in plane spiral micromixer and spiral micromixer with spiral obstacle are discussed below.

5.3.1 Effect of geometry

The mass fraction contours of plane spiral micromixer and spiral micromixer with spiral obstacle are manifested in Figure 5.10. As manifested in this figure, a spiral micromixer with spiral obstacle is better than a plane spiral micromixer. Mixing index value at an outlet of spiral micromixer with a spiral obstacle is much (M_i = 0.994) than that of the plane spiral micromixer whose value is (M_i = 0.684) at the Reynolds number 80.

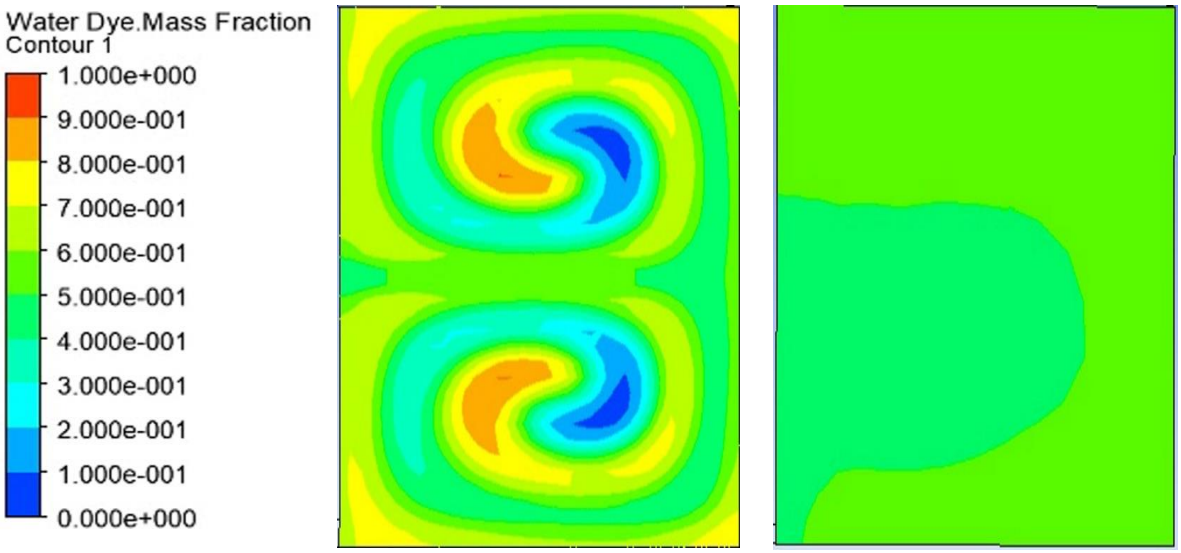

(a) (b)

Fig.5.10 Mass fraction contours of micromixer at an outlet for (a) plane spiral (b) plane spiral with a spiral obstacle at Re = 80.

Figure 5.11 manifests a contour of mass fraction along the spiral length at a central plane in plane spiral micromixer and spiral micromixer spiral obstacle. The red color reveals the first species (water) and the blue color reveals the second species (water dye). When the color is changed into green characterizes a mixture.

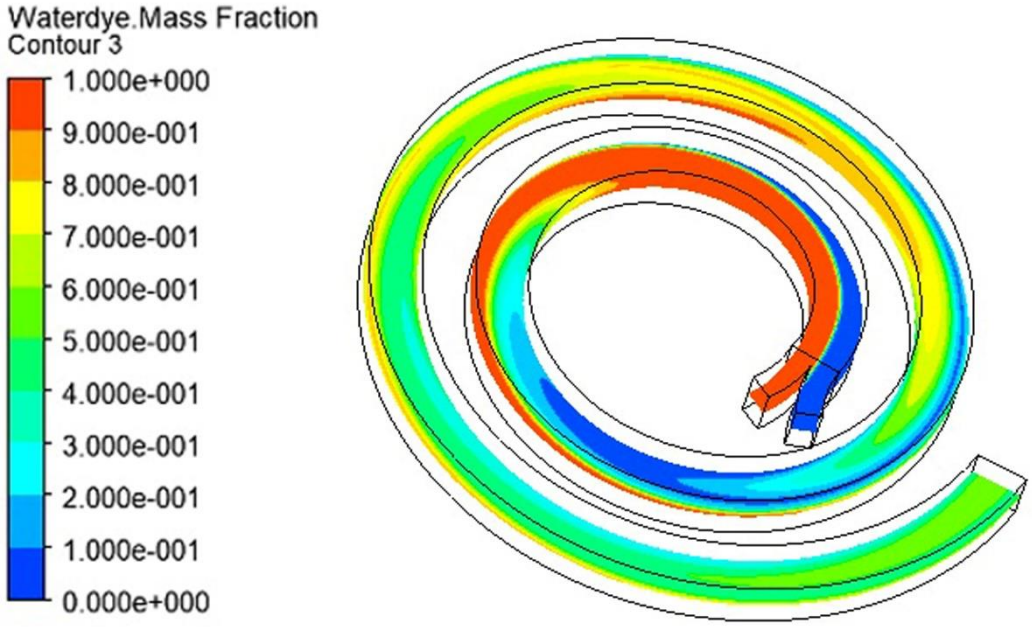

(a)

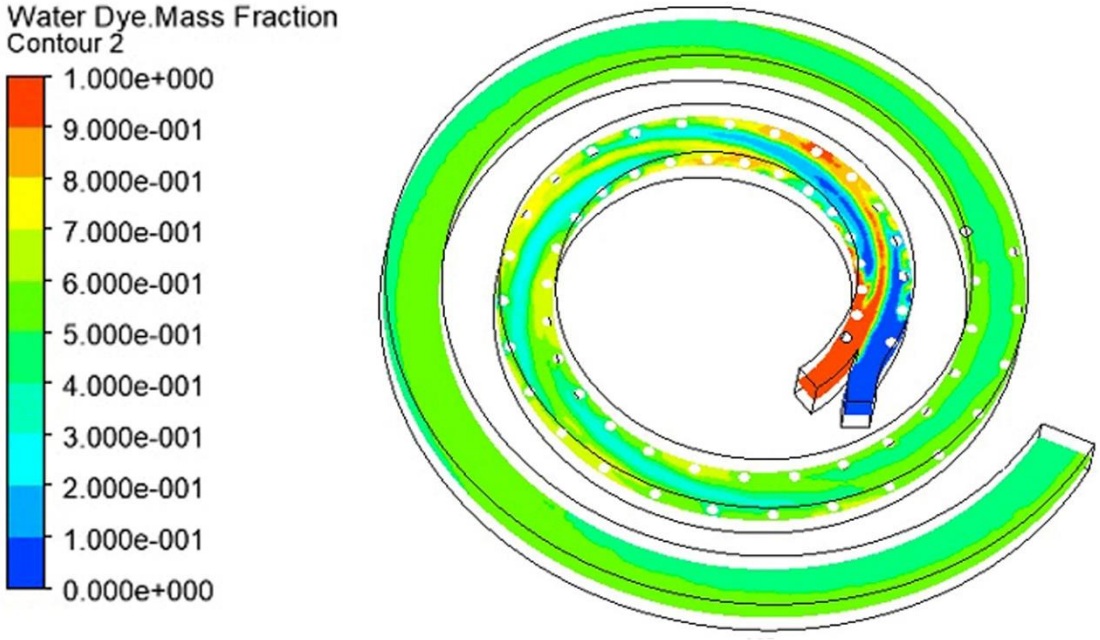

(b)

Fig.5.11 Contour of mass fraction across the spiral length at the central plane for (a) plane spiral (b) plane spiral with a spiral obstacle at Re = 80.

The streamlines rely on the fraction of mass throughout the spiral length in plane spiral micromixer and spiral micromixer with spiral obstacle are exhibited in figure 5.12.

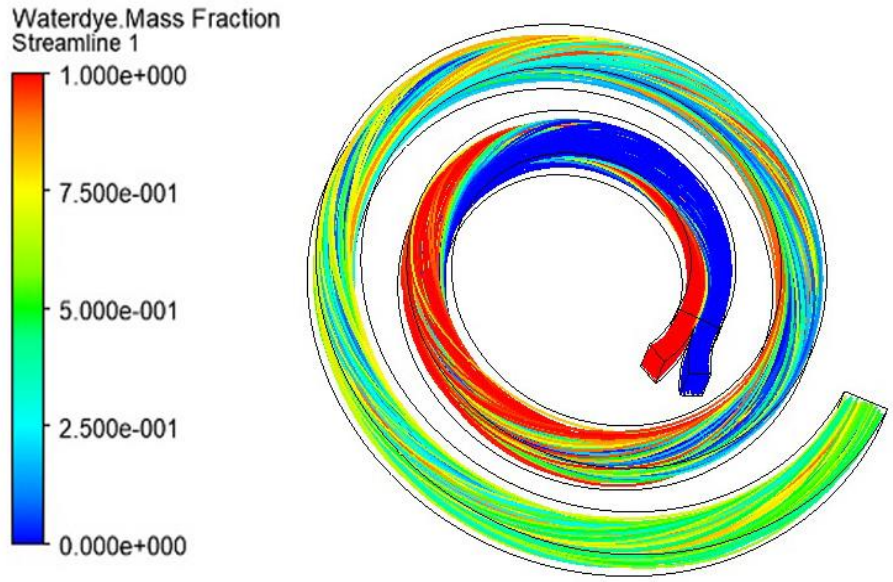

(a)

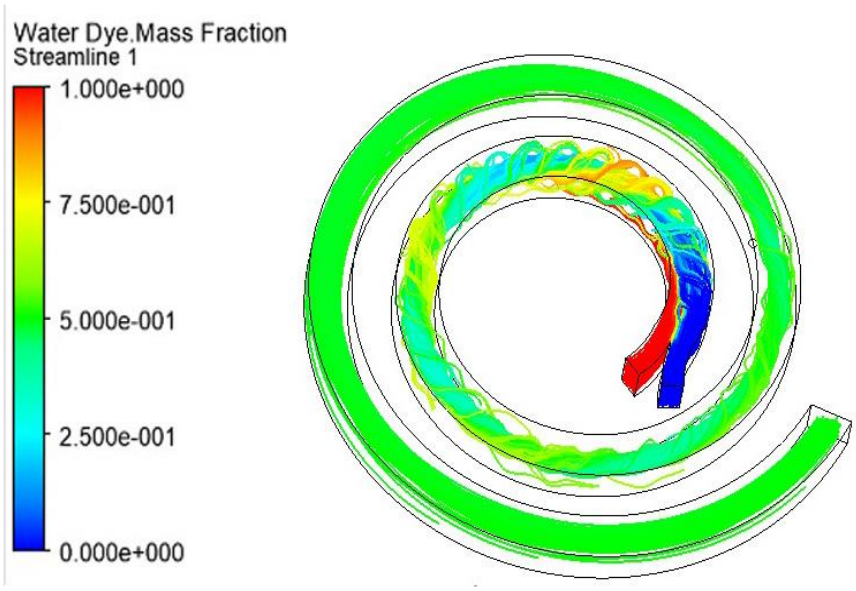

(b)

Fig.5.12: Streamlines rely on species concentration for (a) plane spiral (b) plane spiral with a spiral obstacle at Re = 80.

5.3.2 Effect of increasing inlets velocity in terms of Reynolds number

The increasing Reynolds numbers (i.e. increasing inlet velocity) effect on the mixing index in two micromixer plane spiral and the plane spiral with spiral obstacle was monitored. For this aim, the simulation work was carried out at different Reynolds numbers (1, 30, 50, 80, 112, 125) for plane spiral micromixer and spiral micromixer with spiral obstacle having the same length. Figure 5.13 manifests mixing index estimation with different Reynolds numbers for plane spiral microchannel and plane spiral with spiral obstacle microchannel. As manifested in the current graph, the mixing index in the plane spiral with spiral obstacle microchannel increases unexpectedly with increasing Reynolds numbers.

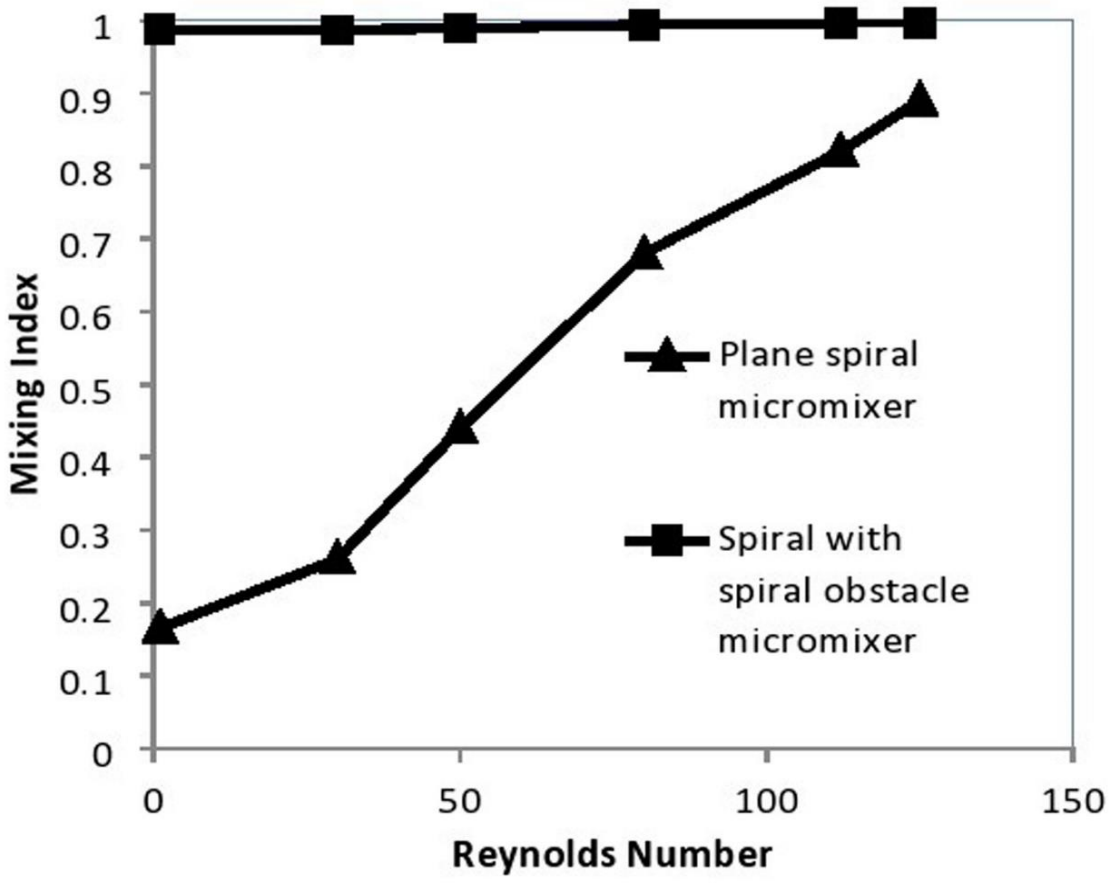

Fig.5.13 Numerated mixing index to the plane spiral microchannel and spiral with spiral obstacle microchannel at several Reynolds numbers

Figure 5.14 manifests pressure drop in plane spiral microchannel and spiral with spiral obstacle microchannel at several Reynolds numbers. As viewed in the present graph, the pressure drop in the spiral with spiral obstacle micromixer is more supreme than the plane spiral micromixer.

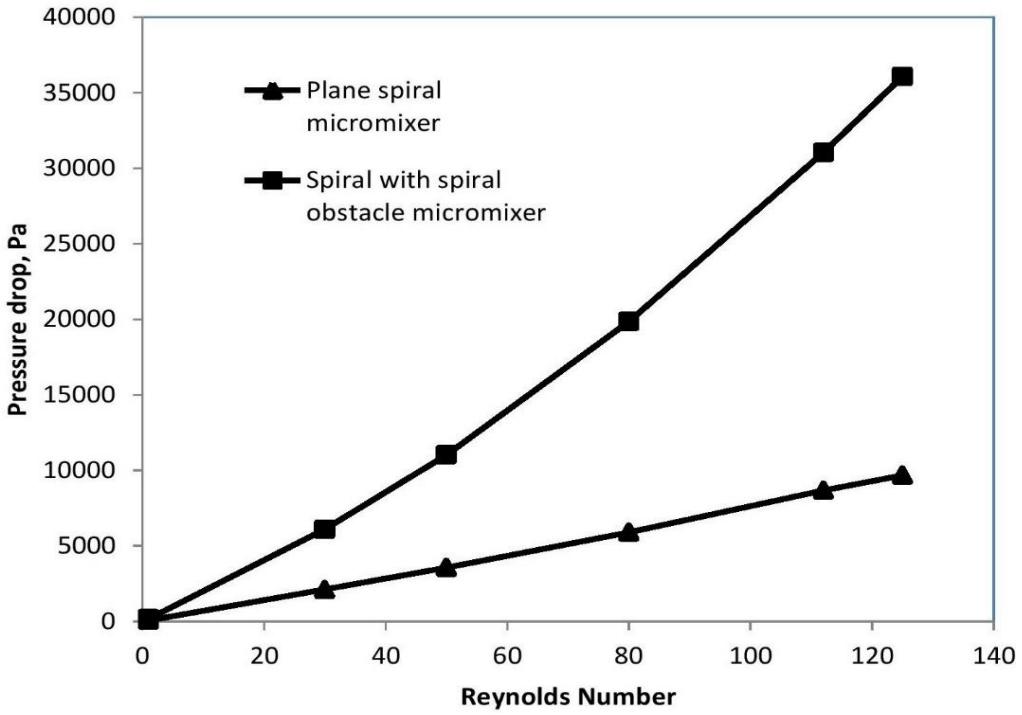

Fig.5.14 Pressure downfall in the plane spiral micromixer and spiral with spiral obstacle micromixer at several Re

5.3.3 Impression of channel's curvature

In present portion, impact of channel's curvature is inspected by mixing quality of spiral with spiral obstacle micromixer. For this target, three spiral with spiral obstacle micromixers having equal lengths but with different initial microchannel radii of 0.5mm, 2mm, and 3mm were examined. The calculated mixing index of the spiral with spiral obstacle microchannels is exhibited in Figure 5.15. As exhibited in this graph, the initial microchannel radius of 0.5 mm reveals higher mixing index values than the other two radius micromixers.

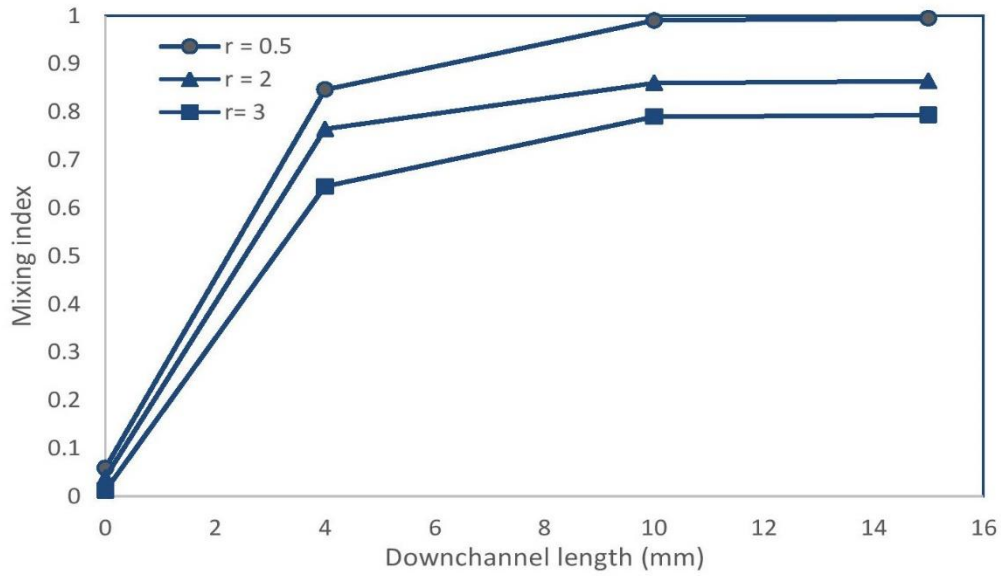

Fig.5.15: Calculated mixing index of three spiral with spiral obstacle micromixers with different initial channel radius

5.3.4 Impression of microchannel's cross-section

Present portion targets to test combination procedure in the spiral having spiral obstacle micromixers with varied rectangular cross-sections. To obtain this aim, four spiral having spiral obstacle micromixers with equal hydraulic diameter (200μm), but different aspect ratios (1.5, 1.25, 1, 0.6) were analyzed. The mixing index for all four designs is numerated at an outlet of microchannels and numerated data is displayed in Figure 5.16. This figure shows that square cross-section microchannel (aspect ratio =1) provides highest mixing index value. The vertical cross-section microchannel (aspect ratio equal to 0.6) provides marginally less mixing index in comparison to square cross-section microchannel. Also, vertical cross-section microchannel provides higher mixing index value than horizontal cross-section microchannel.

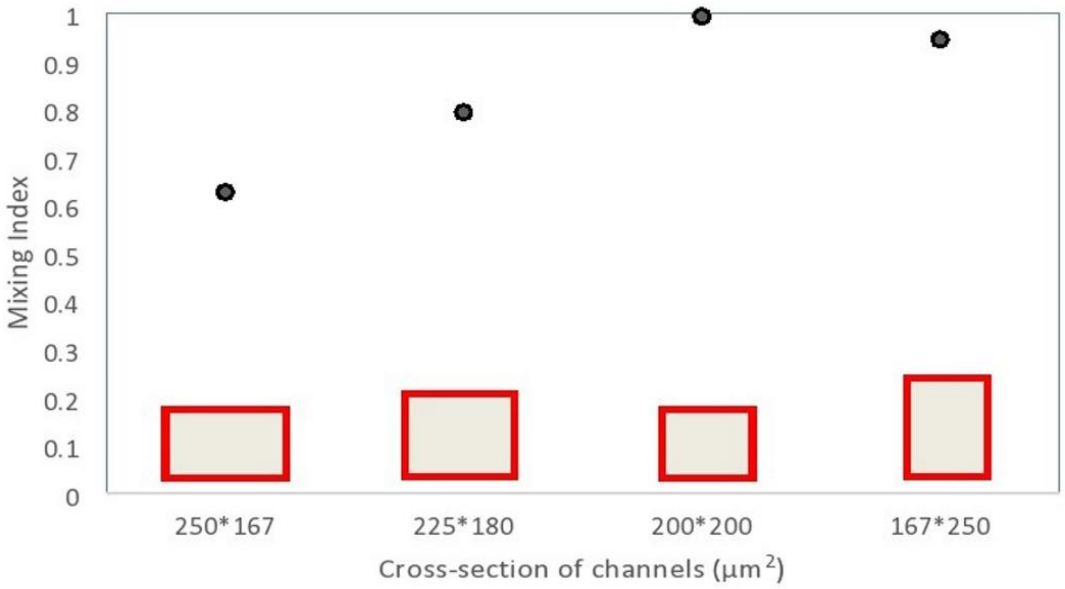

Fig.5.16 Calculated mixing index at outlet of four spiral with spiral obstacle micromixers with different rectangular cross-sections.

5.3.5 Impression of distance between two consecutive turns of spiral with spiral obstacle microchannel

In present portion, impact of distance between two consecutive turnings of spiral with spiral obstacle microchannel is calibrated. For this target, four concerns were screened with different centre-to-centre distances, S = 2W, S = 4W, S = 6W, and S = 8W considering other parameters were the same. The mixing index for these cases was numerated along the down-channel length is shown in Figure 5.17. As displayed in this figure, the spiral with spiral obstacle micromixer having smallest footmark gives higher mixing quality at the same length. Reducing the centre-to-centre distance of spiral with spiral obstacle micromixer has an identic impact as reducing its initial radius; decrement of this factor enhances the Dean flow, as well as then increases the amalgam in spiral with spiral obstacle micromixer.

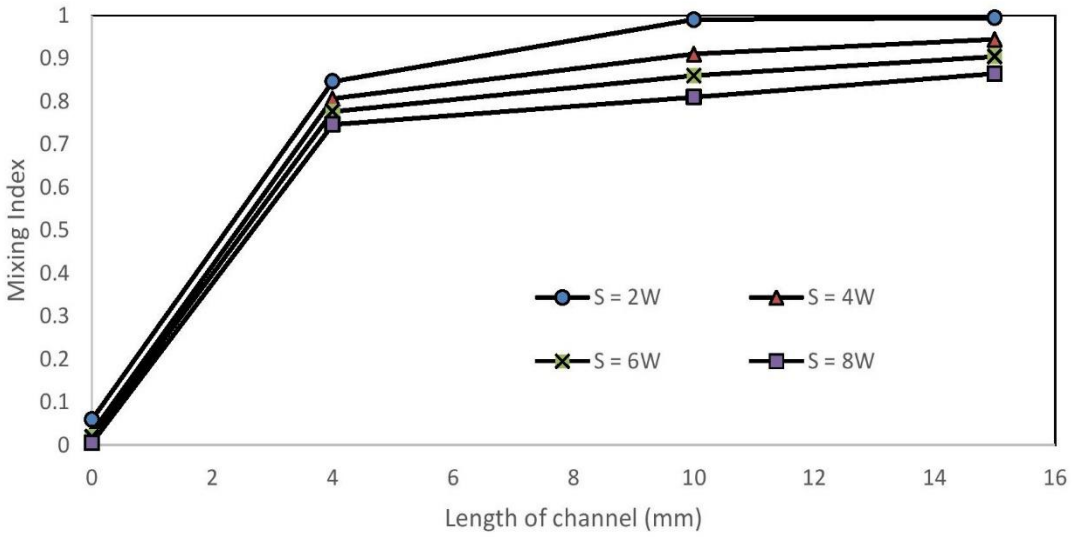

Fig.5.17 Computed mixing index versus mixing channel length at an outlet for the four spiral with spiral obstacle micromixers with different centre-to-centre distances.

5.4 **Mixing and flow analysis in spiral microchannel with cylindrical obstacles, rectangular obstacles, triangular obstacles**

As discussed in Chapter 4, inserted cylindrical obstacles have a diameter of 0.06mm, and height of cylindrical obstacles is 0.18mm. When inserting rectangular obstacles with length, width, as well as height are 100 µm, 50 µm, and 180 µm respectively. The rectangular obstacles are placed offset from the centre line. The gap between two successive rectangular obstacles is 200 µm. The clearance between rectangular obstacle and main mixing channel wall is 10 µm and when inserting triangular obstacles having a base length of 200 µm, width of 200 µm, pitch length of 300 µm, and height of obstacle is 75 µm. Flow and mixing behaviour of water and water dye in spiral microchannel with cylindrical obstacles, rectangular obstacles, and triangular obstacles are discussed below.

5.4.1 Impact of geometry

The mass fraction contours of cylindrical obstacles micromixer, rectangular obstacles micromixer, and triangular obstacles micromixer are manifested in Figure 5.18. Mixing index value at an outlet of spiral micromixer with cylindrical obstacles is (M_i = 0.983), spiral micromixer with rectangular obstacles is (M_i = 0.988), and spiral micromixer with triangular obstacles is (M_i = 0.976) at the Reynolds number 80.

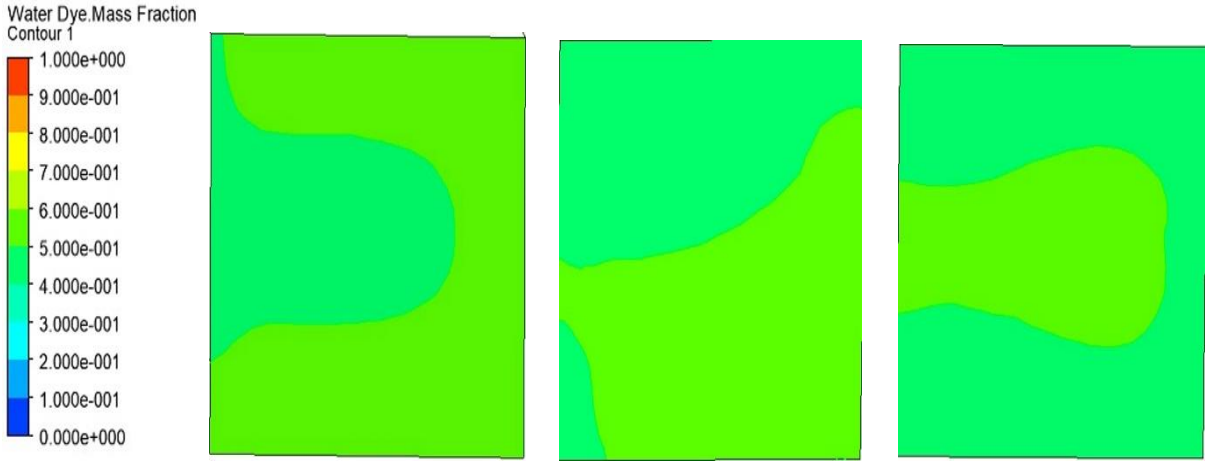

(a) (b) (c)

Fig.5.18 Contours of a fraction of mass to the micromixer at an outlet for (a) cylindrical obstacles (b) rectangular obstacles (c) triangular obstacles at Re = 80.

Figure 5.19 manifests a contour of mass fraction along the spiral length at a central plane in cylindrical obstacles micromixer, rectangular obstacles micromixer, and triangular obstacles micromixer. The red color shows the first species (water) and the blue color shows the second species (water dye). When the color is changed into green characterizes a mixture.

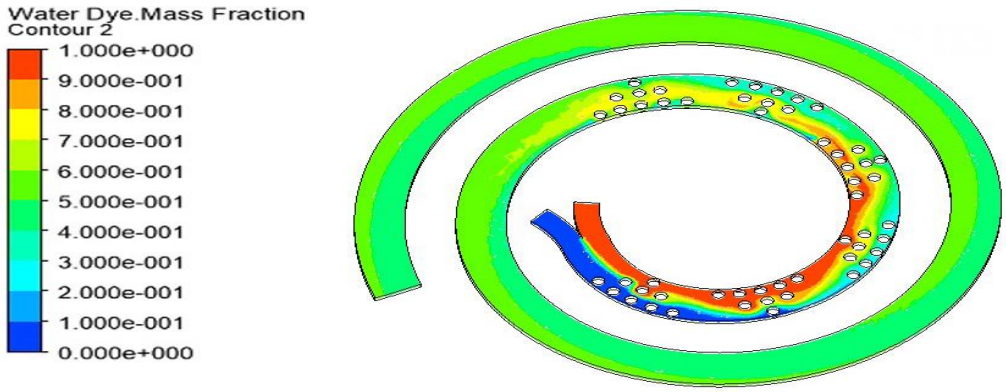

(a)

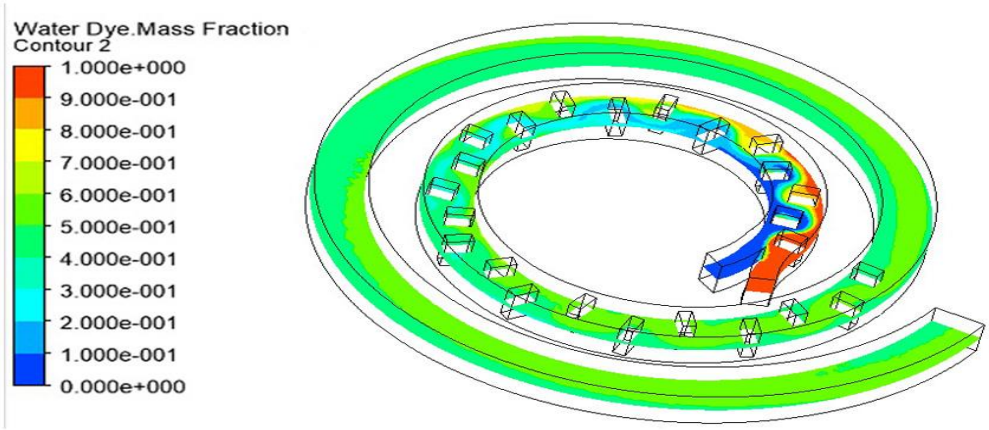

(b)

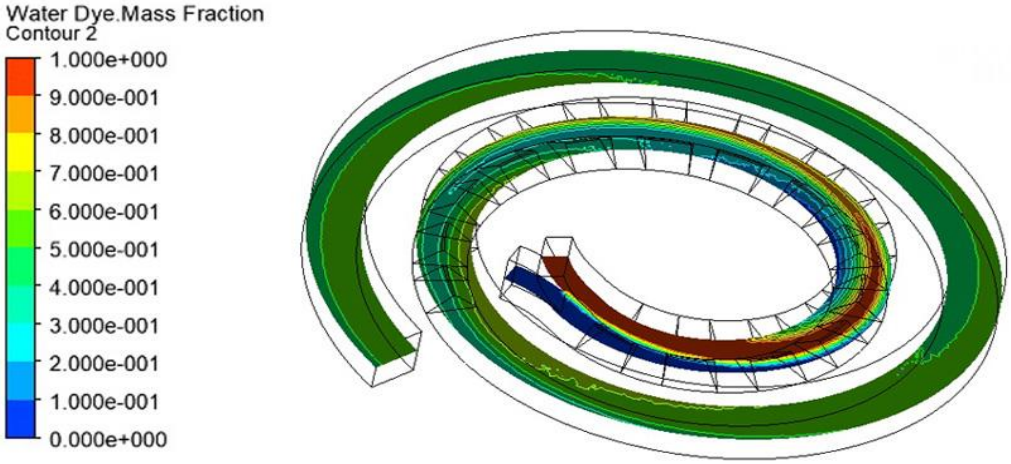

(c)

Fig.5.19: Contour of mass fraction along the spiral length at central plane for (a) cylindrical obstacles (b) rectangular obstacles (c) triangular obstacles at Re = 80.

Streamlines rely on the fraction of mass throughout the spiral length in cylindrical obstacles micromixer, rectangular obstacles micromixer, and triangular obstacles micromixer are exhibited in Figure 5.20.

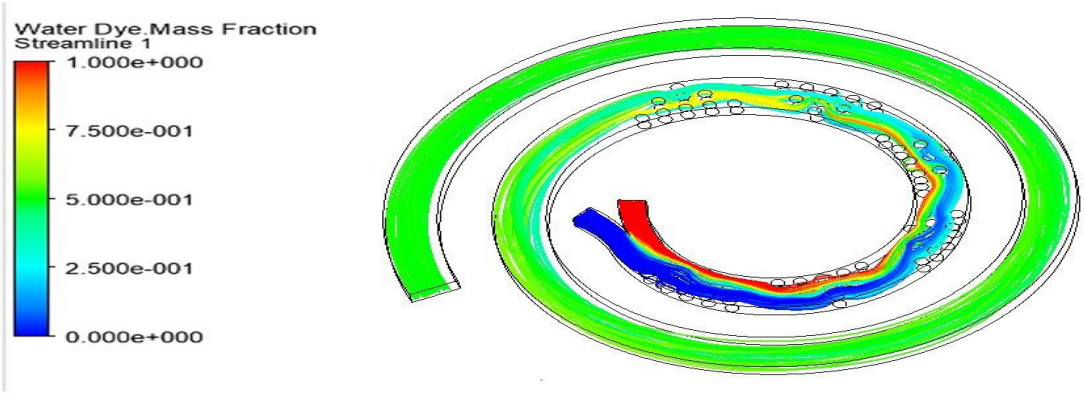

(a)

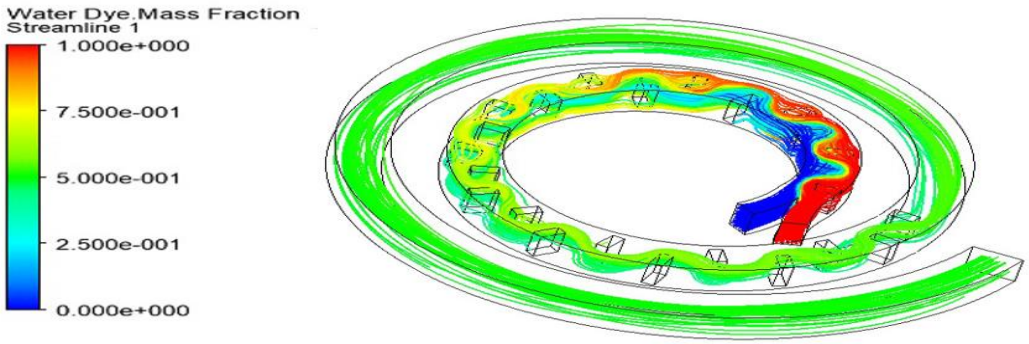

(b)

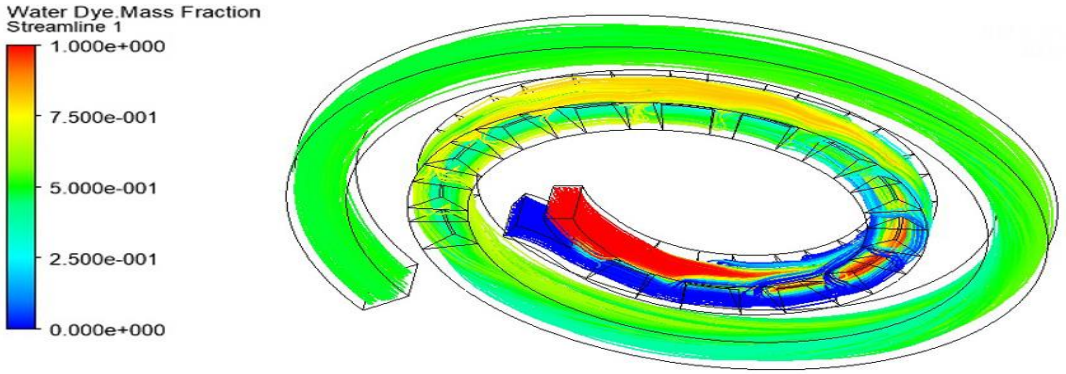

(c)

Fig.5.20: Streamlines rely on species concentration for (a) cylindrical obstacles (b) rectangular obstacles (c) triangular obstacles at Re = 80.

Comparison of Mixing index and Pressure downfall values of Plane spiral micromixer, Spiral micromixer with spiral obstacle, Cylindrical obstacles micromixer, Rectangular obstacles micromixer, and Triangular obstacles micromixer are displayed in table 5.1 and table 5.2 respectively.

Table 5.1: Mixing index at several Reynolds numbers

Inlet Velocity (m/sec)	Reynolds Number	Mixing Index (MI)				
		Plane spiral micromixer	Spiral with triangular obstacles	Spiral with cylindrical obstacles	Spiral with rectangular obstacles	Spiral with spiral obstacle
0.005	1	13.53 %	67.81 %	74.70 %	82.18 %	98.84 %
0.15	30	26.85 %	90.06 %	96.06 %	99.51 %	98.78 %
0.25	50	44.08 %	97.16 %	97.92 %	99.04 %	98.95 %
0.4	80	68.44 %	97.65 %	98.30 %	98.83 %	99.46 %
0.56	112	82.60 %	97.88 %	98.47 %	99.40 %	99.71 %
0.625	125	84.20 %	97.90 %	98.57 %	99.59 %	99.75 %

Table 5.2: Pressure drop at several Reynolds numbers

Inlet Velocity (m/sec)	Reynolds Number	Pressure Drop				
		Plane spiral micromixer	Spiral with triangular obstacles	Spiral with cylindrical obstacles	Spiral with rectangular obstacles	Spiral with spiral obstacle
0.005	1	70.006	152.26	337.77	217.14	176.04
0.15	30	2113.46	4723.94	10612.77	7657.38	6104.02
0.25	50	3564.008	8107.59	18588.38	14861.63	11034.58
0.4	80	5896.41	13661.87	32047.90	29098.36	19854.27
0.56	112	8673.03	20415.52	48311.61	48646.57	31044.78
0.625	125	9883.017	23424.19	55457.42	57799.41	36073.50

From Table 5.1, a spiral with spiral obstacle micromixer provides highest mixing index value. Spiral with rectangular obstacles provides the next higher mixing index value after the spiral with spiral obstacle micromixer. From Table 5.2, a spiral with rectangular obstacles micromixer gives highest pressure drop at Reynolds number 112 and 125, while at Reynolds number 1, 30, 50, and 80, a spiral with cylindrical obstacles gives highest pressure drop.

5.5 Mixing and flow analysis in square section spiral microchannel and circular section spiral microchannel

As discussed in Chapter 4, for the comparison of square cross-section micromixer as shown in Figure 4.3 as well as circular cross-section micromixer as shown in Figure 4.9, the hydraulic diameter of mixing channel and inlets channel of both geometries (circular and square cross-section) was taken same.

5.5.1 Influence of Configuration

To illustrate numerical outcomes, mixing quality of simulations is likened to an exit of square as well as circular cross-section spiral microchannel. The dissemination of fraction of mass of micromixer to the square cross-section as well as circular cross-section for Reynolds number 125 is displayed in Figure 5.21. The mass fraction contour exhibits that mixing performance of circular cross-section micromixer is superior to square cross-section micromixer. Mixing index esteem at the outlet to the mixing channel in circular cross-section form is (M= 92.95) as well as to the mixing channel in square cross-section form is (M = 84.20).

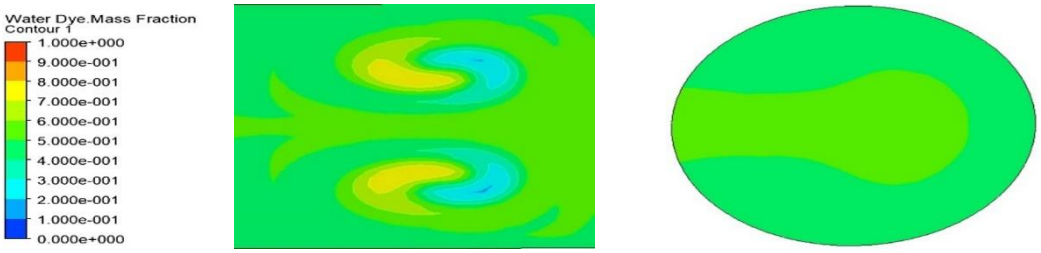

(a) (b)

Fig.5.21: Fraction of mass contours of micromixer (a) square cross-section (b) circular cross-section at Re = 125.

Figure 5.22 exhibits a concentration contour throughout the spiral length to the square cross-section as well as circular cross-section micromixer. The contour exhibits that for this Reynolds

number, mixing increases conformably from the junction point to an exit. The red color represents one fluid (water) and the blue color represents another fluid (dye diluted in water). When combination has happened, depicts green color.

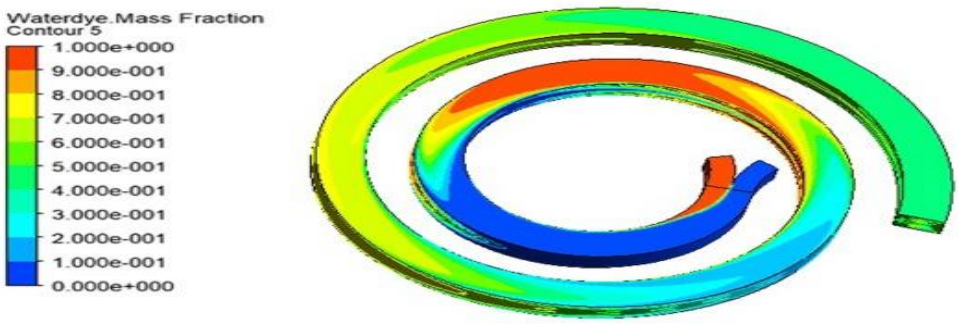

(a)

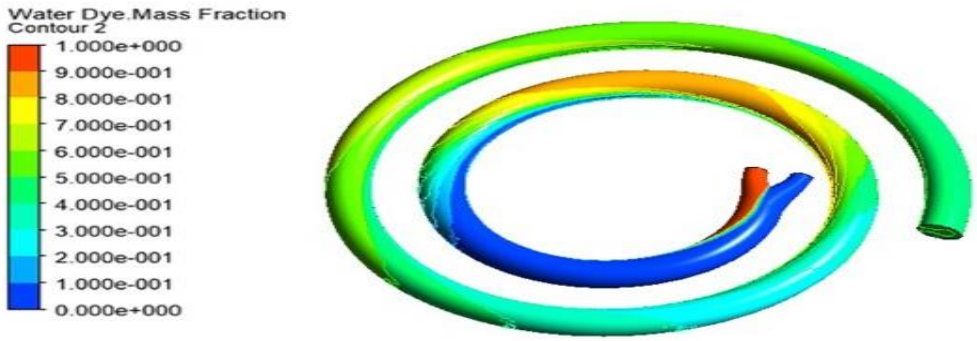

(b)

Fig.5.22 Concentration contour throughout the spiral length for (a) square cross-section micromixer (b) circular cross-section micromixer at Re = 125.

The mixing is much incited via secondary flow created because of centrifugal force in concern of circular cross-section micromixer as likened to square cross-section micromixer. Hereupon chaotic advection is immensely dominant in circular cross-section spiral microchannel as likened to square cross-section spiral microchannel, which exquisitely enhances combination. This coalescence can be viewed via streamlines depending on fraction of mass. Streamlines based on fraction of mass throughout the spiral length in square as well as circular cross-section micromixer are delineated in Figure 5.23. Contours of concentration at four varied positions

beginning from the junction point for square cross-section micromixer and circular cross-section micromixer are displayed in figure 5.24 as well as figure 5.25 exhibits plots of velocity vector at an exit of micromixer square and circular cross-section. For Reynolds number equal to 125, flow sample is almost similar in these two channels, as well as velocity vectors are curvilinear to a micromixer wall throughout the cross-section.

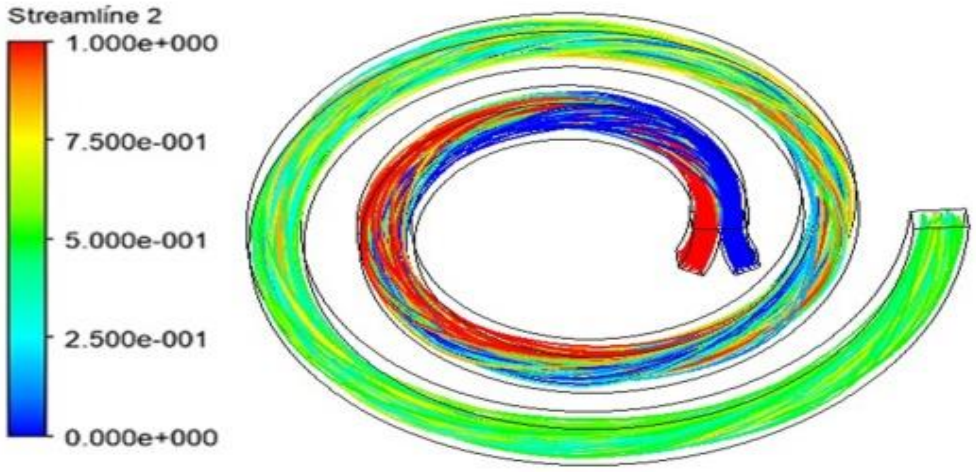

(a)

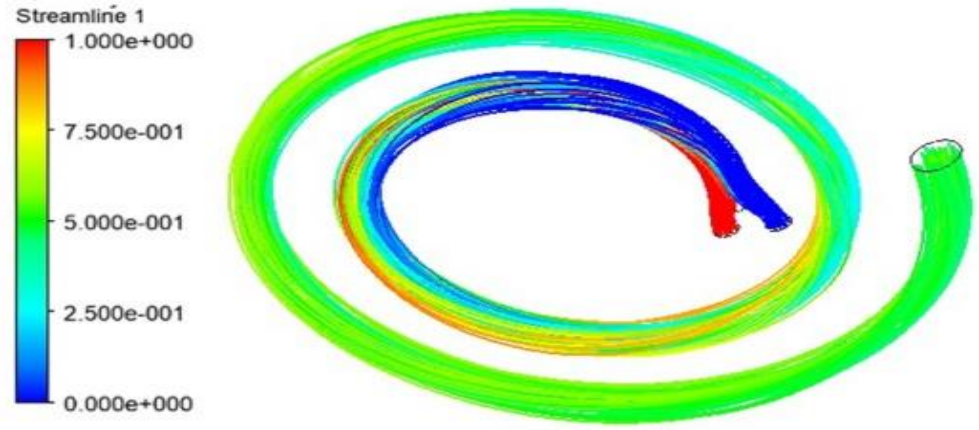

(b)

Fig.5.23 Streamlines rely on a fraction of mass for micromixer of (a) square cross-section (b) circular cross-section at Re = 125.

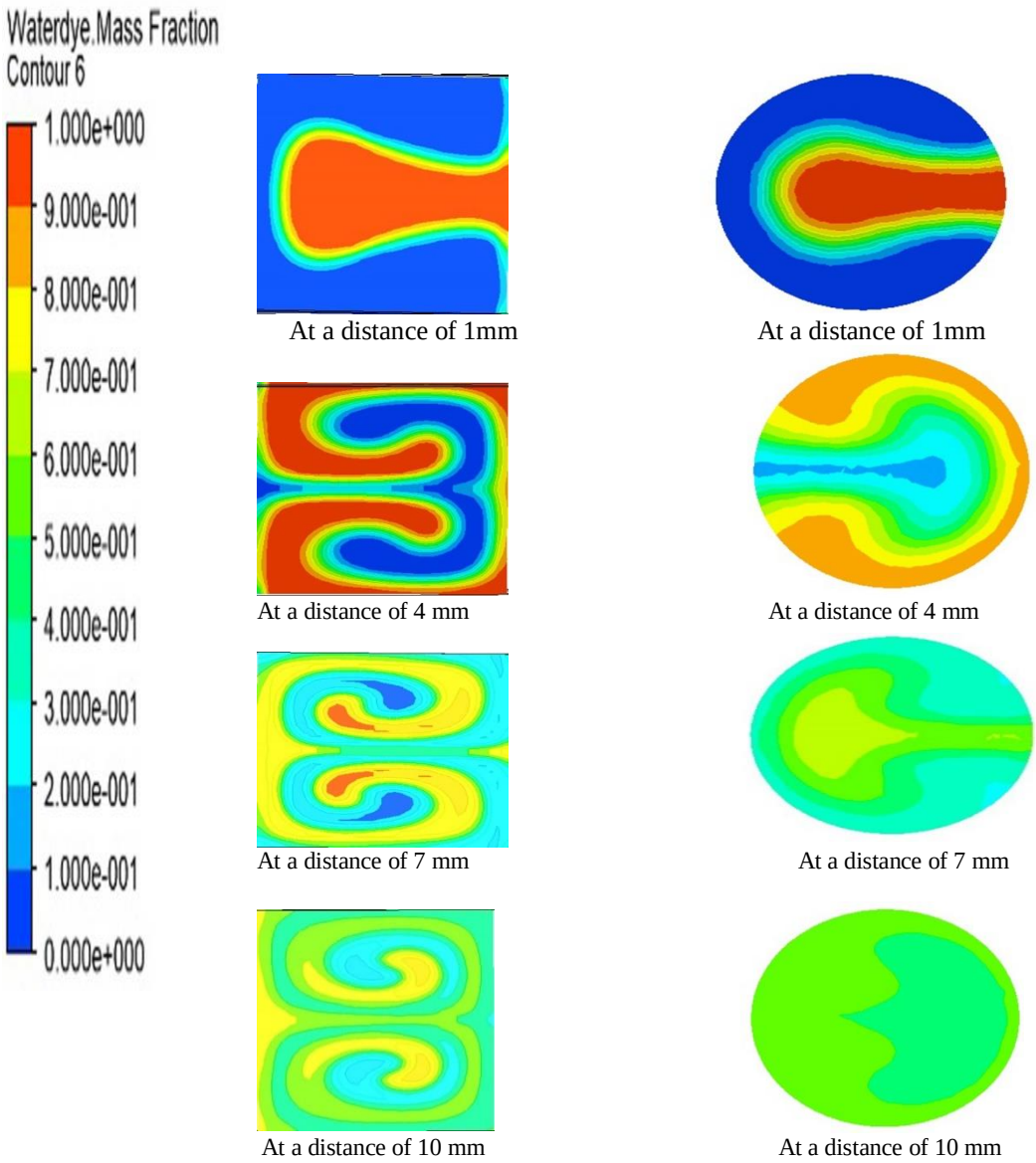

Fig.5.24 Contour of fraction of mass at four varied positions beginning from junction point for micromixer of (a) square cross-section (b) circular cross-section at Re = 125.

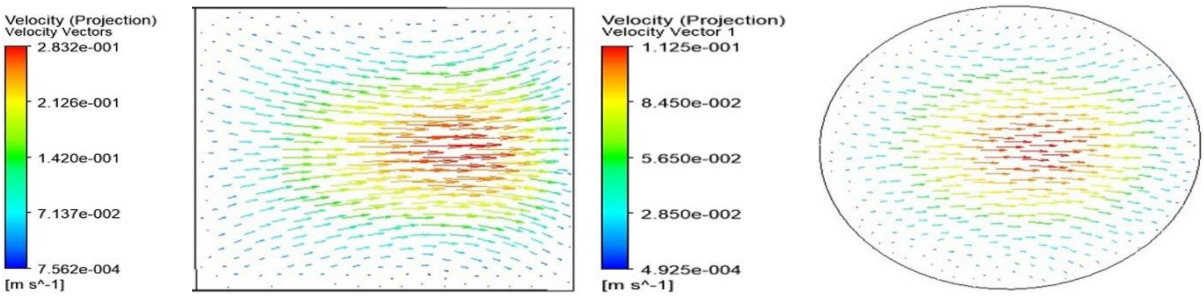

(a) (b)

Fig.5.25 Plot of velocity vectors for micromixer of (a) square cross-section (b) circular cross-section at Re = 125.

5.5.2 Effect of increasing inlets velocity in terms of Reynolds number

The Reynolds number impressiveness on mixing index in pair of micromixer square as well as circular cross sections was studied. The simulation procedure was carried out at Reynolds numbers (1, 30, 50, 80, 112, and 125) to the square cross-section micromixer as well as circular cross-section micromixer with the same length. Figure 5.26 shows the graph amid mixing index as well as Reynolds numbers in which circular cross-section micromixer have a superior mixing index.

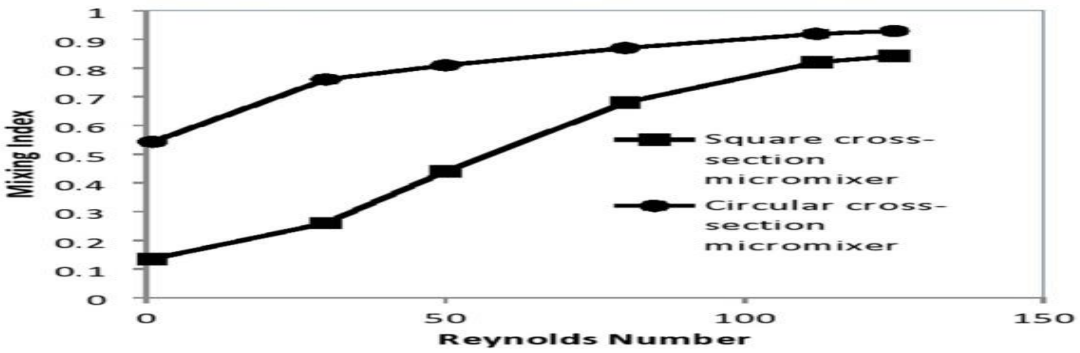

Fig.5.26 Mixing index esteems to the square as well as circular cross-section micromixer at several Reynolds numbers.

The explanation of mixing eventuate demands perusal of pressure downfall between entrance and exit of mixing channel and this gets much valued in case of passive micromixers since pressure drops immediate an idea of energy which will be urged to pump the liquids from the

entrance to exit. Hereupon, it is essential to scrutinize pressure downfall in a channel. The mixing procedure utilizes power inputs in terms of pressure downfalls. Figure 5.27 shows a variation to pressure drop for two cross-sections at several Reynolds numbers. For these two cases, pressure drops have been estimated to be the microchannels having equal down-channel lengths. Pressure drop increase abruptly after the increase of Reynolds number in the condition of square cross-section microchannel. The circular cross-section micromixer exhibits a minor pressure downfall than square cross-section micromixer since there are no sharp edges in circular cross-section micromixer. Figure 5.28 exhibits regimes of mixing quality across down-channel length for Reynolds number 125. Mixing increases well-neatly throughout micromixer length as explicated in this graph.

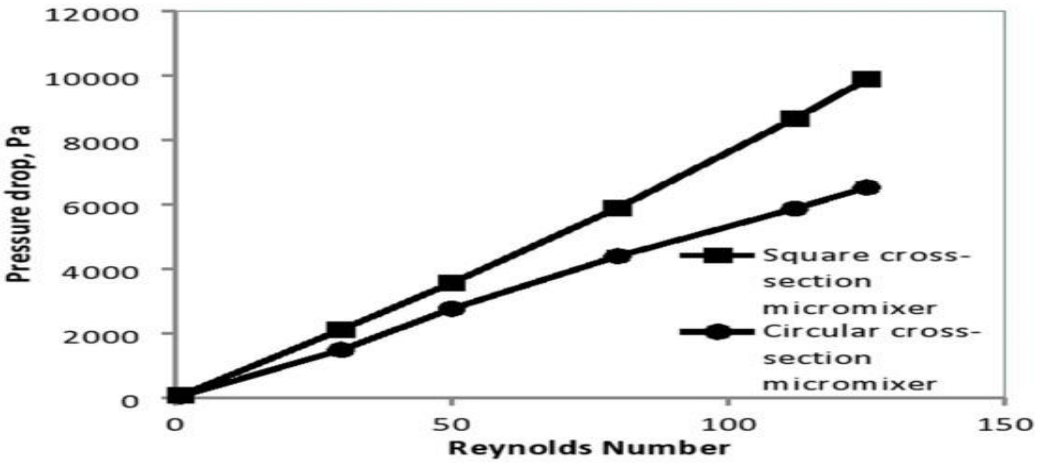

Fig.5.27 Variation of the pressure downfall versus Reynolds number for duo cross-section.

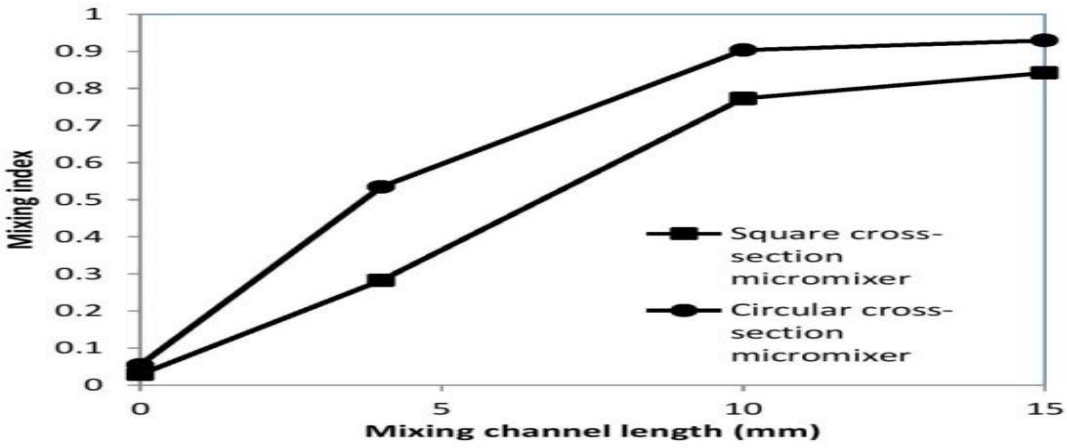

Fig.5.28 Variation of mixing index across mixing channel length at Re =125.

5.6 Mixing and flow analysis in plane spiral microchannel and twisted spiral microchannel

As discussed in Chapter 4, for comparison between plane spiral micromixer and twisted spiral micromixer, length in profile direction is selected identical for both situations (Plane spiral and Twisted spiral micromixer).

5.6.1 Effect of geometry

The mass fraction contours of microchannel plane spiral and twisted spiral are exhibited in Figure 5.29. As exhibited in this figure, a twisted spiral microchannel is better than a plane spiral microchannel. This is primely due to the impacts of swirling flow because of the twisted microstructure. Also, the second effect can be observed by seeing the streamlines. The effect is partially similar to fluid flow like a wavy form at each turn by twisting the geometry. The mixing index esteem at an outlet of twisted spiral microchannel is more (M_i = 0.961) than that of the plane spiral microchannel whose value is (M_i = 0.826).

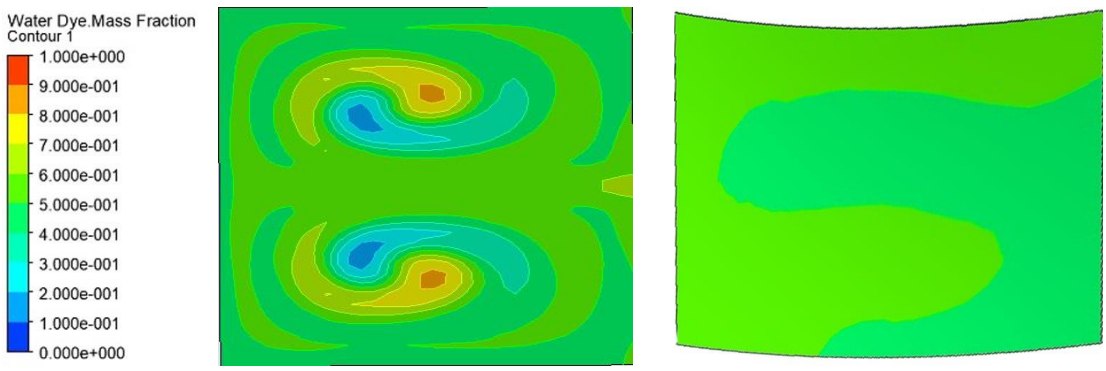

(a) (b)

Fig.5.29 Contours of fraction of mass of micromixer at an outlet for (a) plane spiral (b) twisted spiral at Re = 112

Figure 5.30 shows a contour of mass fraction along the spiral length in plane spiral micromixer and twisted spiral micromixer. The red color signifies the first species (water) and the blue color signifies the second species (water dye). When the color is changed to green designate a mixture.

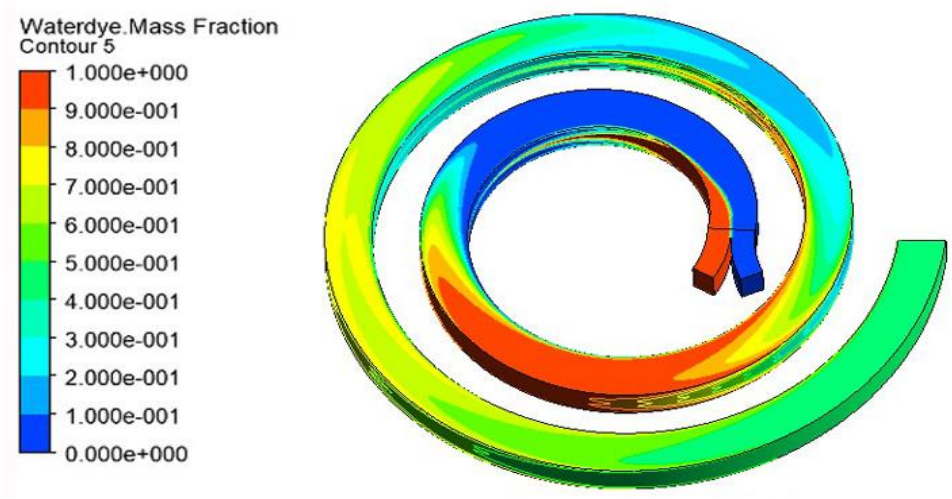

(a)

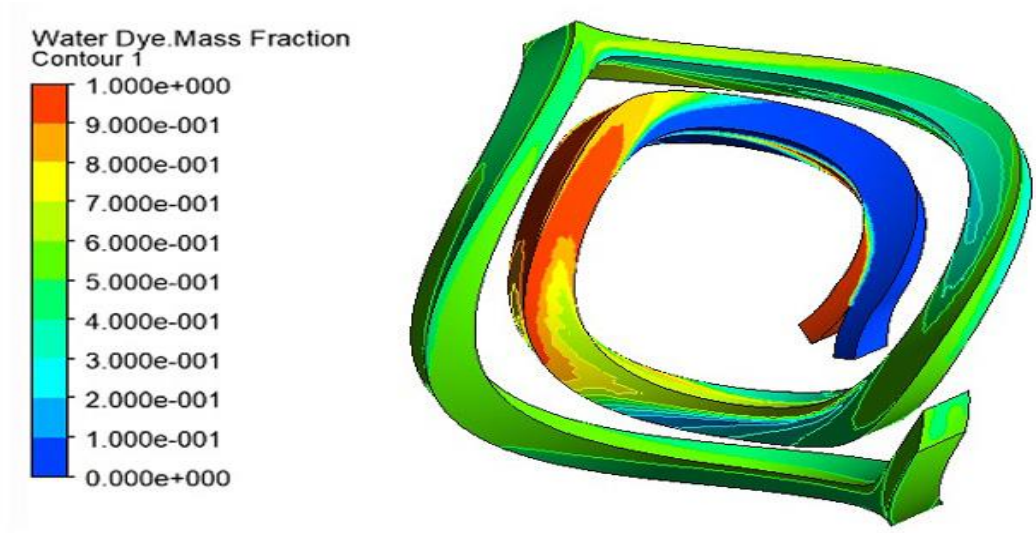

(b)

Fig.5.30: Contour of fraction of mass across the spiral length for (a) plane spiral (b) twisted spiral at Re = 112.

At a low Reynolds number, twisted spiral exertions fluids dominant to growth in molecular diffusion. For a supreme Reynolds number, flow is in control of secondary flow erected because of centrifugal force, which appreciably enhances mixing procedure. This sensation can be predicted by streamlines rely on species concentration for plane spiral and twisted spiral micromixer at Re = 112. The streamlines founded on the fraction of mass throughout the spiral length in plane spiral microchannel and twisted spiral microchannel are exhibited in Figure 5.31. The contour of species concentration at five different locations in plane spiral microchannel and twisted spiral microchannel is displayed in Figure 5.32. As exhibited in this figure, we can see that as distance from junction point of both spiral geometry increases, the mixing quality is increasing and attained highest esteems at the outlet. In concern of twisted spiral, obtained higher mixing quality at each different location of plane spiral micromixer. The velocity vectors plot at the outlet of the plane spiral micromixer and twisted spiral microchannel is exhibited in Figure 5.33. For Reynolds number = 112, flow pattern is different in these two microchannels. At the outlet of the plane spiral micromixer, velocity vectors exhibit the generation of two small vortices having just downstream turns. At the outlet of twisted spiral micromixer, velocity vectors exhibit the stronger transverse vorticals flows having just an upstream turn. So at this Reynolds number =112, twisted spiral exhibits higher mixing efficiency.

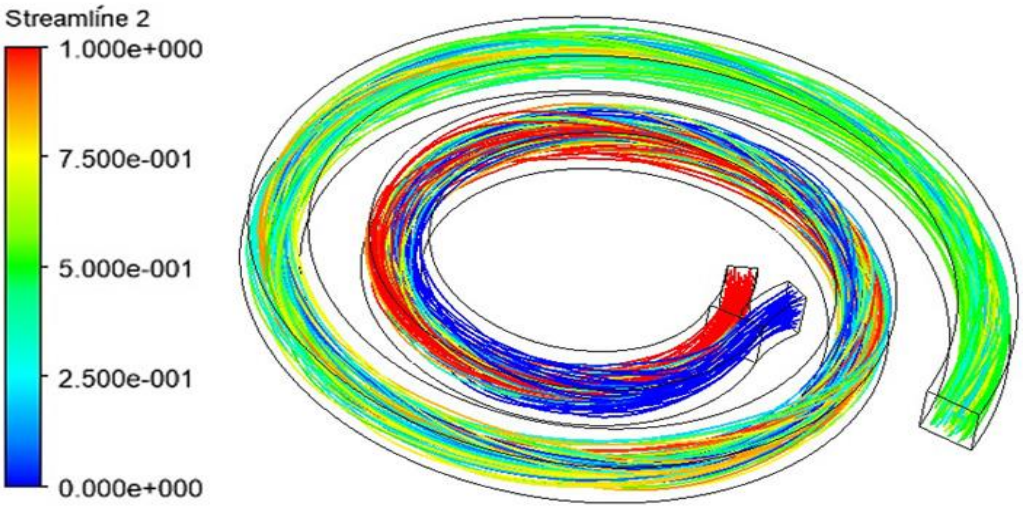

(a)

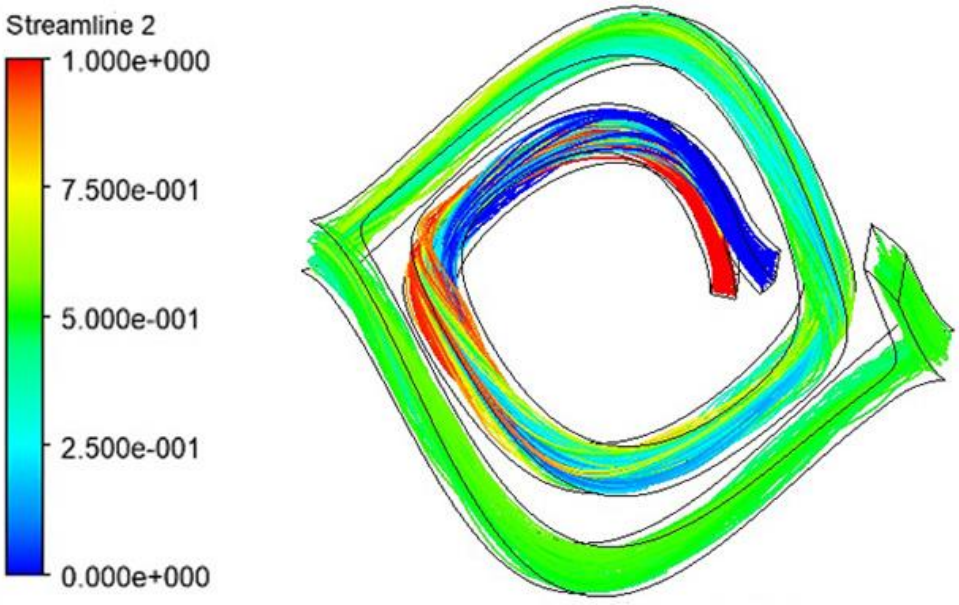

(b)

Fig.5.31: Streamlines rely on fraction of mass for (a) plane spiral (b) twisted spiral at Re = 112.

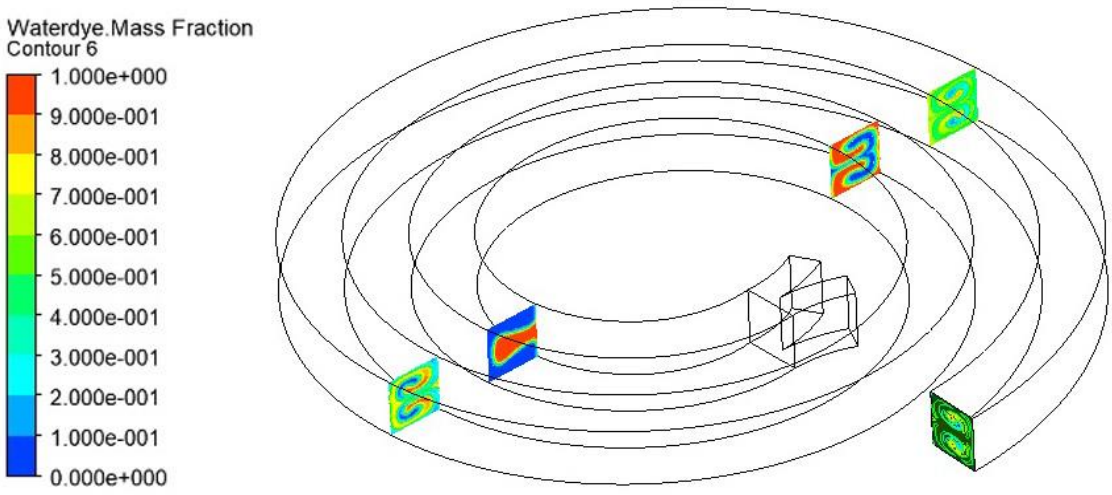

(a)

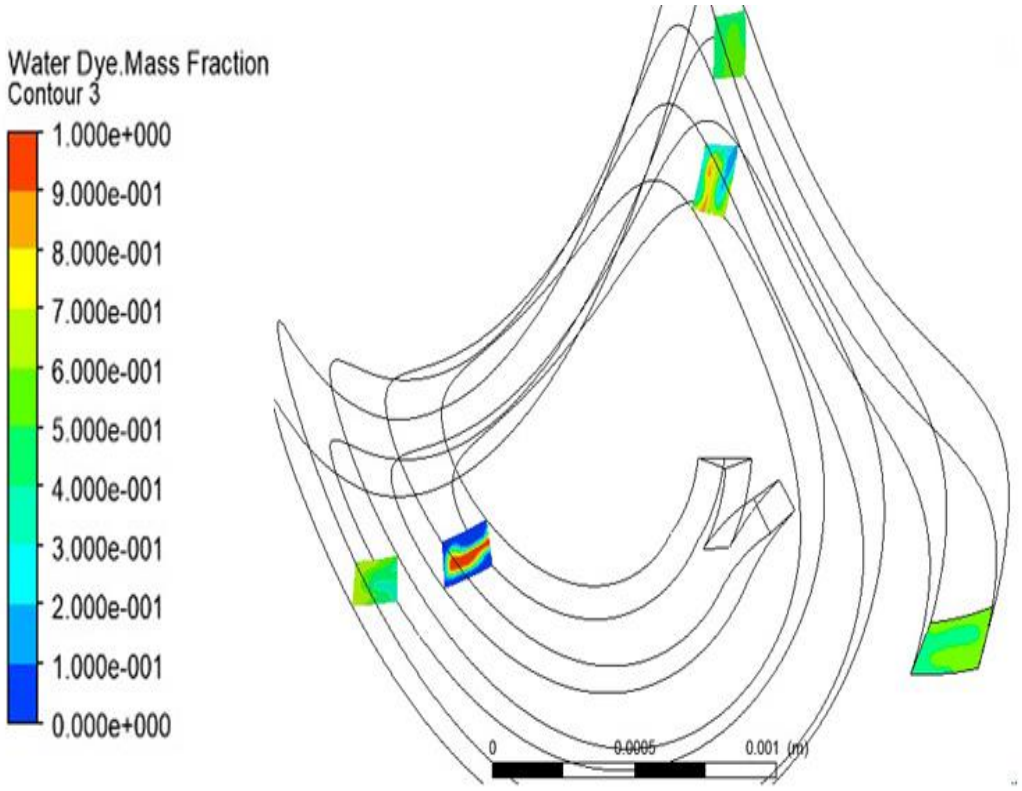

(b)

Fig.5.32: Species concentration contour at five varied positions for (a) plane spiral (b) twisted spiral at Re =112.

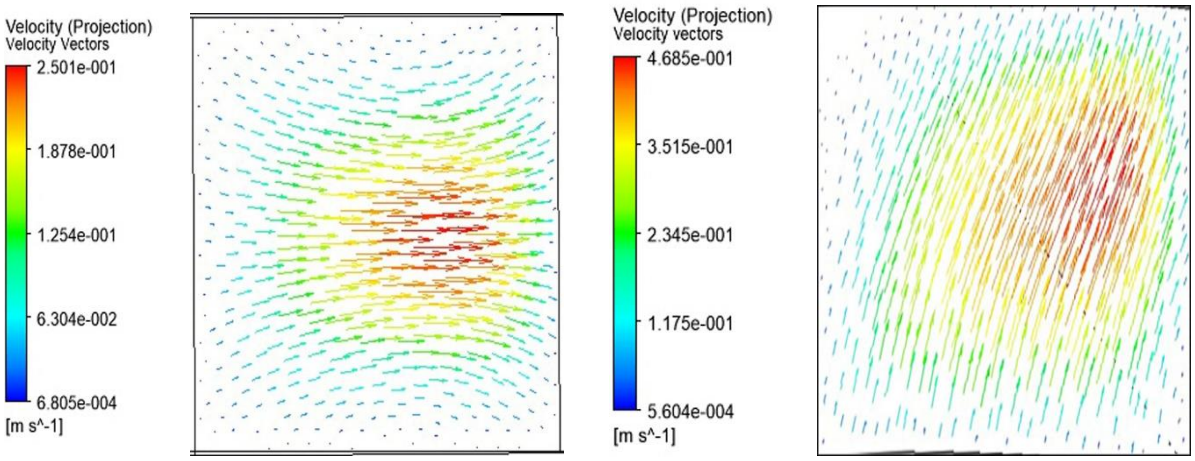

(a) (b)

Fig.5.33: Velocity vectors plot at an outlet of (a) plane spiral micromixer (b) twisted spiral micromixer at Re = 112.

5.6.2 Effect of increasing inlets velocity

The increasing Reynolds numbers (i.e. increasing inlet velocity) impact on the mixing quality in two micromixer plane spiral and the twisted spiral was monitored. For this target, the simulation process was carried out at various Reynolds numbers (1, 30, 50, 80, 112, 125) for plane spiral micromixer and twisted spiral micromixer having equal lengths. Figure 5.34 displays mixing index estimation with different Reynolds numbers for plane spiral microchannel and twisted spiral microchannel. As exhibited in present figure, mixing index in the twisted spiral mixer improves abruptly with rising Reynolds numbers. Beyond Dean number definite value, secondary flow in a perpendicular direction to the main flow arises in spiral micromixer. The stirring effect is generated due to secondary flow in the spiral micromixer. Thus grants to improvement of mixing procedure in spiral micromixer. The secondary flow enhances as the velocity increases in the spiral micromixer, hence mixing procedure intensifies with it. Also, this stirring effect is more in case of twisted spiral within a

swirling motion. So twisted spiral micromixer manifests to be a superior alternative because of its supreme mixing quality at all the esteems of Reynolds number as likened to plane spiral micromixer.

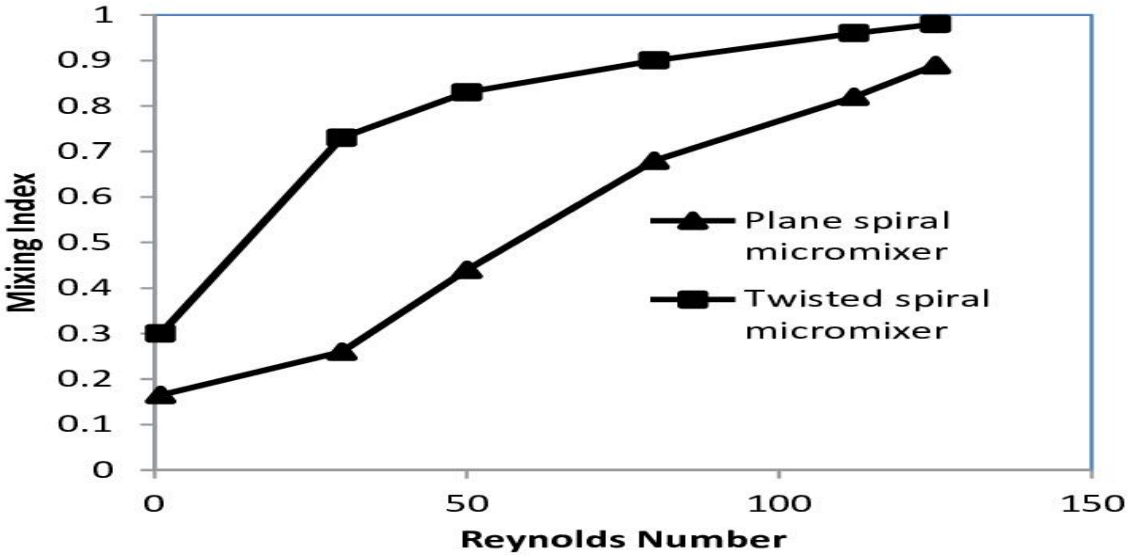

Fig.5.34: Numerated mixing index to the plane spiral microchannel and twisted spiral microchannel at several Reynolds numbers.

As altercated above that microchannel twisted spiral is immensely versed than the plane spiral microchannel. The numerated pressure drop reveals the dissipated energy in the system. Figure 5.35 shows pressure down in plane spiral microchannel and twisted spiral microchannel at several Reynolds numbers. As viewed in the present graph, pressure downfall in a twisted spiral micromixer is more than the plane spiral micromixer. The higher pressure downfall occurs in the microchannel due to the Chaotic advection mechanism, which generates a secondary flow proceeded by centrifugal force. Also as we know that best mixing is generally inclusive of high pressure falls. The high pressure falls motivated a large amount of power loss that will influence actual outcomes of the mixing. Furthermore, mixing index to the plane spiral microchannel and twisted spiral microchannel was numerated with the mixing channel length. Figure 5.36

exhibits mixing index value with the mixing channel length to the plane spiral microchannel and twisted spiral microchannel. As exhibited in this figure, by increasing the mixing channel length from the junction point, obtained a higher mixing index value. Alteration of mixing quality at four variegated locations throughout the length of mixing channel in the three-dimensional twisted spiral micromixer is exhibited in figure 5.37.

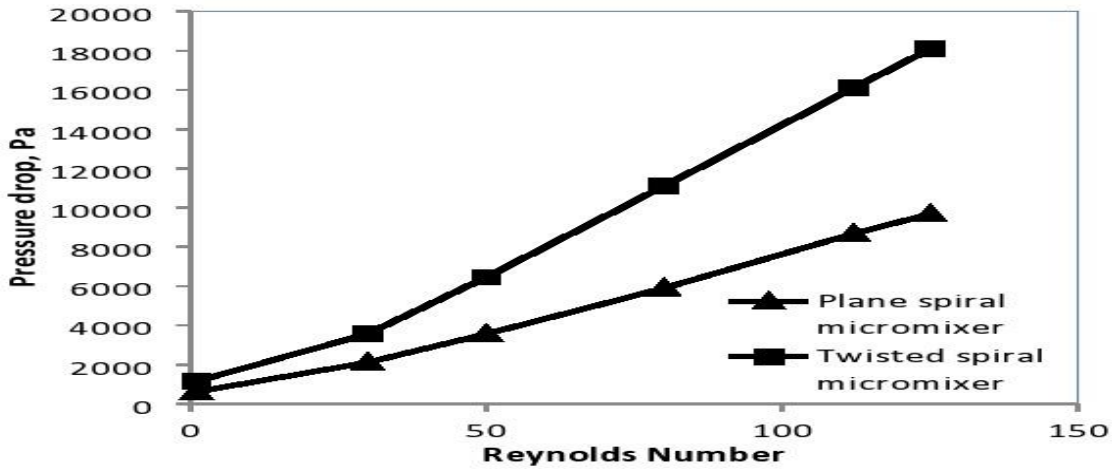

Fig.5.35 Pressure downfall in the plane spiral microchannel and twisted spiral microchannel at several Re

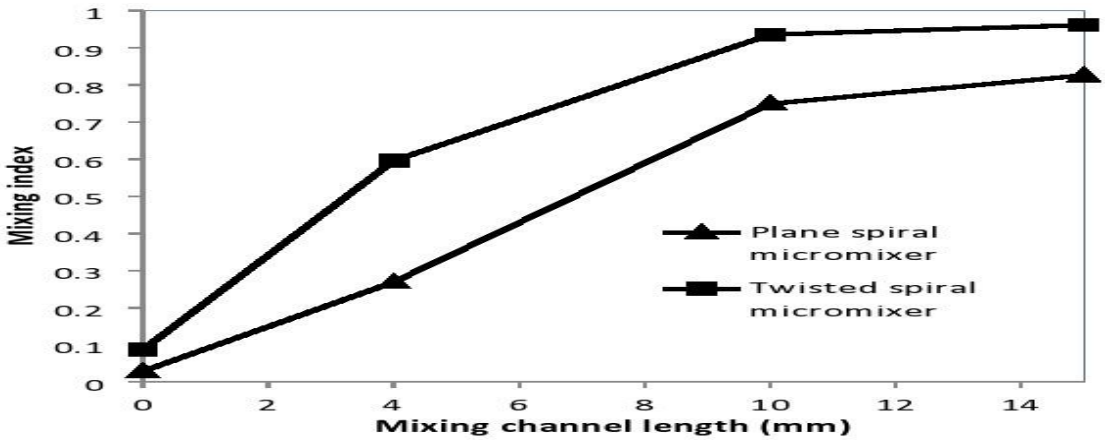

Fig.5.36: Mixing index along the mixing channel length to plane spiral microchannel and twisted spiral microchannel.

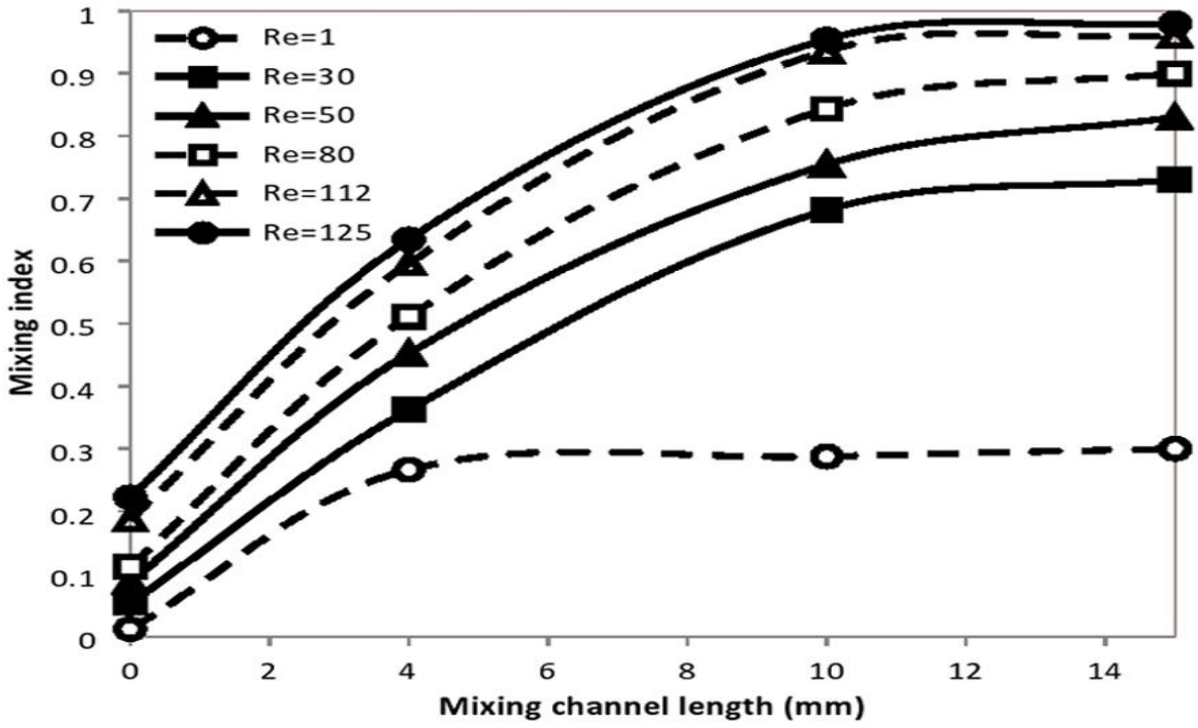

Fig.5.37 Mixing index variation at four variegated locations throughout the length of the mixing channel for twisted spiral micromixer.

CHAPTER-6

CONCLUSIONS

In this research mixing quality of micromixers in six cases, firstly mixing performance and flow characterization in the T junction unbending as well as T junction having bend structure, the second section includes numerical results of T form straight microchannel, offset insertions T form straight microchannel, and offset insertions T junction having bend form mixing channel, thirdly mixing efficiency and flow features in a plane spiral micromixer and spiral micromixer with spiral obstacle and also the study of parameters like effect of increasing inlet velocity, impact of microchannel's curvature, impact of channel's cross-section, and impact of distance amid two consecutive turns of spiral micromixer with spiral obstacle, fourthly numerical results of an effect of cylindrical obstacles, rectangular obstacles, triangular obstacles in case of spiral microchannel, fively simulation results comparison of square section spiral mixer as well as circular section spiral mixer, sixly the effect of twisted spiral geometry are being analyzed for Newtonian fluid water. A Computational Fluid Dynamics simulation tool, ANSYS FLUENT, has been utilized to carry out simulations. The conclusions are under mentioned that can be made rely on the simulated outcomes.

(1) Micromixer with bend turns provides a supreme mixing index ($M_i = 45.9$ %) to that of an unbending mixing channel ($M_i = 28$ %) at the Reynolds number 500, because of chaotic advection mechanisms. The pressure downfall in T form having bend turns is gradually higher than T form unbending. As mixing bend's structure enhances, mixing index also enhances.

(2) T form straight microchannel, offset insertions T form straight microchannel, and offset insertions T junction having bend form mixing channel have been simulated. It was

gained that offset insertions T junction having bend form gives a promoted mixing quality ($M_i = 51.4\ \%$) than that of T form straight microchannel ($M_i = 28\ \%$) and offset insertions T form straight microchannel ($M_i = 46.8\ \%$) at the Reynolds number 500, because of enhanced aspect ratio as well as chaotic advection. Pressure downfall in offset insertions T junction having bend form mixing channel is increased than T form straight microchannel but moderately increased than offset insertions T form straight microchannel.

(3) Simulation results show spiral micromixer with a spiral obstacle ($M_i = 99.4\ \%$) is more efficient than a plane spiral micromixer ($M_i = 68.4\ \%$) at the Reynolds number 80. Rising the fluid's inlet velocity in a spiral with spiral obstacle micromixer enhances mixing quality rapidly as compared to a plane spiral micromixer. Enhancing the fluid's velocity in the spiral with spiral obstacle microchannel strengthens the two counter-rotating vortices and hence rises mixing procedure. It is obtained that initial radius of spiral with spiral obstacle micromixer is the prime factor for increasing the fluids mixing. Reducing the initial radius of microchannel enhances the swirling flow, and hence, compacting the size of microchannel enhances its mixing quality. The study of microchannel's cross-section (different aspect ratios) exhibits that mixing quality of square cross-section is the best. The secondary flow (Dean Flow) much fruitfully stirs the fluids within this square cross-section. Further reducing the centre-to-centre distance of a spiral with spiral obstacle micromixer has a similar impact as reducing the initial radius, so it is concluded that compacting the device increases its mixing performance.

(4) The effect of cylindrical obstacles, rectangular obstacles, and triangular obstacles in case of spiral microchannel were also studied. It is found that a spiral with spiral obstacle micromixer provides highest mixing index value ($M_i = 99.4\ \%$). Spiral with rectangular obstacles provides the next higher mixing index value (M_i = 98.8 %) after the spiral with spiral

obstacle micromixer. It is also found that a spiral with rectangular obstacles micromixer gives highest pressure drop at Reynolds number 112 and 125, while at Reynolds number 1, 30, 50, and 80, a spiral with cylindrical obstacles gives highest pressure drop out of the five proposed geometry.

(5) The simulation study of amalgam in square and circular cross-section mixers has been analyzed. Pure water and Dye diluted in water have been selected as operating liquids for amalgam. Navier-Stokes equation in 3D investigates flow region and combination to the Reynolds numbers 1 to 125. It was concluded that circular cross-section micromixer exhibits a higher mixing index ($M_i = 92.95\ \%$) than square cross-section micromixer ($M_i = 84.20\ \%$) at Re = 125, because of their enhanced swirling strength. The swirling strength is evaluated as the ratio of the tangential velocity of the liquid to the main velocity across a cross-section. In both micromixers, the pressure drops abruptly increase by increasing Reynolds number. The circular cross-section mixer exhibits lower pressure falls than the square cross-section mixer. The intention of present investigation is to obtain two goals which are a higher mixing index and minor pressure falls in micromixer. The circular cross-section mixing channel has accomplished both norms, so this cross-section is superior for liquid mixing. In factual exercises, the gubernation of a Lab-on–chip device is not impressed via pressure downfall. The geometry performs a significant contribution, so this circular cross-section mixing channel has a better potential for usage in lab-on-chip devices.

(6) The plane spiral microchannel and twisted spiral microchannel have been simulated. The water and water with dye were taken as mixing fluids. 3-D Navier-stokes was utilized to examine mixing phenomena at a vast limit of the Reynolds number (Re = 1 to 125). It was concluded that a twisted spiral micromixer renders an improved mixing index ($M_i = 96.1\ \%$)

than a plane spiral micromixer ($M_i = 82.6\ \%$) at Re = 112, because of the effect of swirling flow due to twisted geometry. The proposed modified micromixer twisted spiral attained the mixing index of 98 % at Re = 125. It is as well found that the mixing index esteem rises with the rising the length of mixing channel from the junction point. In two microchannels, pressure drop in a twisted spiral microchannel is more than in a plane spiral microchannel due to a more intensive chaotic advection mechanism. In practical application, pressure drop does not affect the operation of a microchip. The geometry of the system is prominent. This proposed geometry shape has a high potential for the application of the lab on a chip device.

Various configurations and parameters are studied in this work, in which a spiral with spiral obstacle microchannel provides the best mixing performance even at a low Reynolds number, so the optimal design parameter is the length of the spiral obstacle. As the length of the spiral obstacle increases, mixing quality also increases.

SCOPE FOR FUTURE WORK

(1) In future studies, the experimental implementation of the presented ideas in this thesis can be done to enhance the mixing quality of micromixers.

(2) Future research will be centered on the impact of nanoparticles in microchannel by enforcing an exterior magnetic field.

(3) To design the next formatio mixer, the incidence of cavitation interior of the mixer will be pondered in future. As well, future interpretations will be centered on computational explication of mixing of various fluids such as water-ethanol mixture, water-ink mixture, blood mixture, etc since mixing quality rely on the diffusion coefficient of fluids mixture.

(4) The future scope will be centered on the optimization of spiral micromixers with obstacles and more than one phase mixing will also be analyzed.

REFERENCES

[1] Afzal, A., & Kim, K. Y. (2013). Three-objective optimization of a staggered herringbone micromixer. Sensors and Actuators B, 192, 350-360.

[2] Afzal, A., & Kim, K. Y. (2015). Convergent–divergent micromixer coupled with pulsatile flow. Sensors and Actuators B, 211, 198-205.

[3] Ansari, M. A., & Kim, K. Y. (2009). A numerical study of mixing in a microchannel with circular mixing chambers. AIChE Journal, 55(9), 2217-2225.

[4] Ansari, M. A., & Kim, K.Y. (2009). Parametric study on mixing of two fluids in a three-dimensional serpentine microchannel. Chemical Engineering Journal, 146, 439-448.

[5] Alam, A., & Kim, K. Y. (2012). Mixing performance of a planar micromixer with circular chambers and crossing constriction channels. Sensors and Actuators B, 176, 639-52.

[6] Alam, A., & Kim, K. Y. (2012). Analysis of mixing in a curved microchannel with rectangular grooves. Chemical Engg. Journal, 181-182:708-716.

[7] Ansari, M. A., Park, C. W., Hur, N., & Kim, D. (2013). Non-aligned bilayer square wave bend microchannel for mixing. J. of Mech. Science and Technology, 27(12), 3851-3859.

[8] Alam, A., Afzal, A., & Kim, K.Y. (2014). Mixing performance of a planar micromixer with circular obstructions in a curved microchannel. Chemical Engg. Research & Design, 92, 423-34.

[9] Alijani, H., Özbey, A., Karimzadehkhouei, M., & Kosar, A. (2019). Inertial Micromixing in Curved Serpentine Micromixers with Different Curve Angles. Fluids, 4, 204.

[10] Altay, R., Yetisgin, A. A., Erdem, K., & Kosar, A. (2021). The effect of varying radius of curvature on mixing in elliptical spiral microchannels. Chemical Engineering and Processing: Process Intensification, 164, 108401.

[11] Balasubramaniam, L., Arayanarakool, R., Marshall, S. D., Li, B., Lee, P. S., & Chen, P. C. Y. (2017). Impact of cross-sectional geometry on mixing performance of spiral microfluidic channels characterized by swirling strength of Dean-vortices. Journal of Micromechanics and Microengineering, 27, 095016.

[12] Chen, X., Li, T., Zeng, H., Hu, Z., & Fu, B. (2016). Numerical and experimental investigation on micromixers with serpentine microchannels. International Journal of Heat and Mass Transfer, 98, 131-140.

[13] Calado, B., & Santos, A. D. (2015). Characterization of mixing regimes of Newtonian fluid flows in asymmetrical T- shaped micromixers. Experimental Thermal and Fluid Science, 72, 218-227.

[14] Chen, X., & Zhao, Z. (2017). Numerical investigation on layout optimization of obstacles in a three-dimensional passive micromixer. Analytica Chimica Acta, 964, 142-149.

[15] Casanova, J. O., & Lai, C. H. (2018). CFD study on laminar mixing at a very low Reynolds number by pitching and heaving a square cylinder. Computers and Fluids, 168, 318-327.

[16] Cetkin, E., & Miguel, A. F. (2019). Constructal branched micromixers with enhanced mixing efficiency: Slender design, sphere mixing chamber, and obstacles. International Journal of Heat and Mass Transfer 131, 633-644.

[17] Chen, X., & Shen, J. (2016). Numerical analysis of mixing behaviors of two types of E-shape micromixers. International Journal of Heat and Mass Transfer, 106, 593-600.

[18] Cortes-Quiroz, C. A., Azarbadegan, A., Johnston, I. D., & Tracey, M. C. (2014). Analysis and design optimization of an integrated micro pump micromixer operated for bio-MEMS applications. 4th Micro and Nano Flows Conference, 7-10.

[19] Dauyeshova, B., & Monaco, E. (2018). Numerical simulation of diffusion process T-shape micromixer using Shan -Chen Lattice Boltzmann Method. Computers and Fluids, 167, 229-240.

[20] Dundi, T. M., Raju, V. R. K., & Chandramohan, V. P. (2019). Numerical evaluation of swirl effect on liquid mixing in a passive T-micromixer. Australian Journal of Mechanical Engineering, https://doi.org/10.1080/14484846.2019.1626527.

[21] Dundi, M., Raju, V. R. K., & Chandramohan, V. P. (2019). Characterization of enhanced liquid mixing in T-T mixer at various Reynolds numbers. Asia-Pac J Chem Eng., 14(2), e2298.

[22] Deval, J., Tabeling, P., & HO, C. M. (2002). A dielectrophoretic chaotic mixer. Proc. MEMS 02, 15th IEEE Int. Workshop Micro Electromechanical System, pp 36-9.

[23] Duryodhan, V. S., Chatterjee, R., Singh, S. G., & Agrawal, A. (2017). Mixing in a planar spiral microchannel. Experimental Thermal and Fluid Science, https://doi.org/10.1016/j.expthermflusci.2017.07.024.

[24] Engler, M., Kockmann, N., Kiefer, T., & Woias, P. (2004). Numerical and experimental investigations on liquid mixing in static micromixers. Chemical Engineering Journal, 101, 315-322.

[25] Eribol, P. & Uguz, A. K. (2015). Experimental investigation of electrohydrodynamic instabilities in microchannels. The European Physical Journal Special Topics, 224, 425-434.

[26] Ghadami, S., Esfahan, R. K., Saidi, M. S., & Firoozbakhsh, K. (2017). Spiral microchannel with a stair-like cross-section for size-based particle separation. Microfluid Nanofluid., 21, 115.

[27] Gidde, R. R., Pawar, P. M., Ronge, B. P., Misal, N. D., Kapurkar, R. B., & Parkhe, A. K. (2017). Evaluation of mixing performance in a planar passive micromixer with circular and square mixing chambers. Microsystem Technologies, https://doi.org/10.1007/s00542-017-3686-0.

[28] Hadigol, M., Nosrati, R., Nourbakhsh, A., & Raisee, M. (2011). Numerical study of electroosmotic micromixing of non-Newtonian fluids. Journal of Non-Newtonian Fluid Mechanics, 166, 965-971.

[29] Hengzi, W., Pio, I., Erol, H., Syed, M., & Rowan, D. (2001). Mixing of liquids using obstacles in microchannels. Proceedings of SPIE, Vol. 4590.

[30] Haeberle, S., Brenner, T., Schlosser, H. P., Zengerle, R., & Ducree, J. (2005). Centrifugal Micromixer. Chem. Eng. Technol., 28 (5), 613-616.

[31] Haghighinia, A., & Movahedirad, S. (2019). Fluid micro-mixing in a passive microchannel: Comparison of 2D and 3D numerical simulations. International Journal of Heat and Mass Transfer, 139, 907-916.

[32] Hsieh, S. S., Lin, J. W., & Chen, J. H. (2013). Mixing efficiency of Y-type micromixers with different angles. Int. J. of Heat and Fluid Flows, 44, 130-39.

[33] Hossain, S., Ansari, M. A., & Kim, K. Y. (2009). Evaluation of the mixing performance of three passive micromixers. Chemical Engineering Journal, 150, 492-501.

[34] Husain, A., Khan, F. A., Huda, N., & Ansari, M. A. (2017). Mixing performance of split and recombine micromixer with offset inlets. Microsyst Technol, https://doi.org/10.1007/s00542-017-3516-4.

[35] He, M., Li, W., Zhang, M., Zhang, J. (2019). Numerical investigation on the efficient mixing of over bridged split and recombine micromixer at low Reynolds number. Microsystem Technologies, https://doi.org/10.1007/s00542-019-04317-2.

[36] Izadpanah, E., Hekmat, M. H., Azimi, H., Hoseini, H., & Rabiee, M. B. (2018). Numerical simulation of mixing process in T-shaped and DT-shaped micromixers. Chemical Engineering Communications, https://doi.org/10.1080/00986445.2017.1396216.

[37] Ishii, K., Hihara, E., & Munakata, T. (2020). Mechanism of temperature-difference-induced spiral flow in microchannel and investigation of mixing performance of a non-invasive micromixer. Applied Thermal Engineering, 174, 115291.

[38] Javed, S. F., & Zunaid, M. (2020). Numerical investigation inside spiral passive micromixer using nanofluid. International Journal of Mechanical and Production Engineering Research and Development, 9825-9834.

[39] Jain, S., & Unni, H. N. (2020). Numerical modelling and experimental validation of passive microfluidic mixer designs for biological applications. AIP Advances, 10, 105116.

[40] Jacobson, S. C., McKnight, T. E., & Ramsey, J. M. (1999). Microfluidic devices for electrokinetically driven parallel and serial mixing. Anal. Chem., 71, 4455-4459.

[41] Jr., John D. Anderson (1995). Computational Fluid Dynamics: basics with applications, McGraw-Hill series in Mechanical Engineering, Singapore.

[42] Kouadri, A., Douroum, E., Lasbet, Y., Naas, T. T., Khelladi, S., & Makhlouf, M. (2021). Comparative study of mixing behaviors using non-Newtonian fluid flows in passive micromixers. International Journal of Mechanical Sciences, 201, 106472.

[43] Khoshmanesh, K., Almansouri, A., Albloushi, H., Yi, P., Soffe, R. & Zadeh, K. K. (2015). A multi-functional bubble-based microfluidic system. https://doi.org/10.1038/srep09942.

[44] Khaydarov, V., Borovinskaya, E. S., & Reschetilowski, W. (2018). Numerical and experimental investigations of a micromixer with chicane mixing geometry. Appl. Sci., 8, 2458.

[45] Kurnia, J. C., & Sasmito, A. P. (2019). Performance evaluation of liquid mixing in T-junction passive micromixer with twisted tape insert. Ind. Eng. Chem. Res., https://doi.org/10.1021/acs.iecr.9b04535.

[46] Li, T., & Chen, X. (2017). Numerical Investigation of 3D novel chaotic micromixer with Obstacles. International Journal of Heat and Mass Transfer, 115, 278-282.

[47] Lobasov, A. S., & Minakov, A. V. (2018). Analyzing mixing quality in a T-shaped micromixer for different fluids properties through numerical simulation. Chemical Engineering & Processing, 124, 11-23.

[48] Liu, X., & Lu, Y. (2019). Highly efficient and flexible preparation of water-dispersed Fe3O4 nanoclusters using a micromixer. Particuology, 45, 42-48.

[49] Lobasov, A. S., Shebeleva, A. A., Shebelev, A. V., & Minakov, A. V. (2020). Numerical investigation of the mixing efficiency of fluids in the micromixer with a cylindrical section of a swirl flow. AIP Conference Proceedings, https://doi.org/10.1063/5.0000786.

[50] Mouheb, N. A., Malsch, D., Montillet, A., Solliec, C., & Henkel, T. (2012). Numerical and experimental investigations of mixing in T-shaped and cross-shaped micromixers. Chemical Engineering Science, 68, 278-289.

[51] Madana, V. S. T., & Ali, B. A. (2020). Numerical investigation of engulfment flow at low Reynolds numbers in a T-shaped microchannel. Phys. Fluids, 32, 072005.

[52] Mouza, A. A., Patsa, C. M., & Schonfeld, F. (2008). Mixing performance of a chaotic micro-mixer. Chemical Engg. Research and Design, 86, 1128-34.

[53] Mondal, B., Mehta, S. K., Patowari, P. K., & Pati, S. (2018). Numerical study of mixing in wavy micromixers: comparison between a raccoon and serpentine mixer. Chemical Engineering and Processing – Process Intensification, https://doi.org/10.1016/j.cep.2018.12.011.

[54] Mondal, B., Pati, S., & Patowari, P. K. (2020). Fabrication of wavy micromixer using soft lithography technique. Materials Today: Proceedings, 26, 1271-1278.

[55] Mashaei, P.R., Asiaei, S., & Hosseinalipour, S. M. (2020). Mixing efficiency enhancement by a modified curved micromixer; a numerical study. Chemical Engineering and Processing- Process Intensification, https://doi.org/10.1016/j.cep.2020.108006.

[56] Mondal, B., Pati, S., & Patowari, P. K. (2021). Serpentine square wave microchannel fabrication with WEDM and soft lithography. Materials Today: Proceedings, 46, 8513-8518.

[57] Nguyen, T. N. T., Kim, M. C., Park, J. S., & Lee, N. E. (2008). An effective passive microfluidic mixer utilizing chaotic advection. Sensors and Actuators B, 132, 172-81.

[58] Nouri, D., Hesari, A. Z., & Fard, M. P. (2017). Rapid mixing in micromixers using magnetic field, Sensors and Actuators A, 255, 79-86.

[59] Nezhad, J. R., & Mirbozorgi, S. A. (2018). An immersed boundary-lattice Boltzmann method to simulate chaotic micromixers with baffles. Computers and Fluids, 167, 206-214.

[60] Nazari, M., Rashidi, S., & Esfahani, J. A. (2019). Mixing process and mass transfer in a novel design of induced-charge, electrokinetic micromixer with a conductive mixing chamber. Int. communication in H. M .T, 108, 104293.

[61] Ngo, I. L., Lai, T. K., Choi, H. J., Le, H. T. T., Kim, G. M., Dang, T. D. (2020). A study on mixing performance of dean flows through spiral microchannel under various effects. Phys. Fluids., 32, 022004.

[62] Puccetti, G., Tosi, M., Pulvirenti, B., & Morini, G. L. (2015). Flow patterns of an air-water mixture at the exit of a micro T-junction. Experimental Thermal and Fluid Science, 67, 62-69.

[63] Prakash, R., Zunaid, M., & Samsher. (2021). Simulation analysis of mixing quality in T-junction micromixer with bend mixing channel. Materials Today: Proceedings, 47, 3833-3838.

[64] Prakash, R., Zunaid, M., & Samsher. (2021). Numerical study of mixing index in offset inlets 3-D T mixer with bend shape mixing channel. Journal of Engineering Research, 9, 131-141.

[65] Pradeep, A., Raveendran, J., T, R., Nair, B. G., & Babu T.G. S. (2016). Computational simulation and fabrication of smooth edged passive micromixers with alternately varying diameter for efficient mixing. Microelectronic Engineering, 165, 32-40.

[66] Prakash, R., Zunaid, M., & Samsher. (2022). Numerical investigation on mixing phenomena in an offset inlets spiral microchannel. Materials Today: Proceedings, 61, 21-26.

[67] Quiroz, C. A. C., Azarbadegan, A., & Zangeneh, M. (2014). Evaluation of flow characteristics that give higher mixing performance in the 3-D T-mixer versus the typical T-mixer. Sensor and Actuators B, 202, 1209-19.

[68] Quiroz, C. A. C., Azarbadegan, A., & Zangeneh, M. (2016). Effect of channel aspect ratio of 3-D T-mixer on flow patterns and convective mixing for a wide range of Reynolds number. Sensors and Actuators B, 239, 1153-1176.

[69] Qian, S., & Bau, H. H. (2005). Magneto-hydrodynamic stirrer for stationary and moving fluids. Sensors and Actuators B: Chemical, 106 (2), 859-870.

[70] Qian, J. Y., Li, X. J., Gao, Z. X., & Jin, Z. J. (2019). Mixing efficiency and pressure drop analysis of liquid-liquid two phases flow in serpentine microchannels. Journal of Flow Chemistry, https://doi.org/10.1007/s41981-019-00040-1.

[71] Qamareen, A., Ansari, M. A., Alam, S. S., & Alazzam, A. (2021). Modulation of secondary flows in curved serpentine micromixers. Chemical Engineering Communications, https://doi.org/10.1080/00986445.2021.1887153.

[72] Rahimi, M., Akbari, M., & Parsamoghadam, M. A. (2014). CFD study on effect of channel confluence angle on fluid flow pattern in asymmetrical shaped microchannels. Computers and Chemical Engineering, 73, 172-182.

[73] Ritter, P., Osorio-Nesme, A., & Delgado, A. (2016). 3D numerical simulations of passive mixing in a microchannel with nozzle-diffuser-like obstacles. International Journal of Heat and Mass Transfer, 101, 1075-1085.

[74] Rahmannezhad, J., & Mirbozorgi, S. A. (2019). CFD analysis and RSM-based design optimization of novel grooved micromixers with obstructions. International journal of heat and mass transfer, 140, 483-497.

[75] Rao, L. T., Goel, S., Dubey, S. K., & Javed, A. (2019). Performance Investigation of T-Shaped Micromixer with Different Obstacles. Journal of Physics: Conf. Series., 1276, 012003.

[76] Raza, W., Hossain, S., & Kim, K. Y. (2017). Effective mixing in a short serpentine split and recombination micromixer. Sensors and Actuator B, 258, 381-392.

[77] Ruijin, W., Beiqi, L., Dongdong, S., & Zefei, Z. (2017). Investigation on the splitting-merging passive micromixer based on Baker's transformation. Sensors and Actuator B, 249, 395-404.

[78] Sökmen, C. N. (2010). Effect of property variations on the mixing of laminar supercritical water streams in a T-junction. International Communications in Heat and Mass Transfer, 38, 85-92.

[79] Seo, H. S., & Kim, Y. J. (2012). A study on the mixing characteristics in a hybrid type microchannel with various obstacle configurations. Materials Research Bulletin, 47, 2948-2951.

[80] Solehati, N., Bae, J., & Sasmito, A. P. (2014). Numerical investigation of mixing performance in microchannel T-junction with wavy structure. computers and Fluids, 96, 10-19.

[81] Santana, H. S., Tortola, D. S., Jr., J. L. S., & Taranto, O. P. (2017). Biodiesel synthesis in micromixer with static elements. Energy Conversion and Management, 141, 28-39.

[82] Silva, J. P., Santos, A. D., & Semiao, V. (2017). Experimental characterization of pulsed Newtonian fluid flows inside T- shaped micromixers with variable inlets widths. Experimental Thermal and Fluid Science, 89, 249-258.

[83] Santana, H. S., Silva Jr, J. L., & Taranto, O. P. (2019). Optimization of micromixer with triangular baffles for chemical process in milli devices. Sensors and Actuators B: Chemical, 281, 191-203.

[84] Shimizu, H., & Uetsuji, Y. (2022). Fluid-structure and electric coupled analysis of a valveless microfluidic system using metal-capped piezoelectric actuator. Sensors and Actuators A: Physical, 333, 113232.

[85] Shi, X., Huang, S., Wang, L., & Li, F. (2019). Numerical analysis of passive micromixer with novel obstacle design. Journal of Dispersion Science and Technology, https://doi.org/10.1080/01932691.2019.1699428.

[86] Shinde, A. B., Patil, A. V., & Patil, B. V. (2021). Enhance the mixing performance of water and ethanol at micro-level using geometrical modifications. Materials Today: Proceedings, 46, 460-470.

[87] Shah, I., Aziz, S., Soomro, A. M., Kim, K., Kim, S. W., & Choi, K. H. (2020). Numerical and experimental investigation of Y-shaped micromixers with mixing units based on cantor fractal structure for biodiesel applications. Microsystem Technologies, https://doi.org/10.1007/s00542-020-05036-9.

[88] Scherr, T., Quitadamo, C., Tesvich, P., Park, D. S. W., Tiersch, T., Hayes, D., Choi, J. W., Nandakumar, K., & Monroe, W. T. (2012).A planar microfluidic mixer based on logarithmic spirals. J. Micromech.Microeng, 22, 055019.

[89] Tsai, T. H., Liou, D. S., Kuo, L. S., & Chen, P. H. (2009). Rapid mixing between Ferro-nanofluid and water in a semi-active Y-type micromixer. Sensors and Actuators A, 153, 267-73.

[90] Tokas, S., & Zunaid, M. (2020). Computational analysis of passive mixing in T-micromixer with Non-newtonian blood. International Journal of Mechanical and Production Engineering Research and Development, 10(3), 9889-9898.

[91] Termizi, S. N. A. A., Khor, C. Y., Nawi, M. A. M., Ahmad, N., Ishak, M. I., Rosli, M. U., & Jamalludin M. R. (2020). Computational Fluid Dynamics (CFD) Simulation on mixing in T-shaped micromixer. Materials Science and Engineering, 932, 012006.

[92] Tokas, S., Zunaid, M., & Ansari, M. A. (2020). Numerical investigation of the performance of 3D-helical passive micromixer with Newtonian fluid and non-Newtonian fluid blood, Asia-Pacific Journal of Chemical Engineering, e 2570.

[93] Tokas, S., Zunaid, M., & Ansari, M. A. (2021). Non-Newtonian fluid mixing in a Three-Dimensional spiral passive micromixer. Materials Today: Proceeding, 47, 3947-3952.

[94] Vatankhah, P., & Shamloo, A. (2018). Parametric study on mixing process in an in-plane spiral micromixer utilizing chaotic advection. Analytica Chimica Acta, 1022, 96-105.

[95] Veldurthi, N., Chandel, S., Bhave, T., & Bodas, D. (2015). Computational fluid dynamic analysis of poly (dimethyl siloxane) magnetic actuator based micromixer. Sensors and Actuators B, 212, 419-24.

[96] Versteeg, H., & Malalasekra, W. (2007). An Introduction to Computational Fluid Dynamics, Second Edition, Pearson Education Limited, U.K.

[97] Wong, S. H., Bryant, P., Ward, M., & Wharton, C. (2003). Investigation of mixing in a cross-shaped micromixer with static mixing elements for reaction kinetics studies. Sensors and Actuator B, 95, 414-424.

[98] Wong, S. H., Ward, M. C. L., & Wharton, C. W. (2004). Micro T-mixer as a rapid mixing micromixer. Sensors and Actuator B, 100, 359-379.

[99] Wang, L., Wu, W., & Li, X. (2013). Numerical and experimental investigation of mixing characteristics in the constructal tree-shaped microchannel. *Int. J. of H. M. T*, 67, 1014-23.

[100] Wu, J. W., Xia, H. M., Zhang, Y. Y., Zhao, S. F., Zhu, P., & Wang, Z. P. (2018). An efficient micromixer combining oscillatory flow and divergent circular chambers. Microsystem Technologies, https://doi.org/10.1007/s00542-018-4193-7.

[101] Wang, T., Xie, T., & Xu, C. (2020). Numerical investigations of micro –SLM extraction/stripping in a spiral channel. Chemical Engineering Science, 212, 115344.

[102] Xu, Z., Li, C., Vadillo, D., Ruan, X., & Fu, X. (2011). Numerical simulation on fluid mixing by effects of geometry in staggered oriented ridges micromixers. Sensors and Actuator B, 153, 284-292.

[103] Xia, G. D., Li, Y.F., Wang, J., & Zhai, Y. L. (2016). Numerical and experimental analyses of planar micromixer with gaps and baffles based on field synergy principle. International Communications in Heat and Mass Transfer, 71, 188-196.

[104] Xu, W., He, X., Gao, L., Xia, T., & Yu, Z. (2018). Influence of different inlet conditions on micromixer. International Journal of Fluid Machinery and systems, https://doi.org/10.5293/IJFMS.2018.11.2.205.

[105] Xu, C., Zhong, Y., Zheng, Y., Huang, W., Chaojin., & Xu, B. (2019). Micromixing-assisted preparation of TiO2 films from ammonium hexafluorotitanate and urea by liquid phase deposition based on simulation of mixing process in T-shaped micromixer. Ceramic International, 45, 11325-11334.

[106] Xu, J., & Chen, X. (2019). Mixing performance of a fractal-like tree network micromixer based on Murray's law. Int. Journal of H.M.T., 141, 346-352.

[107] Yang, J., Qi, L., Chen, Y., & Ma, H. (2013). Design and Fabrication of a Three Dimensional Spiral Micromixer. Chin. J. Chem., 31, 209-214.

[108] Yuan, S., Jiang, B., Peng, T., Li, Q., & Zhou, M. (2021). An investigation of flow patterns and mixing characteristics in a cross-shaped micromixer within the laminar regime. Micromachines, 12, 462.

[109] Zhang, S., Chen, X., Wu, Z., & Zheng, Y. (2019). Numerical study on stagger Koch fractal baffles micromixer. International Journal of Heat and Mass Transfer, 133, 1065-1073.

[110] Zare, P., & Talebi, S. (2019). Numerical simulation of geometry effect on mixing performance in L-shaped micromixers. Chemical Engineering Communications, https://doi.org/10.1080/00986445.2019.1613228.

[111] Zhang, S., & Chen, X. (2019). Secondary bonding of PMMA micromixer with high pressure. Microchemical Journal, 144, 339-344.

[112] Zou, L., Gong, Y., Chen, L., Yi, X., & Liu, W. (2021). Design and evaluation of two-dimensional passive micromixer based on unbalanced convergence-divergence-splits and reverse-collisions-recombination. Chemical Engineering Science, 244, 116816.

LIST OF PUBLICATIONS BASED ON RESEARCH WORK

Paper Published in International Journals

1. Prakash, R., Zunaid, M. & Samsher "Numerical study of mixing index in offset inlets 3-D T mixer with bend shape mixing channel" Journal of Engineering Research, 9, (2021), 131-141. https://doi.org/10.36909/JER.ICARI.15275. (SCIE, I.F. 0.38).

2. Prakash, R., Zunaid, M. & Samsher "Design and Simulation of the Spiral Micromixer with chaotic advection" Journal of Applied Fluid Mechanics, 16 (4), (2023), 739-749. https://doi.org/10.47176/JAFM.16.04.1450. (SCIE, I.F. 1.15).

Paper Published in International Conferences

1. Prakash, R., Zunaid, M. & Samsher "Simulation analysis of mixing quality in T-junction micromixer with bend mixing channel" Materials Today Proceedings, Volume 47, (2021), 3833-3838. https://doi.org/10.1016/J.MATPR.2021.03.172.
2. Prakash, R., Zunaid, M. & Samsher "Numerical investigation on mixing phenomena in an offset inlets spiral microchannel" Materials Today Proceedings, Volume 61, (2022), 21-26. https://doi.org/10.1016/J.MATPR.2022.03.299.

BIOGRAPHICAL PROFILE OF RESEARCHER

Ranjan Prakash had worked as an Assistant Professor in the Department of Mechanical Engineering, Vishveshwarya Group of Institutions, Dadri from July 2012 to May 2020. He received his Bachelor's degree in Mechanical Engineering from V. I. E. T, Dadri. He completed his Master's Degree in Fluids Engineering from Motilal Nehru National Institute of Technology (MNNIT), Allahabad, India and Ph.D. from Delhi Technological University, Delhi. His research interest includes Microfluidics, Micromixing, and Design of efficient micromixer. He has published four research papers in international journals and conferences. He qualified GATE examination and he has more than ten years of teaching experience.